

METEOROLOGICAL OFFICE

149116

1 DEC 1986

LIBRARY

ADVANCED LECTURES 1986

DYNAMICS

OF

ROTATING FLUIDS

DRS HIDE, JOHNSON, READ & WHITE

PERMISSION TO QUOTE FROM THIS DOCUMENT MUST BE OBTAINED FROM THE PRINCIPAL,  
METEOROLOGICAL OFFICE COLLEGE, SHINFIELD PARK, READING, RG2 9AU.

Lecture 1: Basic theory

Equations of motion, continuity and thermodynamic energy

In the usual notation these are

$$\left. \begin{aligned} \frac{D\mathbf{u}}{Dt} + 2\boldsymbol{\Omega} \times \mathbf{u} + g\mathbf{k} + \frac{1}{\rho} \nabla p &= \mathbf{F} \\ \frac{D\rho}{Dt} + \rho \nabla \cdot \mathbf{u} &= 0 \\ c_v \frac{DT}{Dt} - \frac{p}{\rho^2} \frac{D\rho}{Dt} &= Q \end{aligned} \right\} \textcircled{A}$$

Here  $\boldsymbol{\Omega}$  = rotation rate of frame relative to which the velocity  $\mathbf{u}$  is measured,  $F$  and  $Q$  are the frictional force and diabatic heating per unit mass, and  $\mathbf{k}$  is unit vector in the direction of apparent vertical. The perfect gas equation  $p = \rho RT$  will also be assumed.

From (A) we can derive several important relations:

Total energy budget

$$\frac{d}{dt} \int \rho \left\{ \frac{1}{2} \mathbf{u}^2 + gz + c_v T \right\} d^3r = \int \rho (\mathbf{u} \cdot \mathbf{F} + Q) d^3r \quad \textcircled{B}$$

(so long as the bounding surfaces are rigid, or  $\rho \rightarrow 0$  at "infinity").

Vorticity equation

Defining  $\boldsymbol{\zeta} = \nabla \times \mathbf{u}$  ("relative vorticity") we find

$$\frac{D\boldsymbol{\zeta}}{Dt} + (\boldsymbol{\zeta} + 2\boldsymbol{\Omega}) \nabla \cdot \mathbf{u} - (\boldsymbol{\zeta} + 2\boldsymbol{\Omega}) \cdot \nabla \mathbf{u} + \nabla \left( \frac{1}{\rho} \right) \times \nabla p = \nabla \times \mathbf{F} \quad \textcircled{C}$$

(a) Suppose (as seems reasonable) that the frictional force  $\mathbf{F}$  vanishes if the relative velocity  $\mathbf{u}$  is zero. Then it is clear that, if  $\mathbf{u} = 0$ , then  $\nabla \left( \frac{1}{\rho} \right) \times \nabla p = 0$ . So if  $\nabla \left( \frac{1}{\rho} \right) \times \nabla p \neq 0$  (baroclinic fluid) we

must have  $\underline{u} \neq 0$  i.e. there must be motion. This is the Jeffreys-Bjerknes theorem.

(b) For motion of a rapidly rotating fluid, the dominant balance (away from boundary layers) is between the baroclinic term and the term  $(2\underline{\Omega} \cdot \nabla)\underline{u}$ :

$$2\underline{\Omega} \frac{\partial \underline{u}}{\partial \zeta} \doteq [\nabla(\frac{1}{\rho}) \times \nabla p]$$

(where the  $\zeta$  axis is parallel to  $\underline{\Omega}$ ).

From this:

(i) for a barotropic fluid we may conjecture  $\frac{\partial \underline{u}}{\partial \zeta} = 0$  which is the Proudman-Taylor theorem;

(ii) for a baroclinic fluid, considering the components of  $\underline{u}$  perpendicular to  $\underline{\Omega}$ , we can derive the familiar thermal wind equation.

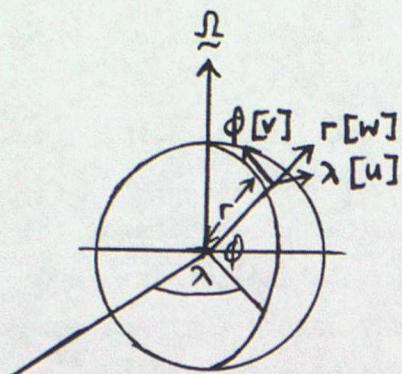
(c) For inviscid, adiabatic motion (and with no further approximation) it follows that

$$\frac{D}{Dt} \left\{ \frac{(\underline{z} + 2\underline{\Omega}) \cdot \nabla \theta}{\rho} \right\} = 0 \quad (D)$$

where  $\theta$  = potential temperature. The quantity in curly brackets is called the Ertel potential vorticity. Result (D) is one of the most important in fluid dynamics. (See Hide (1977) for further discussion of (a) - (c). See Hoskins et al (1986) for more on potential vorticity, and White (1978) for an elementary discussion of energetics, and for references.)

#### Angular momentum: an example

The momentum equation of (A) can of course be used to derive a conservation relation for angular momentum. We can, however, illustrate some important ideas by adopting the reverse procedure - deriving one component of the momentum equation on a sphere by considering the axial angular momentum balance of a parcel of air (at latitude  $\phi$ ) moving with relative velocity  $\underline{u} = (u, v, w)$  relative to the rotating Earth. See diagram.



If the mass of the parcel is  $\rho \delta \tau$ , its angular momentum  $A_\lambda$  about the polar axis is

$$\rho \delta \tau \{ (\Omega r \cos \phi + u) r \cos \phi \}$$

Now

$$\frac{DA_\lambda}{Dt} = r \cos \phi \left\{ \text{net force on parcel} \right\}$$

or

$$\frac{DA_\lambda}{Dt} = r \cos \phi \left\{ \rho \delta \tau F_\lambda - \frac{1}{r \cos \phi} \frac{\partial p}{\partial \lambda} \delta \tau \right\}$$

(where  $F_\lambda$  is the zonal component of the frictional force per unit mass). Using  $w = D r / Dt$ ,  $r D \phi / Dt = v$  we derive, in only a few lines

$$\frac{Du}{Dt} + \frac{u w}{r} - \frac{u v}{r} \tan \phi - 2 \Omega v \sin \phi + 2 \Omega w \cos \phi + \frac{1}{\rho r \cos \phi} \frac{\partial p}{\partial \lambda} = F_\lambda \quad (E)$$

Of course, the same result can be derived by isolating the zonal ( $\lambda$ ) component of the vector momentum equation. The derivation used here emphasises that a complicated equation may express a simple physical principle. This is interesting in itself; but a further implication is that we should be very careful how we approximate equations such as (E).

### Divergence, spin vectors and helicity

The vorticity and energy equations result from applying the operations  $\nabla \times$  and  $\underline{u} \cdot$  to the momentum equation. By applying  $\nabla \cdot$  and  $\underline{u} \times$  instead we obtain equations for the divergence  $\nabla \cdot \underline{u}$  and  $\underline{u} \times \frac{D \underline{u}}{Dt}$ . The latter quantity is related to the spin vector  $\underline{S} \equiv \underline{u} \times \frac{D \underline{u}}{Dt} / \underline{u}^2$  which gives the rate of change of direction of motion of a fluid element (measured in the osculating plane of its trajectory). See Lecluyse and Neumann (1986). Another quantity of interest is the helicity  $\underline{H} = \underline{u} \cdot \underline{z}$  - see, for example, Hide (1976).

## Hamiltonian formulation

The equations of motion may be written in Hamiltonian form. This is of more than academic interest, because the conservation laws (for energy, potential vorticity, &c.) arise as symmetry properties of the Hamiltonian. Hence by making approximations in the Hamiltonian, and deriving the implied equations of motion, we may ensure that analogues of all the conservation laws are retained in approximate models. See Salmon (1983, 1985) for details and further references.

## Various fluid models

As well as the perfect gas model the following are often encountered:

### (i) Incompressible fluid

Nonhydrostatic motion may be allowed, but density  $\rho$  is assumed independent of pressure, and  $\rho = \rho(T)$  at most, this variation being accounted for only in the "buoyancy" term of the vertical momentum equation (the "Boussinesq approximation"). Incompressibility is often assumed in modelling the motion of liquids (e.g. in oceanography and laboratory experiments). It is also applied in modelling some atmospheric flows - after appropriate scale analysis - in which case  $\rho = \rho(T, z)$  may be the adopted functional form. Note that incompressibility does not allow acoustic (elastic) modes to be produced.

### (ii) Shallow water model

If the fluid is incompressible, homogeneous ( $\rho = \text{constant}$ ), shallow (depth  $h \ll$  horizontal scale of motion) and free ( $F=Q=0$ ) the governing equations reduce to

$$\begin{aligned} \frac{D\underline{v}}{Dt} + 2\underline{\Omega} \times \underline{v} + g \nabla h &= 0 \\ \frac{Dh}{Dt} + h \nabla \cdot \underline{v} &= 0 \end{aligned} \quad (F)$$

(where  $\underline{v}$  = horizontal velocity vector)

This is the shallow water model. It is used in many theoretical and numerical studies (see, for example, Salmon (1985)). Note that gravity and rotational (Rossby) modes are allowed; Longuet-Higgins (1968) gives a detailed account.

The hydrostatic primitive equations

The forms used in GCMs and many forecasting models are

$$\left. \begin{aligned} \frac{Du}{Dt} - \frac{uv \tan \phi}{a^2} - 2\Omega v \sin \phi + \frac{1}{\rho a \cos \phi} \frac{\partial P}{\partial \lambda} &= F_\lambda \\ \frac{Dv}{Dt} + \frac{u^2 \tan \phi}{a^2} + 2\Omega u \sin \phi + \frac{1}{\rho a} \frac{\partial P}{\partial \phi} &= F_\phi \\ g + \frac{1}{\rho} \frac{\partial P}{\partial z} &= 0 \end{aligned} \right\} (G)$$

Justification by scale analysis (for quasi-horizontal motion) is tedious and will not be given here. Note that the above set is energetically consistent, and that the shallow atmosphere approximation ( $r \approx a =$  Earth's radius) has been made.

A useful Cartesian approximation to (G) is obtained by setting  $f = 2\Omega \sin \phi$ , neglecting the metric terms and using rectangular coordinates :

$$\left. \begin{aligned} \frac{Du}{Dt} - fv + \frac{1}{\rho} \frac{\partial P}{\partial x} &= F_x \\ \frac{Dv}{Dt} + fu + \frac{1}{\rho} \frac{\partial P}{\partial y} &= F_y \\ g + \frac{1}{\rho} \frac{\partial P}{\partial z} &= 0 \end{aligned} \right\} (H)$$

$f = f_0 =$  constant is the 'f-plane approximation'.  $f = f_0 + \beta y$ , where  $\beta =$  constant, is the ' $\beta$ -plane approximation'. These approximations are widely used in theoretical studies.

The semi-geostrophic (SG) and quasi-geostrophic (QG) approximations

In (H),  $\frac{D}{Dt} = \left( \frac{\partial}{\partial t} + \mathbf{u} \cdot \nabla \right)$ . The SG approximation retains this relation, but sets  $\mathbf{u} = \mathbf{u}_g, \mathbf{v} = \mathbf{v}_g$  elsewhere in the acceleration terms :

$$\left. \begin{aligned} \frac{Du_g}{Dt} - fv + \frac{1}{\rho} \frac{\partial P}{\partial x} &= F_x \\ \frac{Dv_g}{Dt} + fu + \frac{1}{\rho} \frac{\partial P}{\partial y} &= F_y \end{aligned} \right\} (SG)$$

Here the geostrophic flow  $\mathbf{v}_g$  is defined by  $\mathbf{v}_g = \frac{1}{\beta f_0} \mathbf{k} \times \nabla P$ , where  $\rho_0 = \rho_0(z)$ .

The QG approximation goes one step further, and sets  $\underline{u} = \underline{v}_g$  in the definition of the material derivative :

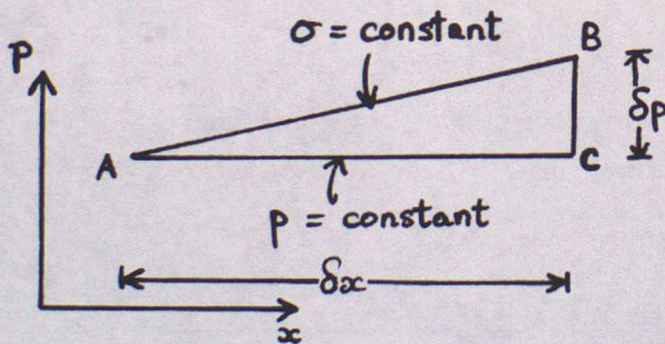
$$\begin{aligned} \left( \frac{\partial}{\partial t} + \underline{v}_g \cdot \nabla \right) u_g - fv + \frac{1}{\rho} \frac{\partial p}{\partial x} &= F_x \\ \left( \frac{\partial}{\partial t} + \underline{v}_g \cdot \nabla \right) v_g + fu + \frac{1}{\rho} \frac{\partial p}{\partial y} &= F_y \end{aligned} \quad (\text{QG})$$

Similar replacements are made in the other prognostic equations.

For further details on SG, see Hoskins (JAS, 1975). Because  $\nabla \cdot \underline{v}_g = 0$ , neither SG nor QG implies gravity modes; they are therefore "filtered models".

### Vertical coordinate systems

For compressible atmospheres the following systems may be encountered in conjunction with the primitive equations and filtered models : height  $z$ , pressure  $p$  (or  $\ln p$ ,  $p^{R/c_p}$  & c), potential temperature  $\theta$ ,  $\sigma = p/p_{\text{surface}}$ ,  $\epsilon = \theta/\theta_{\text{surface}}$ . The only identity which it is necessary to know (or to be able to derive quickly) is illustrated by the transformation from  $p$  to  $\sigma$  of a horizontal derivative of any scalar  $Q$ :



$$\begin{aligned} \delta Q_{AB} &= \delta Q_{AC} + \delta Q_{CB} \\ &= \left. \frac{\partial Q}{\partial x} \right|_p \delta x + \left. \frac{\partial Q}{\partial p} \right|_x \delta p \end{aligned}$$

$$\begin{aligned} \boxed{\left. \frac{\partial Q}{\partial x} \right|_\sigma} &= \left. \frac{\partial Q}{\partial x} \right|_p + \left. \frac{\partial Q}{\partial p} \right|_x \left. \frac{\partial p}{\partial x} \right|_\sigma \\ &= \left. \frac{\partial Q}{\partial x} \right|_p + \frac{1}{p_{\text{surface}}} \left. \frac{\partial Q}{\partial \sigma} \right|_x \left. \frac{\partial p}{\partial x} \right|_\sigma \end{aligned}$$

There is currently great interest in the use of  $\theta$  as vertical coordinate ('isentropic coordinates'); see Hoskins et.al (1985).

## References

- Hide, R.            1976    Geophys.fluid dynamics,7, 157-161  
                         1977    Quart.J.R.Met.Soc.,103, 1-28
- Hoskins, B.J.    1975    J.Atmos.Sci.,32, 233-242  
\_\_\_\_\_        1985    Quart.J.R.Met.Soc.,111, 877-946
- McIntyre, M.E.  
and Robertson,A.W.
- Lecluyse, A.    1986    Ibid,,112, 285-288  
and Neumann,J.
- Longuet-Higgins 1968    Phil.Trans., A 132, 511-607
- Salmon, R.       1983    J.Fluid.Mech., 132, 431-444  
                         1985    Ibid, 153, 461-477
- White, A.A.      1978    Weather, 33, 408-416 & 446-457

LECTURE 2: THE 'PHILOSOPHY' OF LABORATORY EXPERIMENTS

Before embarking upon a more detailed examination of results from a particular range of experiments, it is instructive to consider the underlying basis for regarding laboratory experiments as contributing information relevant to dynamical meteorology and oceanography. An intimately related question is "what is meant by the term 'model' in meteorology and oceanography, and what purpose does it serve?". The following discussion offers some remarks which are intended to 'set the scene' for future presentations, by elucidating the general role of laboratory experiments in fluid mechanics and atmospheric science, and that of the thermally-driven rotating annulus as a particular example of relevance to general circulation studies in meteorology.

1. 'Models' in basic and applied science

In engineering and applied sciences, the term 'model' is commonly used to represent a device which imitates the behaviour of a physical system as closely as possible, but on a different (usually smaller) scale. The aim of such a model is normally to evaluate the behaviour of the physical system under practical conditions, for reasons connected with the exploitation of that system for economic, social, military or other purposes. Numerical weather prediction (NWP) models, for example, clearly fall into this category. By their very nature, such models are extremely complicated entities. Like the atmosphere itself, therefore, it is generally impossible to comprehend fully the complex interactions of physical processes and scales of motion that result in their synoptic behaviour. The success of these models can only really be judged by the accuracy of their predictions as directly verified against subsequent atmospheric observations. Climate models, on the other hand, are often comparable in complexity to those used for NWP, yet are frequently used in attempts to answer questions of economic, social or military importance for which little atmospheric data may be available to verify their conclusions (e.g. the CO<sub>2</sub> problem, the 'nuclear winter' debate etc...).

In constructing such models and interpreting their results, it is necessary to make use of a different class of model - the 'conceptual' or 'theoretical' model - which may represent only a tiny subset of the processes active in the

much larger, applications-oriented model, but whose behaviour may be completely understood (both qualitatively and quantitatively) from first principles. To arrive at such a complete level of understanding, however, it is usually necessary to make such models extremely simple in construction and highly idealised. An important prototype of such a model in fluid mechanics is that of dimensional or 'scale' analysis (a hybrid form of the technique was called 'inspectional analysis' by Birkhoff 1960), in which an entire problem is reduced to a determination of the essential balance of forces, and the consequent dependence of one or more observable (dimensionless) parameter on others in the form of power-law exponents. Following a systematic scale analysis, it is often possible to arrive at a scheme of approximations to the full mathematical description of a problem (e.g. the Navier-Stokes equations) which may then permit analytical solutions to be obtained. The quasi-geostrophic approximation is another important prototype, discussed in detail in this course (and elsewhere, see e.g. Gill 1982), which enables a number of essential dynamical processes (barotropic and baroclinic instabilities, Rossby waves, 'free modes' etc....) to be studied in simplified forms.

For the basic researcher, such models are an essential device to aid and advance understanding. The latter is achievable because simple models enable theories and hypotheses to be formulated in a way which may be tested (i.e. falsified, in the best traditions of the scientific method) against observations (e.g. of the atmosphere of the Earth and of other planets) and/or experiments. The ultimate aim of such studies in atmospheric science are an overall framework which sets in perspective all planetary atmospheres, of which the Earth's is but one example (see Lorenz 1967; Hide 1969, 1977; Hoskins 1983; Fig. 1).

The role of laboratory fluid mechanics experiments in this scheme would seem to be as models firmly in the second category. Compared with the atmosphere, they are clearly much simpler in their geometry, boundary conditions and forcing processes (diabatic and mechanical). Their behaviour is therefore governed by a system of equations which can be stated exactly (i.e. no controversial parametrisations are necessary), although exact mathematical solutions may still be impossible to obtain. Unlike the atmosphere, however, it is possible to carry out controlled experiments in the laboratory to study dynamical processes in a

real fluid without recourse to dubious approximations (necessary to analytical studies). For certain purposes, therefore, laboratory experiments can complement studies using complex numerical models, especially since (a) experiments have virtually infinite resolution compared with their numerical counterparts (subject only to the continuum hypothesis!) and (b) they are very cheap to run! In the context of simple analytical models of atmospheric processes, it is sometimes possible (though by no means automatically true) that a suitably-designed laboratory experiment can be used to obtain a physical realisation of that model in a real fluid, provided certain scaling assumptions (for 'dynamical similarity') can be satisfied (e.g. Birkhoff 1960). Such an experiment can be regarded as a 'test bed' for that model under highly controlled conditions.

In discussing the role of laboratory experiments, however, it is not entirely true to say that they have no direct role in the construction of more complex, applications-oriented models. Because the numerical techniques used (finite-difference schemes, etc.) in such models of the atmosphere can also be used to simulate flows in the laboratory under similar scaling assumptions, laboratory experiments can also be useful 'test beds' for directly verifying the accuracy of such techniques in a far more rigorous way than is possible using atmospheric data alone (indeed this role is explicitly recognised, for example, in the World Climate Programme, and will be discussed in Lecture 7).

## 2. General circulation studies and the rotating annulus

If the central problem concerning the global circulation of the Earth's atmosphere is that of 'predicting from the laws of classical physics that the atmosphere is necessarily organized as it is', then any approach towards obtaining such a prediction should include a minimal number of essential physical ingredients. At its most basic level, the general circulation is but one example of thermal convection due to impressed differential heating in the horizontal in a fluid of low viscosity and thermal conductivity. Laboratory experiments investigating such a problem should therefore include at least these features, and be capable of satisfying scaling requirements for dynamical similarity to the relevant scales of motion in the atmosphere. Such experimental systems may then be regarded as representing the general circulation in the absence of various complexities associated e.g. with radiative transfer,

atmospheric chemistry, boundary layer turbulence, planetary curvature, topography etc. (although the latter can be included in a systematic way if required, see Lecture 5).

Experiments of this type are by no means a recent phenomenon, with examples published as long ago as the 18th and 19th centuries (e.g. Vettin 1884; Exner 1923; see Fultz 1951 for a review of this early work). The modern development of experiments on the general topic of rotating fluids was begun by Taylor (1923), who also contributed greatly to the theoretical development of the subject. It was not until the late 1940s, however, that Fultz began a systematic series of experiments at the University of Chicago on rotating fluids subject to horizontal differential heating in an open cylinder (hence resulting in the obsolete term 'dishpan experiment'), and set the subject onto a firm footing (see Fultz et al. 1959). Independently and around the same time, Hide (1958) began his first series of experiments at the University of Cambridge on flows in a differentially heated rotating annulus, and it is the latter system which we now consider in detail.

### 3. Flow regimes and transitions in the rotating annulus

The typical construction of the annulus is illustrated schematically in Fig. 2, and consists of a working fluid (usually a viscous liquid, such as water or silicone oil) contained in the annular gap between two coaxial, circular, thermally-conducting cylinders, which can be rotated about their common (vertical) axis. The cylindrical sidewalls are maintained at constant but different temperatures (though see Lecture 6), with a (usually horizontal) thermally-insulating lower boundary and an upper boundary which is also thermally-insulating and either rigid or free (i.e. without a lid).

Although a number of variations of these boundary conditions have been investigated experimentally, all such experiments are found to exhibit the same three main flow regimes over the range of conditions studied. These consist of axisymmetric flow (in some respects analogous to Hadley flow in the Earth's tropics) at very low rotation rate  $\Omega$ , regular waves at moderate  $\Omega$ , and highly irregular aperiodic flow at the highest rotation rates attainable. In addition, axisymmetric flows occur at all values of  $\Omega$  at a sufficiently low temperature difference  $\Delta T$ . The location of these regimes are usually plotted on a 'regime

diagram' with respect to the two most important dimensionless parameters, viz. a stability parameter (or 'thermal Rossby number')  $\Theta$  ( $\equiv g\alpha\Delta Td/[\Omega(b-a)]^2$ , where  $g$  is the acceleration due to gravity, and  $\alpha$  the cubical expansion coefficient of the fluid) and a Taylor number  $Ta$  ( $\equiv \Omega^2(b-a)^5/[\nu^2d]$ , where  $\nu$  is the kinematic viscosity - see Fig. 3).

The regular waves may be either steady (apart from a slow drift) or 'vacillating' (i.e. with a periodic or nearly periodic time dependence). 'Amplitude vacillation' occurs in association with transitions towards a lower wavenumber (obtained by reducing  $\Omega$  and/or increasing  $\Delta T$ ), and is characterised by periodic modulation of the wave amplitude and phase speed. 'Structural vacillation' (also known as 'shape' or 'tilted-trough vacillation') occurs as the irregular flow transition is approached, and is characterised by a nearly periodic tilting of the wave axis. This becomes more pronounced as  $\Omega$  is increased, until the regular flow pattern breaks down into fully irregular flow. Another important property characteristic of the regular flow regime is that of intransitivity (i.e. multiple equilibrium states), in which two or more alternative flows with differing azimuthal wavenumber  $m$  can occur for a given set of parameters. The state obtained depends upon the initial conditions. In addition, transitions between different states in the regular regime, achieved by slowly changing the external parameters, often exhibit hysteresis, in that the location of a transition in parameter space depends upon the direction from which that transition is approached (e.g.  $m = 3 \rightarrow 4$  does not occur at the same point as  $m = 4 \rightarrow 3$ ). The latter properties are intimately connected with non-linear effects in the flow (e.g. see Pippard 1985) arising from the advection of heat and momentum in the fluid.

From a consideration of the conditions under which waves occur in the annulus (especially the location in parameter space of the 'upper symmetric' transition, see Fig. 3) and a comparison with the results of linear instability theory (e.g. see Lecture 3), it is concluded that the waves in the annulus are fully-developed manifestations of baroclinic instability (often referred to as 'sloping convection' from the geometry of typical fluid trajectories, e.g. see Lecture 3 and Hide & Mason 1975). Since these flows occur in the interior of the annulus (i.e. outside ageostrophic boundary layers) under conditions appropriate to quasi-geostrophic scaling, a dynamical similarity to the large-

scale mid-latitude cyclones in the Earth's atmosphere is readily apparent, though with rather different boundary conditions. A more detailed discussion of the properties of these flows is given by Hide (1969, 1977) and Hide & Mason (1975). Implicit in this conclusion is the implication that the waves develop in order to assist in the transfer of heat both upwards (enhancing the static stability) and horizontally down the impressed thermal gradient. The effect of baroclinic waves on heat transfer (including laboratory measurements) will be discussed in more detail in Lectures 6 and 7.

#### 4. Other experimental systems?

The regime structure for the thermal annulus is remarkable in exhibiting highly regular and predictable non-axisymmetric flows over a wide range of parameters. If such a regime structure were to apply generally to any fluid system, it could have important implications for theories of atmospheric predictability. Evidence for regular flow regimes in systems more closely akin to planetary atmospheres is currently sparse (e.g. see James & Gray 1983), although the atmospheres of Mars and Jupiter display some intriguing examples of highly persistent and regular features (e.g. see Leovy 1979; Lecture 6). It is of interest, therefore, to compare the regime structure of the thermally-driven annulus with that of other fluid systems in the laboratory which investigate quite different dynamical processes.

##### a) The two-layer annulus or cylinder

Another system which exhibits baroclinic instability in a different form to that of the thermal annulus is found in the rotating, two-layer experiment (e.g. see Hart 1979). Two immiscible liquids of differing density ( $\Delta\rho$ ) are placed in an open circular cylinder or coaxial annulus (see Fig. 4(a)) which can, like the thermal annulus, be rotated about its vertical axis of symmetry. Motions are driven by rotating the rigid upper boundary of the fluid at a different rate to the rest of the apparatus, imparting a vertical shear which causes an axisymmetric deformation of the fluid interface (thereby storing potential energy in a way analogous to the sloping isotherms in the thermal annulus). Baroclinic instability occurs via non-axisymmetric deformations of that interface, thereby transferring angular momentum (rather than heat). A

significant advantage of this system in the study of sloping convection is that it is more amenable to mathematical analysis than the thermally-driven system (e.g. see Pedlosky 1979).

The regime diagram is schematically shown in Fig. 4(b), plotted vs an inverse Rossby number  $R_o$  ( $\equiv \Delta\Omega/[2\Omega(b-a)]$ , where  $\Delta\Omega$  is the difference in rotation rate between the apparatus and the lid) and a Froude number  $F$  ( $\equiv \rho_o [2\Omega(b-a)]^2/[g\Delta\rho D]$ )  $\sim 1/\theta$ , see §3 above). At low  $F$  and/or very small  $R_o$ , all flows are axisymmetric, while at  $F > 5$  with moderate  $R_o$ , waves are found to occur. As in the thermal annulus, these waves are regular and steady at moderate values of  $F$ , and undergo periodic modulations at larger values. At the highest values of  $F$  attainable, the flow becomes irregular and aperiodic, much as observed for the thermal annulus.

#### b) Rayleigh-Benard convection

The properties of thermal convection without rotation in the presence of an unstable thermal gradient in the vertical have been studied for many years (e.g. see Swinney & Gollub 1985 for a review). The regime structure is found to depend significantly upon the aspect ratio  $D/L$  (where  $D$  and  $L$  are vertical and horizontal length scales respectively). Fig. 5 shows a typical regime diagram for low aspect ratio systems (from Krishnamurti 1973), in which flow type depends mainly upon the Rayleigh number  $A$  ( $\equiv g\alpha\Delta T D^3/\kappa\nu$ , where  $\kappa$  is the thermal diffusivity of the fluid) and the Prandtl number  $P$  ( $\equiv \nu/\kappa$ ). No convection occurs at all when  $A < A_c$  ( $\sim 1500$ ). When  $A > A_c$ , convection begins in the form of steady, 2-dimensional rolls, the precise form and orientation of which depending upon the lateral boundaries. As  $A$  continues to increase, the rolls give way first (at high  $P$ ) to steady, 3-dimensional cells, then to time-dependent flows, which can be regular and periodic (especially at low  $P$ ) before finally becoming irregular and turbulent. For large aspect ratio systems, there is little evidence for regular behaviour at the onset of convection, with the flow rapidly becoming irregular and turbulent (with the development of plumes etc.).

### c) Taylor-Couette flow

The instability of a homogeneous fluid subject to mechanical shear at its boundaries is another classical problem in fluid mechanics, and was extensively studied (both theoretically and experimentally) by Taylor (1923). To study the flow in the laboratory, the fluid is usually contained in an annulus of narrow gap width  $(b - a)$  and large depth, in which the inner and outer cylindrical sidewalls may be rotated independently (at  $\Omega_a$  and  $\Omega_b$  - see Fig. 6(a)). The flow obtained depends principally upon Reynolds or Taylor numbers defined by  $\Omega_a$ ,  $\Omega_b$ ,  $a$  and  $b$  (i.e.  $R_{ea} \equiv \Omega_a a^2/\nu$  etc.) and the main aspect ratios of the apparatus. Because the experimental arrangement is simple and easy to control (and has applications connected with the lubrication of bearings), it has received wide attention, especially in recent years, in connection with its transitions to turbulent flow (e.g. see Swinney & Gollub 1985 for a review).

At low values of  $R_e$ , the flow is uniform throughout the apparatus, in response to the imposed shear. Above a critical value of  $R_e$  (related to the Rayleigh criterion for inviscid centrifugal instability), the flow develops a series of steady axisymmetric rolls which are periodic along the rotation axis (Taylor vortices). As  $R_e$  is increased further, the rolls develop waves in the azimuthal direction ('wavy vortex flow'), and the flow becomes doubly-periodic (see Fig. 6(b), taken from Coles 1965). At much higher values of  $R_e$ , further instabilities occur until fully turbulent flow is obtained, although the detailed sequence of events is highly complicated (the sequence is discussed in some detail by Andereck et al. 1986). Intransitivity in the number of Taylor vortices obtained at a given set of parameters in the regular flow regime is often exhibited much more strongly in the Taylor-Couette system than in the thermal annulus, in the sense that many more different states may be obtained at a given set of parameters.

## 5. 'Universal' behaviour and Dynamical Systems

The above examples serve to demonstrate (and the list is by no means exhaustive) that the presence of steady symmetric, regular periodic, and irregular flow regimes are the norm rather than the exception in fluid mechanics (at least for systems characterised by a degree of spatial symmetry in their boundary conditions). Some justification for this conclusion has recently

emerged from studies of the general theory of non-linear dynamical systems, of which fluid flows may be but a single example.

A dynamical system may be loosely defined as one whose state is fully determined by its position in a suitably-defined phase-space, and whose evolution in time (i.e. its time derivatives) depends solely upon its current position in phase-space. Numerous other examples of dynamical systems are found outside hydrodynamics, including non-linear optics, electronics, engineering structures, chemical reactions, and even certain processes in living organisms (e.g. see Cvitanovic 1984; Pippard 1985 for reviews). Of particular interest has been the identification of a number of sequences by which systems may undergo transitions ('bifurcations') from steady to irregular behaviour via regular, periodic states, and in which irregular behaviour may involve only a relatively small number of the available degrees of freedom in a way first identified by Lorenz (1963 - 'deterministic chaos' !!!). The latter is in complete contrast to earlier classical theories of the transition to turbulence (Landau & Lifshitz 1959), in which turbulence and irregular flow was associated with the excitation of a very large number of degrees of freedom.

The possible applications of these theoretical developments to real systems continues to be an active area of research activity....(e.g. see Bell et al. 1986).

#### REFERENCES

- Andereck, C. D., Liu, S. S. & Swinney, H. L., 1986. 'Flow regimes in a circular Couette system with independently rotating cylinders', J. Fluid Mech., **164**, 155-183.
- Bell, M. J., Johnson, D. W., Read, P. L. & Small, R. M., 1986. 'Phase-space analysis of rotating, thermally-driven baroclinic flows: a feasibility study', Meteorological Office, Met. O. 21 Internal Report IR/86/4.
- Birkhoff, G., 1960. Hydrodynamics: A Study in Logic, Fact and Similitude, Princeton University Press.

- Coles, D., 1965. 'Transition in circular Couette flow', J. Fluid Mech., 21, 385-425.
- Cvitanovic, P., 1984. Universality in Chaos, Adam Hilger.
- Exner, F. M., 1923. 'Uber die Bildung von Windhosen und Zyklonen', S. B. Akad. Wiss. Wien, Abt. IIa, 132, 1-16.
- Fultz, D., 1951. 'Experimental analogies to atmospheric motions', Comp. Meteor., 1235-1248.
- Fultz, D., Long, R. R., Owens, G. V., Bowan, W., Kaylor, R. & Weil, J., 1959. 'Studies of thermal convection in a rotating cylinder with some implications for large-scale atmospheric motions', Met. Mon., 4, Boston, Amer. Met. Soc.
- Gill, A. E., 1982. Atmosphere-Ocean Dynamics, Academic Press.
- Hart, J. E., 1979. 'Finite amplitude baroclinic instability', Ann. Rev. Fluid Mech., 11, 147-172.
- Hide, R., 1958. 'An experimental study of thermal convection in rotating liquid', Phil. Trans. R. Soc. Lond., A250, 442-478.
- Hide, R., 1969. 'Some laboratory experiments on free thermal convection in a rotating fluid subject to a horizontal temperature gradient and their relation to the theory of the atmospheric general circulation', in The Global Circulation of the Atmosphere (ed. G. A. Corby), London, R. Met. Soc., 196-221.
- Hide, R., 1977. 'Experiments with rotating fluids', Quart. J. R. Met. Soc., 103, 1-28.
- Hide, R. & Mason, P. J., 1975. 'Sloping convection in a rotating fluid', Adv. Phys., 24, 47-100.

- Hoskins, B. J., 1983. 'Dynamical processes in the atmosphere and the use of models', Quart. J. R. Met. Soc., **109**, 1-21.
- James, I. N. & Gray, L. J., 1983. 'Regimes of flow in a planet's atmosphere: a numerical study', Weather, **38**, 140-149.
- Krishnamurti, R., 1973. 'Some further studies on the transition to turbulent convection', J. Fluid Mech., **60**, 285-304.
- Landau, L. D. & Lifshitz, E. M., 1959. Fluid Mechanics, Oxford, Pergamon Press.
- Leovy, C. B., 1979. 'Martian meteorology', Ann. Rev. Astron. Astrophys., **17**, 387-413.
- Lorenz, E. N., 1963. 'Deterministic non-periodic flow', J. Atmos. Sci., **20**, 130-141.
- Lorenz, E. N., The Nature and Theory of the General Circulation of the Atmosphere, W.M.O. Geneva, T.P. 115, No. 218, 161pp.
- Pedlosky, J., 1979. Geophysical Fluid Dynamics, Berlin, Springer-Verlag.
- Pippard, A. B., 1985. Response and Stability, Cambridge University Press.
- Swinney, H. L. & Gollub, J. P. (eds.), 1985. Hydrodynamic Instabilities and the Transition to Turbulence (2nd Edition), Topics in Appl. Phys., **45**, Berlin, Springer-Verlag.
- Taylor, G. I., 1923. 'Experiments on the motion of solid bodies in rotating fluids', Proc. R. Soc. Lond., **A104**, 213-218.
- Vettin, F., 1884. 'Experimentale Darstellung von Luftbewegungen unter dem Einflusse von Temperatur-Unterschieden und Rotations-Impulsen', Meteor. Z., **1**, 227-230 & 271-276.

P. L. Read  
August 1986

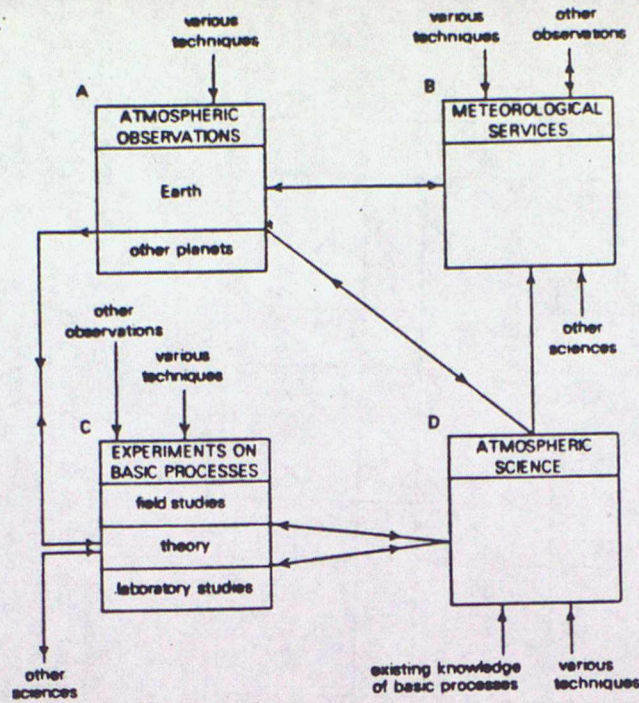
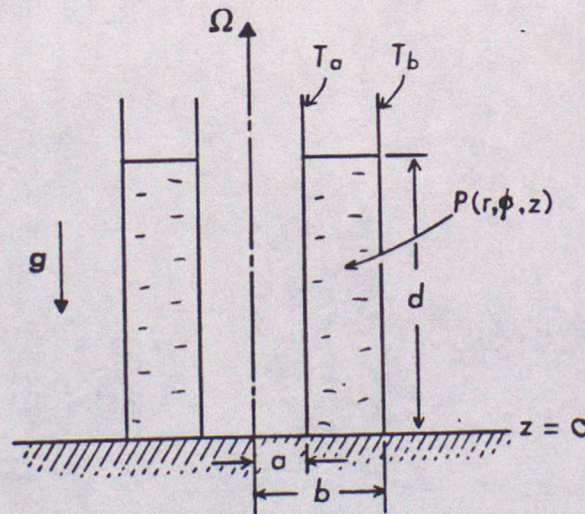


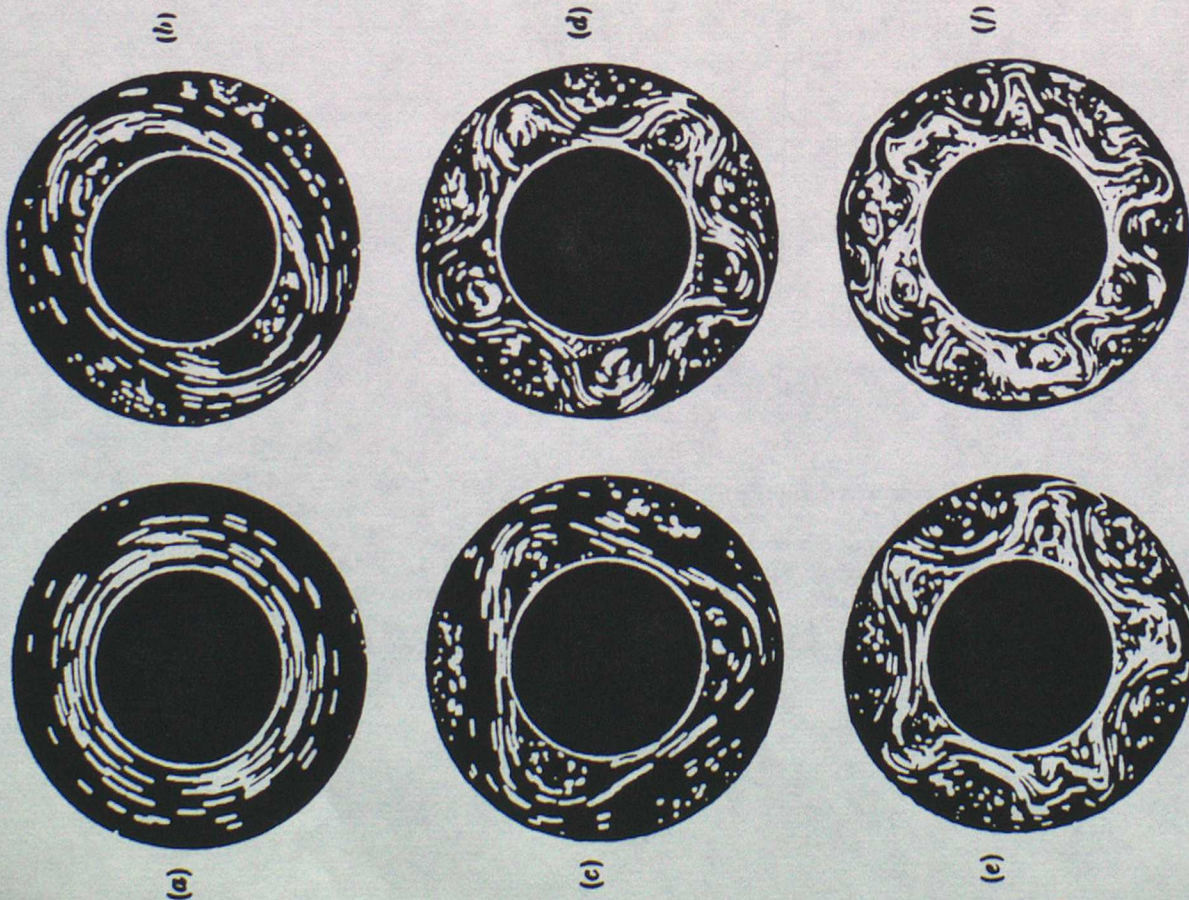
Figure 1. 'An attempt to illustrate the relationship between atmospheric science, applied meteorology and research on basic processes (see text).

Figure 2

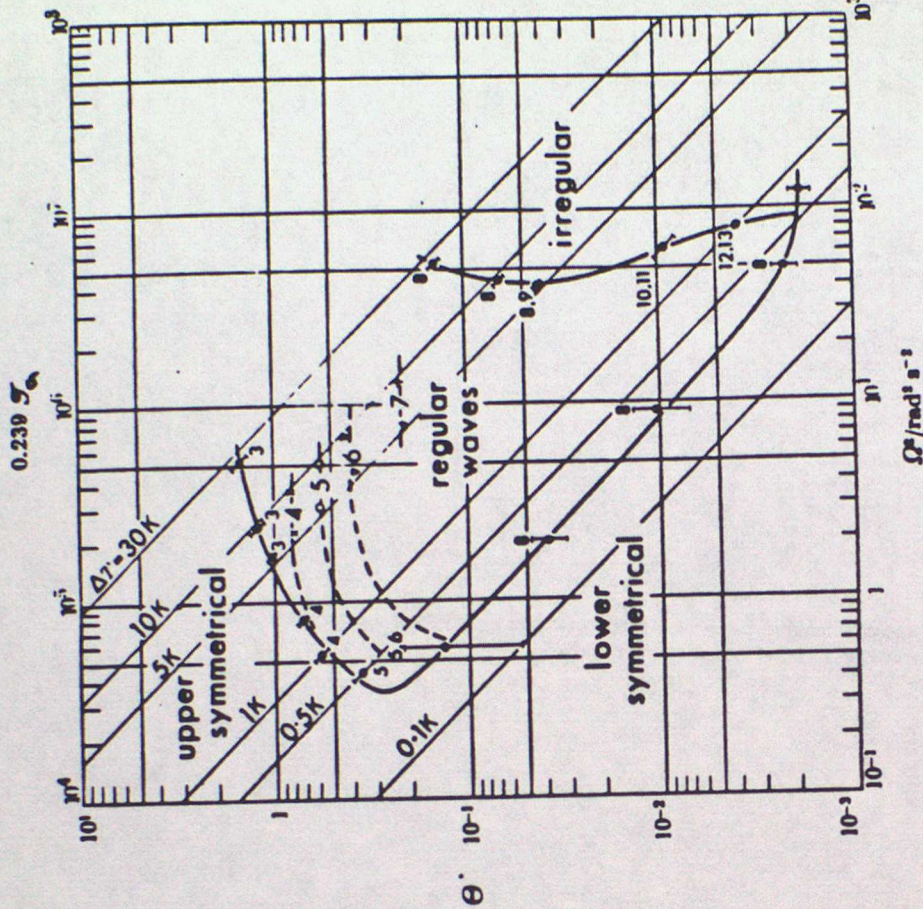


Schematic diagram of a rotating fluid annulus subject to a horizontal temperature gradient, drawn for the case when the upper and lower bounding surfaces are horizontal.  $P$  is a general point with polar coordinates  $(r, \phi, z)$  in a frame of reference rotating with the apparatus:  $\Omega = (0, 0, \Omega)$  is the angular velocity of basic rotation;  $\mathbf{g} = (0, 0, -g)$  is the acceleration of gravity; region occupied by the fluid is  $a \leq r \leq b$ ,  $0 \leq z \leq d$ ;  $T_a$  and  $T_b$  denote the respective temperatures of the cylindrical boundaries,  $r = a$  and  $r = b$ .

Figure 3



Streak photographs illustrating the dependence of the flow type on rotation rate. The values of film exposure duration,  $\Omega$ , and  $\theta$  are, respectively: (a) 1 s, 0.41 rad s<sup>-1</sup> and 7.3; (b) 1 s, 1.07 rad s<sup>-1</sup> and 1.07; (c) 1 s, 1.21 rad s<sup>-1</sup> and 0.84; (d) 2 s, 3.22 rad s<sup>-1</sup> and 0.118; (e) 2 s, 3.91 rad s<sup>-1</sup> and 0.080; (f) 3 s, 6.4 rad s<sup>-1</sup> and 0.030. Other experimental details: working fluid was a water-glycerol solution of mean density  $\bar{\rho} = 1.037$  g cm<sup>-3</sup> and kinematic viscosity  $\nu = 1.56 \times 10^{-3}$  cm<sup>2</sup> s<sup>-1</sup>;  $T_b - T_a$  was maintained steady to better than 0.5 parts per cent at values close to 9 K;  $b - a = 4.64$  cm,  $d = 13.6$  cm; the streak photographs show the flow at a depth of 0.5 cm below the free upper surface.



(9)

Typical régime diagram illustrating the dependence of the mode of convection on the two principal dimensionless parameters required to specify the system, namely  $\Theta = g d [\rho(T_a) - \rho(T_b)] / \{ \rho(T_a + T_b) \} \Omega^2 (b - a)^2$  and  $\mathcal{F} = 4 \Omega^2 (b - a)^2 / \nu^2 d$  (where  $\rho$  denotes density and  $\nu$  the mean coefficient of kinematic viscosity). (Experimental details:  $a = 3.48$  cm,  $b = 6.02$  cm,  $d = 10.0$  cm;  $T = \frac{1}{2}(T_a + T_b) = 20.0^\circ\text{C}$ ; working fluid was water; kinematic viscosity  $\nu = 1.01 \times 10^{-3}$  cm<sup>2</sup> s<sup>-1</sup>; mean density  $\bar{\rho} = \frac{1}{2}[\rho(T_a) + \rho(T_b)] = 0.998$  gm cm<sup>-3</sup>; and  $\nu/\bar{\rho} = 7.19$  ( $\bar{\alpha}$  being the mean coefficient of thermometric conductivity). Over 15 independent dimensionless parameters are required to specify the system completely, and these results can only be applied to much shallower systems or to much larger systems through a correct interpretation of the physical processes involved. Thus, a comparison of the experimental results with baroclinic instability theory shows that the ordinate should be regarded as a measure of the vertical density gradient multiplied by  $g d^2 / \rho \Omega^2 (b - a)^2$  and the abscissa as an (inverse) measure of the ratio of viscous to Coriolis forces multiplied by a factor which depends on the aspect ratio  $d/(b - a)$  and the mean slope of the isotherms in the main body of the fluid.

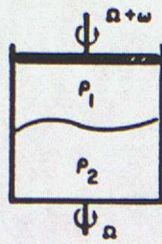


Figure 4(a)  
Schematic diagram of the two-layer baroclinic system (shown for an open cylinder)  $\Delta\rho = \rho_2 - \rho_1$ .

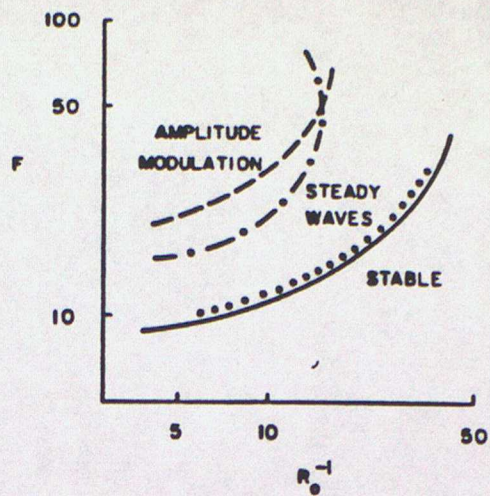


Figure 4b Regime diagram for corotating two-layer flow: — observed neutral curve; ..... predicted neutral curve; - - - transition to amplitude vacillation; - · - · - prediction from spectral model.

Figure 5  
Regime diagram for low aspect-ratio Rayleigh-Bénard convection as a function of Rayleigh and Prandtl number (from Krishnamurti 1973).

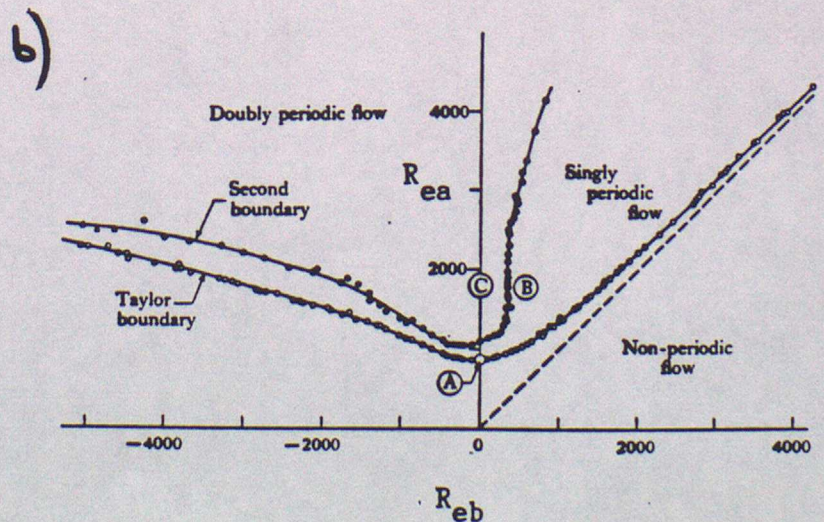
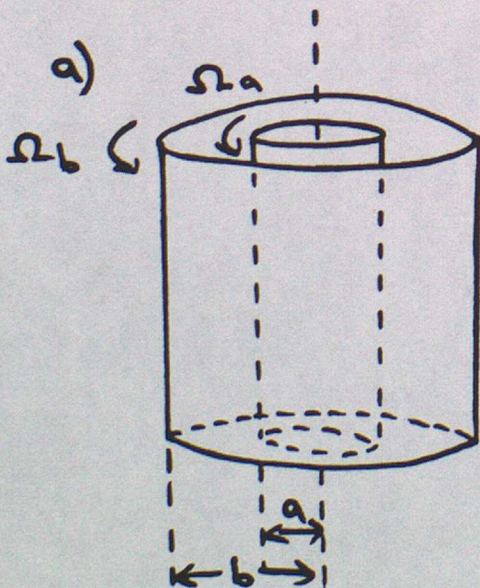
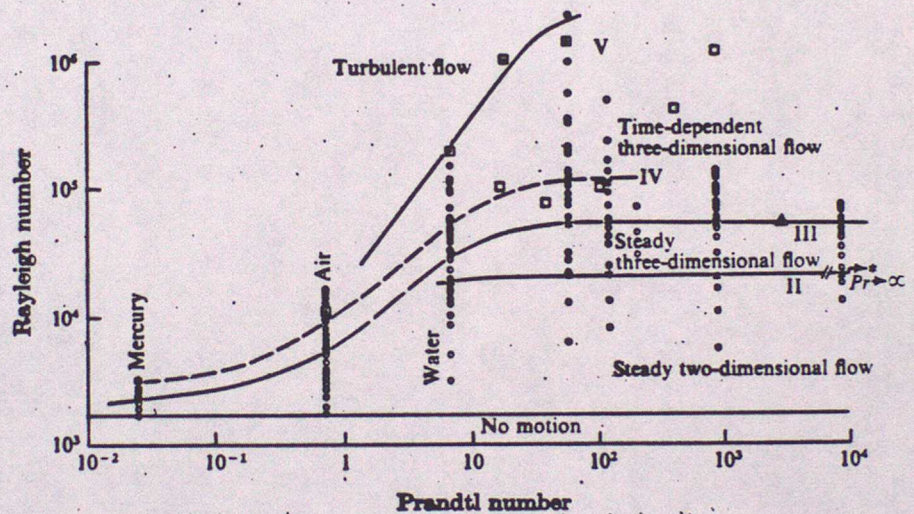


Fig. 6: a) Schematic diagram of the Taylor-Couette system, and b) regime diagram as a function of  $Re_a$  and  $Re_b$  near the onset of Taylor vortices.

Lecture 3 : Linear instability theory

The quasi-geostrophic (QG) model

The QG model was introduced in lecture 1 and will be extensively used in this lecture and the next one. Detailed accounts are given in the text-books by Pedlosky (1979) and Gill (1982). Here we give only a brief outline - assuming an incompressible fluid model,  $\beta$ - plane dynamics and inviscid adiabatic motion (and using height coordinates).

The central quantity is the streamfunction  $\psi$  of the geostrophic wind:  $\underline{v}_g = \frac{1}{f_0 f_0} \underline{k} \times \nabla p' = \underline{k} \times \nabla \psi$  - so  $\psi = p' / \rho_0 f_0$ . (Here, and from now on,  $\nabla$  is the horizontal gradient operator  $(\partial/\partial x, \partial/\partial y)$ .) Primes indicate deviations from horizontal averages; e.g.,  $p' = p - \bar{p}^x$ .) The equation governing the time evolution of  $\psi$  is

$$\left( \frac{\partial}{\partial t} + \underline{v}_g \cdot \nabla \right) \varphi = 0 \quad (1)$$

(assuming adiabatic, inviscid flow). Here  $N = \left( -\frac{g}{\rho_0} \frac{d\rho_0}{dz} \right)^{1/2}$  is the buoyancy frequency and the quantity

$$\varphi \equiv \nabla^2 \psi + f_0^2 \frac{\partial}{\partial z} \left\{ \frac{1}{N^2} \frac{\partial \psi}{\partial z} \right\} + \beta y \quad (2)$$

is known as the quasi-geostrophic potential vorticity. Horizontal boundary conditions are specified via the thermodynamic equation, whose appropriate adiabatic form (see text-books) is

$$\left( \frac{\partial}{\partial t} + \underline{v}_g \cdot \nabla \right) \frac{\partial \psi}{\partial z} + \frac{N^2}{f_0} \psi = 0 \quad (3)$$

Thus, if there are rigid horizontal boundaries at  $z = \pm H/2$  (say) we have simply

$$\left( \frac{\partial}{\partial t} + \underline{v}_g \cdot \nabla \right) \frac{\partial \psi}{\partial z} = 0 \quad \text{at } z = \pm H/2 \quad (4)$$

Given suitable side boundary conditions (such as  $\psi = 0$  on  $y = 0, L$  and cyclic continuity in  $x$ ) and initial conditions, the time evolution of  $\psi$

is thus fully determined. All other quantities are deducible from  $\psi$ :

$$\underline{v}_g = \underline{k} \times \nabla \psi \quad (5) \quad p' = \rho_0 f_0 \psi \quad (6) \quad \rho' = \frac{\rho_0 f_0}{g} \frac{\partial \psi}{\partial z} \quad (7)$$

$$\frac{N^2}{f_0^2} \nabla^2 w + \frac{\partial^2 w}{\partial z^2} = \frac{1}{f_0} \frac{\partial}{\partial z} \left\{ \underline{v}_g \cdot \nabla (\nabla^2 \psi + f) \right\} - \nabla^2 \left\{ \underline{v}_g \cdot \nabla \left( \frac{\partial \psi}{\partial z} \right) \right\} \quad (8)$$

$$\nabla^2 \chi + \frac{\partial w}{\partial z} = 0 \quad (9)$$

Here  $\chi$  is the velocity potential of the irrotational ageostrophic wind  $\underline{v}_a (\equiv \underline{v} - \underline{v}_g = \nabla \chi)$ . (Strictly  $\underline{v}_a$  has a small rotational part - but it is dynamically unimportant.)

### Stability of zonal flows

The QG model is a convenient one for studying the stability of steady zonal flows to large-scale perturbations. Suppose that the zonal flow is  $\bar{u} = \bar{u}(y, z)$ . Perturbations  $\psi$  about this state must obey the linearized form of (1) (and associated boundary conditions):

$$\left( \frac{\partial}{\partial t} + \bar{u} \frac{\partial}{\partial x} \right) \psi' + \frac{\partial \psi'}{\partial x} \frac{\partial \bar{q}}{\partial y} = 0 \quad (10)$$

$$\text{subject to } \left( \frac{\partial}{\partial t} + \bar{u} \frac{\partial}{\partial x} \right) \frac{\partial \psi'}{\partial z} - \frac{\partial \bar{u}}{\partial z} \frac{\partial \psi'}{\partial x} = 0 \quad (11)$$

at rigid horizontal boundaries, and

$$\left. \begin{aligned} \psi' &= 0 \quad \text{at } y = 0, L \\ \psi(x+L_x) &= \psi(x) \end{aligned} \right\} \quad (12)$$

In (10)

$$\psi' \equiv \nabla^2 \psi' + f_0^2 \frac{\partial}{\partial z} \left( \frac{1}{N^2} \frac{\partial \psi'}{\partial z} \right)$$

and

$$\frac{\partial \bar{q}}{\partial y} \equiv \beta - \frac{\partial^2 \bar{u}}{\partial y^2} - f_0^2 \frac{\partial}{\partial z} \left( \frac{1}{N^2} \frac{\partial \bar{u}}{\partial z} \right) \quad (13)$$

(the "potential vorticity gradient").

The general stability problem (which encompasses barotropic, baroclinic and mixed cases) is complicated. However, conditions for stability may be

derived (Blumen (1968, 1978), White (1982)) :

$$\left. \begin{array}{l} \text{If } (\bar{u} - u_0) / \partial \bar{q} / \partial y \leq 0 \text{ everywhere} \\ \text{and } (\bar{u} - u_0) / \partial \bar{u} / \partial z \leq 0 \text{ on } z = +H/2 \\ (\bar{u} - u_0) / \partial \bar{u} / \partial z \geq 0 \text{ on } z = -H/2 \end{array} \right\} \quad (14)$$

for some choice of the constant  $u_0$ , then the flow is stable to all perturbations. (Equivalent conditions for wave-mode perturbations are given by Pedlosky (1964)). Note that a zonal flow may possess horizontal temperature gradients (and hence "available potential energy") and yet be stable. However, many flows which are of interest are unstable; temperature gradients at the horizontal boundaries are instrumental in allowing instability in many cases.

#### The Eady Problem (Eady (1949))

Consider the simple case in which (i)  $\bar{u} = \Delta u z / H$  (ii)  $\beta = 0$  (iii)  $N = \text{constant}$ . The stability problem is now analytically tractable. Wave-modes having

$$\psi' = \text{Re} \{ F(z) \sin ly e^{ik(x-ct)} \}$$

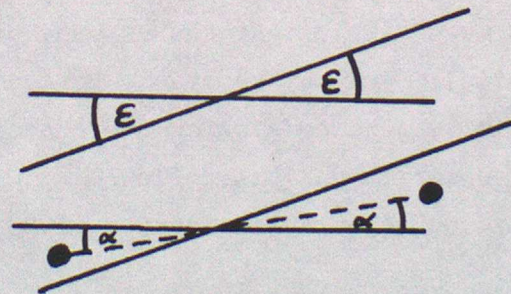
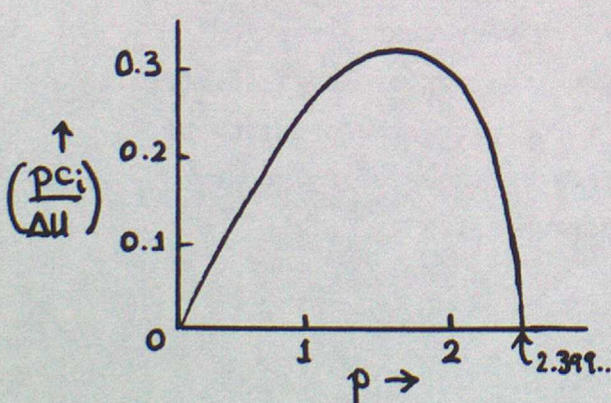
obey

$$\left( \frac{pc_i}{\Delta u} \right)^2 = - \left( \frac{p}{2} - \tanh \frac{p}{2} \right) \left( \frac{p}{2} - \coth \frac{p}{2} \right) \quad (15)$$

Here

$$p = \frac{NH}{f_0} (k^2 + l^2)^{1/2}$$

is a non-dimensional horizontal wavenumber. For  $p \lesssim 2.4$  unstable waves exist - see diagram.



The flow  $\bar{u} = \Delta u z$  has sloping isotherms (and hence sloping isopycnals). Potential energy is released if fluid elements are interchanged at an angle  $\alpha$  to the horizontal which is less than the slope  $\epsilon$  of the mean

isotherms. It is readily shown that the energy release is a maximum if  $\alpha = \frac{1}{2} \epsilon$  (Green 1960). Away from the horizontal boundaries this is achieved in the fastest-growing waves.

Energy arguments provide a useful rationalization of the instability which is found in the Eady problem. But vorticity constraints are at least as important - as the stability conditions (14) show.

Some extensions of the Eady problem can be done analytically. Examples are :

(i) Lower and/or upper boundaries remain axisymmetric but slope meridionally. Opposite boundary slopes can simulate (crudely) a positive or negative  $\beta$ - effect - in that meridional motion is accompanied by vortex stretching or compression (at least as regards the height-average flow). Similar boundary slopes can drastically affect the energy releasing mechanism by dictating trajectory slopes throughout the fluid.

(ii) Ekman layers are present on the upper and/or lower boundaries. In such cases  $z = \pm H/2$  are imagined to be the extremities of the Ekman layers, and  $\omega = \mp \left(\frac{\nu}{2f_0}\right)^{1/2} \nabla^2 \psi$  ( $\nu$  = kinematic viscosity) are applied there.

(iii) Combinations of (i) and (ii).

See Hide and Mason (1975) and Mason (1975) for details.

If  $\beta \neq 0$  the stability problem becomes analytically demanding, but it is understood as a result of the studies by Charney (1947), Green (1960), Garcia and Norscini (1970) and others. Use of a 2-layer or 2-level model makes the problem much simpler (at the expense of assuming a very coarse vertical resolution); see any reputable textbook on dynamical meteorology. Except in a few limiting cases - which are conceptually important - the presence of lateral shear in the basic flow  $\bar{u}$  makes numerical methods of solution essential. See Held and Andrews (1983) for references.

#### Interpretation of results

Zonal flow stability analyses based on QG dynamics leave little doubt that baroclinic instability is an important process in the Earth's atmosphere. Stability analyses based on the SG model (see Hoskins 1976) and on the

hydrostatic primitive equations (see Simmons and Hoskins 1976) support this conclusion - as do numerical integrations into the nonlinear regime (Simmons and Hoskins 1978). However, it must be borne in mind that all these analyses are initial value calculations in which a fairly simple zonal flow is posed and then found to be unstable. One may reasonably ask how such a flow might occur in reality - given that instabilities may be expected to break out as they become dynamically viable, and not to be restrained until the theoretician, in god-like mood, chooses to shout 't=0'. Until recently, theory has paid little attention to stable (or weakly unstable flows) as models of the zonal mean atmosphere. However, there is growing evidence that the atmosphere, in its day-to-day evolution and on the large scale, is often only marginally unstable (see Stone (1978) and Held (1978)). Steady waves in the annulus offer further evidence of this possibility. Another important element has been the recognition of steady, finite-amplitude solutions of the QG equations - the subject of the next lecture.

#### References

- Blumen, W.                    1968 J.Atmos.Sci., 25, 929-931  
                                   1978 Ibid., 35, 1314-1318
- Charney, J. G.                1947 J. Met., 4, 135-163
- Eady, E. T.                    1949 Tellus, 1, 33-52
- Garcia, R. V.                 1970 Ibid., 22, 239-250
- and Norscini, R.
- Gill, A. E.                    1982 Atmosphere-Ocean Dynamics, Academic Press
- Green, J. S. A.                1960 Quart.J.R.Met.Soc., 86, 237-251
- Held, I. M.                    1978 J.Atmos.Sci., 35, 572-576  
                                   1983 Ibid., 40, 2220-2231
- and Andrews, D. G.
- Hoskins, B. J.                1976 Quart.J.R.Met.Soc., 102, 103-122
- Pedlosky, J.                  1964 J.Atmos.Sci., 21, 201-219  
                                   1979 Geophysical Fluid Dynamics, Springer-Verlag
- Simmons, A. J.                1976 J.Atmos.Sci., 33, 1454-1477
- and Hoskins, B. J.  
                                   1978 Ibid., 35, 414-432
- Stone, P. H.                  1978 Ibid., 35, 561-571
- White, A. A.                 1982 Ibid., 39, 2107-2118

Lecture 4 : Free Modes

Linear instability theory offers an explanation for the occurrence of non-axisymmetric motion in the atmosphere, but it has also promoted the notion that the atmosphere is a turbulent fluid (on large horizontal scales). In turbulence, energy and other quantities are passed between different scales of motion by the advection process (which is of course mathematically nonlinear in an Eulerian description). Such processes are undoubtedly important in the atmosphere, yet other possibilities exist : even large amplitude disturbances may not involve cascades of energy. In this lecture we consider analytical models of such free modes.

Steady solutions of the QG system

The QG potential vorticity equation may be written in the form

$$\frac{\partial Q}{\partial t} + J(\psi, Q) = 0 \tag{1}$$

in which  $J(\psi, Q) = \frac{\partial \psi}{\partial x} \frac{\partial Q}{\partial y} - \frac{\partial \psi}{\partial y} \frac{\partial Q}{\partial x}$

(the Jacobian of  $\psi$  and  $Q$  w.r.t.  $x$  and  $y$ ). Note that (1) is the full nonlinear QG form.

Suppose that

$$\frac{\partial}{\partial t} = -c \frac{\partial}{\partial x}$$

where  $c$  is a real constant. Then (1) can be written as

$$J(\psi + cy, Q) = 0 \tag{2}$$

which has solutions of the form

$$Q = F(\psi + cy) \tag{3}$$

where  $F$  is any well-behaved function. According to (3), contours of  $Q$  must be parallel to contours of  $\psi + cy$  ; or, in other words, a coordinate frame must exist in which the  $Q$  and  $\psi$  contours are parallel. Most attention has been paid to cases in which  $F$  is a linear function.

1. Domain-filling solutions

If  $F(x) = -\alpha^2 x$ , then (3) becomes

$$\nabla^2 \psi + \beta y + \frac{f_0^2}{N^2} \frac{\partial^2 \psi}{\partial z^2} = -\alpha^2 \psi - \alpha^2 c y \quad (4)$$

Separating the zonal mean ( $\bar{\quad}$ ) and deviation ( $\prime$ ) parts we find

$$\nabla^2 \psi' + \frac{f_0^2}{N^2} \frac{\partial^2 \psi'}{\partial z^2} = -\alpha^2 \psi' \quad (5)$$

$$-\frac{\partial^2 \bar{u}}{\partial y^2} - \frac{f_0^2}{N^2} \frac{\partial^2 \bar{u}}{\partial z^2} + \beta = -\alpha^2 \bar{u} - \alpha^2 c \quad (6)$$

Solutions exist in the following forms:

(i) barotropic Rossby waves

$$\bar{u} = u_0, \quad \psi = A \frac{\sin kx'}{\cos kx'} \frac{\sin ly}{\cos ly}, \quad c = u_0 - \frac{\beta}{(k^2 + l^2)}$$

(ii) baroclinic Rossby waves

$$\bar{u} = u_0, \quad \psi = A \frac{\sin kx'}{\cos kx'} \frac{\sin ly}{\cos ly} \frac{\sin mz}{\cos mz}, \quad c = u_0 - \frac{\beta}{(k^2 + l^2 + \frac{f_0^2}{N^2} m^2)}$$

(iii) any combination of barotropic and baroclinic Rossby waves and sinusoidal zonal flows having the same total wavenumber:

$$\left. \begin{aligned} \bar{u} &= u_0 + \sum u_{pqr} \frac{\sin py}{\cos py} \frac{\sin qz}{\cos qz} \\ \psi' &= \sum A_{klm} \frac{\sin kx'}{\cos kx'} \frac{\sin ly}{\cos ly} \frac{\sin mz}{\cos mz} \end{aligned} \right\} c = u_0 - \beta/\alpha^2$$

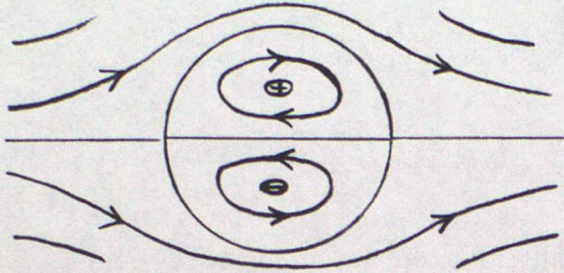
where 
$$p^2 + \frac{q^2 f_0^2}{N^2} = k^2 + l^2 + \frac{m^2 f_0^2}{N^2} = \alpha^2$$

for all components included in the sums.  $[x' = (x - ct)]$

The possibilities in (iii) may be restricted by the boundary conditions, but fairly complicated solutions are obtainable in many cases of interest. See Kuo (1959). Read (1985) and White (1986) have used solutions of this type to model regular waves in the laboratory annulus and to illustrate certain aspects of wave-mean flow non-interaction. Mitchell and Derome (1983) have examined their relevance to the blocking phenomenon in the atmosphere.

## 2. Isolated solutions

Finite amplitude solutions of the form (3) which are spatially isolated can also be found. It is required that  $F$  take on different forms in an interior and exterior region (with matching conditions applied at the boundary). The diagram shows the streamfunction in a solution of this type which has become known as a 'modon'. Most have



been obtained in barotropic or 2-level models. See Stern (1975), Flierl et al (1980) and Tribbia (1985). The character of modons is that the solution is spatially oscillatory in the interior

domain and spatially decaying in the exterior. The conditions applied at the boundary are continuity of streamfunction ( $\equiv$  pressure), tangential velocity and vorticity. The resemblance of modons to the dipole structures seen in blocking pressure fields has prompted much interest.

Modons are not solitons in the true sense (they do not emerge unscathed from collisions). Solitons may be obtained as solutions of the QG model in certain asymptotic limits. See Malanotte-Rizzoli (1982) for a review.

### Approach to free mode form in real geophysical flows

The existence of many finite amplitude solutions of the QG model suggests that steady flow structures might be important in the real atmosphere. Of course, the finite amplitude solutions might be unstable (and in some cases this has been proved) but numerical integrations with the QG equations suggest effective stability in many cases. To investigate approach to free mode form in real fluids we need to evaluate  $Q$  and  $\psi$  at each data or grid point and plot them against one another. If  $Q \approx Q(\psi)$  then the points should collapse on to a line (or curve); in general terms, the spread of points about some mean curve is a measure of departure from free-mode form. For QG numerical models this is an easy enough procedure, but to process real data in the required way is more difficult because of the approximations inherent in the QG model. D.G. Andrews has shown that this difficulty may be

overcome by noting that free mode behaviour may occur in flow governed by the hydrostatic primitive equations. We revert to the forms used in lecture 1 for a perfect gas. In adiabatic, inviscid flow

$$\frac{\partial \underline{v}}{\partial t} + (\underline{v} \cdot \nabla_{\theta}) \underline{v} + f \underline{k} \times \underline{v} + \nabla_{\theta} M = 0 \quad (7)$$

$$\frac{\partial}{\partial t} \left( \frac{\partial p}{\partial \theta} \right) + \nabla_{\theta} \cdot \left( \underline{v} \frac{\partial p}{\partial \theta} \right) = 0 \quad (8)$$

$$\frac{\partial M}{\partial \theta} = \frac{T c_p}{\theta} = c_p \left( \frac{p}{p_0} \right)^{R/c_p} \quad (9)$$

are the  $\theta$ -coordinate forms of the horizontal momentum, continuity and hydrostatic equations.  $M$  (the Montgomery potential) =  $gz + c_p T$ . The (Ertel) potential vorticity in this system is

$$q_E = (f + \zeta_{\theta}) \frac{\partial \theta}{\partial p} ; \zeta_{\theta} = \left( \frac{\partial v}{\partial x} - \frac{\partial u}{\partial y} \right)_{\theta} \quad (10)$$

which is a very simple form (see Hoskins et al (1985)).

Hence

$$\left( \frac{\partial}{\partial t} + \underline{v} \cdot \nabla_{\theta} \right) q_E = 0 \quad (11)$$

represents conservation of  $q_E$ . An advantage of  $\theta$ -coordinates is that there is no vertical motion ( $\dot{\theta} = 0$ ) unless diabatic heating is present. This makes it easy to isolate effects which result from the adiabatic dynamics and effects which do not. Suppose that a free-mode state exists, and that we adopt a coordinate frame in which  $\partial/\partial t = 0$ . Then (8) becomes

$$\nabla_{\theta} \cdot \left( \underline{v} \frac{\partial p}{\partial \theta} \right) = 0 \quad (12)$$

and so  $\underline{v} \frac{\partial p}{\partial \theta} = \underline{k} \times \nabla_{\theta} \chi$ ,

where  $\chi$  is a streamfunction for  $\underline{v} \frac{\partial p}{\partial \theta}$  on isentropic surfaces.

From (11)

$$\frac{\partial p}{\partial \theta} (\underline{v} \cdot \nabla_{\theta}) q_E = 0 \Rightarrow J(\chi, q_E) = 0 \Rightarrow q_E = F(\chi, \theta)$$

Also, from (7)

$$\frac{\partial p}{\partial \theta} (\underline{v} \cdot \nabla_{\theta}) \left\{ \frac{1}{2} \underline{v}^2 + gz + c_p T \right\} = 0 \Rightarrow \frac{1}{2} \underline{v}^2 + gz + c_p T = G(\chi, \theta)$$

These results can be used to set up an analytical free-mode problem, but it turns out to be intractable (in general). However, the results suggest a method of data analysis by which the approach to free mode form may be assessed - we simply plot  $q_E$  (or  $E$ ) against  $\chi$ .

### Almost free modes

In practice, of course, no real geophysical flow is inviscid and adiabatic. The theory must be extended to include (at least) weak forcing. For the QG case this is straightforward. Suppose that

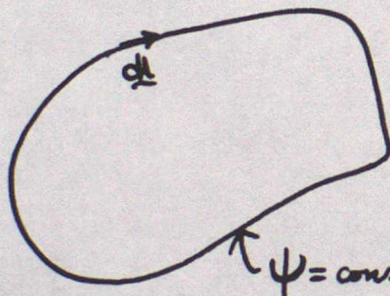
$$q = q_0(\psi) + q_1,$$

where  $|q_1| \ll q_0$ ,

and that the steady state potential vorticity equation is

$$(\underline{v}_g \cdot \nabla) q = F_q + \nabla \cdot (D \nabla q)$$

where  $F_q$  represents some forcing agency and  $D$  is a diffusion coefficient. By integrating over a closed  $\psi$  contour, it is readily shown that



$$\frac{dq_0}{d\psi} = \frac{- \iint F_q dx dy}{\oint D \underline{v}_g \cdot d\underline{l}}$$

Thus the forcing and the diffusion constrain the relation between  $q_0$  and  $\psi$ .

The treatment has been extended to forced cases - with the bonus that some of the uncertainty about the  $q(\psi)$  relation is removed. See Rhines and Young (1982), Pierrehumbert and Malguzzi (1984), Marshall and Nurser (1986), Read et al (1986).

### References

- Flierl, G.R., 1980 Dyn.Atmos.Oceans, 5, 1-41  
 Larichev, V.D.,  
 McWilliams, J.C.  
 and Reznik, G.M.  
 Hoskins, B.J., 1985 Quart.J.R.Met.Soc., 111, 877-946  
 McIntyre, M.E.  
 and Robertson, A.W.

- Kuo, H.L. 1959 J.Met., 16, 524-534
- Malanotte-Rizzoli, P. 1982 Advances in Geophysics, 24, 147-224
- Marshall, J.C. 1986 J.Phys.Oceanog., to appear
- and Nurser, G.
- Mitchell, H.L. 1983 J.Atmos.Sci., 40, 2522-2536
- and Derome, J.
- Read, P.L. 1985 Dyn.Atmos.Oceans, 9, 135-207
- 1986 J.Atmos.Sci., to appear
- Rhines, P.B.
- and White, A.A.
- Rhines, P.B. 1982 J.Fluid Mech., 122, 347-367
- and Young, W.
- Stern, M.E. 1975 J.Mar.Res., 33, 1-13
- Tribbia, J.J. 1984 Geophys.Astrophys.Fluid Dynamics, 30, 131-168
- White, A.A. 1986 Quart.J.R.Met.Soc., 112, 749-773

LECTURE 5Laboratory studies of the effect of topography on fluid motions5.1 Introduction

It is widely recognized that the underlying topography of the earth's atmosphere influences it over a large range of length scales; from the smallest scales where topography can produce local winds in the boundary layer, to lee (gravity) waves downstream from the topography, to mesoscale phenomena such as lee cyclogenesis, right up to stationary planetary scale waves which are regularly observed in climatological mean fields. One approach to gain insight into the nature of these phenomena is to use laboratory experiments to systematically study, in a controlled manner, the effect of topography over a large range of parameter space. The laboratory studies divide naturally into three sections:

- a) non-rotating stratified flow,
- b) rotating homogeneous flow and
- c) rotating stratified flow.

5.2 Non-rotating stratified flow

## 1) Layered flows.

The non-rotating experiments carried out, model atmospheric phenomena with short length and time scales where the earth's rotation is not important for the dynamics. They are considered relevant if viscous effects are small i.e. the Reynolds number  $R_m > 100$ . The Reynolds number is defined as

$$R_m = \frac{Ul}{\gamma} = \frac{\text{Inertia force}}{\text{Viscous force}}$$

where  $U$  = characteristic velocity

$l$  = characteristic length scale

$\gamma$  = kinematic viscosity

The experiments are generally performed by towing a smooth obstacle along the bottom of a long, horizontal tank and the fluid is stratified by using individual layers of constant density separated by abrupt changes in density. Single layer flows have been studied extensively (Long 1954, 1970, 1972), mainly with regard to engineering hydraulics. These experiments are applicable to atmospheric flows when the hydrostatic approximation is satisfied. This requires that the depth of the layer is small compared to the horizontal length scales. Two non-dimensional parameters characterize the resulting flow:

$$\text{Froude number } F_o = \frac{U}{(gd)^{1/2}} = \frac{\text{Inertia force}}{\text{Gravity force}}$$

and  $H = \frac{h}{d}$

where  $g$  = acceleration due to gravity  
 $h$  = height of obstacle  
 $d$  = undisturbed depth of layer

The general properties of single layer hydrostatic flow over an obstacle appear to be understood, with theoretical models (Houghton and Kasahara 1968) being consistent with the observations. Figure 5.1 summarizes the flow regimes obtained. To the left of the curve FAB the flow is either supercritical ( $F_o > 1$ ) or subcritical ( $F_o < 1$ ) and the flow over the obstacle is given by the Bernoulli equation (Tritton 1977). Between EAB and BC a hydraulic jump propagates upstream and in this region below AD a hydraulic jump is attached to the lee of the obstacle (above AD this is only a transient feature). To the right of the curve BC the obstacle height is sufficient to completely block the flow.

Experiments with two-layer flows, where the density jump at the upper interface (air/water) is much greater than at the lower one, have been carried out by Long (1974) and Smith (1976). Similar phenomena are observed in the lower layer for appropriate parameter values as in the single layer experiments. In addition though a hydraulic drop is at seen at the lower interface either when the obstacle height is greater than the initial depth of the lower layer, or when the lower layer is deeper than the upper one.

ii) Continuously stratified flows.

In a stably stratified fluid the tendency for a vertically displaced fluid particle to return to its original level means that waves can be generated. The lee wave phenomena which is schematically shown in figure 5.2 is one example of this. The important non-dimensional parameters are

$N^2 = -g \frac{d\rho_0}{\rho_0 dz}$  where  $N$  is the Brunt-Vaisala frequency (the frequency a vertically displaced particle oscillates about its original position in a stably stratified fluid)

$$K = \frac{Nd}{\pi U} \quad \epsilon = \frac{\pi h}{d} \quad F = \frac{U}{Nh} \quad \text{i.e. } \epsilon KF = 1$$

The first experiments with continuously stratified flows over obstacles were carried out by Long (1955) using a smooth flat obstacle of circular-arc shape. He observed the lee waves found in the parameter range  $0.7 < K < 4.6$ ,  $0.17 < \epsilon < 0.63$  and the results compared favourably with theory. However as the value of  $K$  was increased, alternating horizontal jets became apparent in the vertical just upstream from the obstacle which do not appear in the theoretical solutions. These jets were related to some degree of blocking below the level of the top of the obstacle.

### 5.3 Rotating homogeneous flow.

In rotating systems the coriolis force is of paramount importance and the most appropriate non-dimensional parameters for describing the flow are the Rossby number and Ekman number defined as:

$$\text{Rossby number } R_o = \frac{U}{2\Omega L} = \frac{\text{inertia force}}{\text{coriolis force}}$$

$$\text{Ekman number } E = \frac{\nu}{2\Omega L^2} = \frac{\text{viscous force}}{\text{coriolis force}}$$

where  $\Omega$  = rotation rate (N.B.  $R_o = R_o/E$ )

In a rapidly rotating system, an obstacle may influence the flow throughout the full depth of the fluid to a much greater extent than in a non-rotating system. This is illustrated by the Taylor-Proudman theorem which states that as  $R_o \rightarrow 0$  and  $E \rightarrow 0$  a steady homogeneous flow satisfies

$$(\Omega \cdot \nabla) \mathbf{u} = 0$$

(N.B. This is obtained by taking the curl of the geostrophic equation of motion and using the continuity equation.)

Thus, for convenience, if  $\Omega$  is in the z direction

$$\Omega \frac{\partial u}{\partial z} = 0 \quad \text{or} \quad \frac{\partial u}{\partial z} = \frac{\partial v}{\partial z} = \frac{\partial w}{\partial z} = 0$$

which states that none of the components of the fluid velocity vary in the direction of the rotation vector. This implies that in a system with a solid boundary perpendicular to the rotation axis i.e.  $w = 0$  on the boundary, then

$$\frac{\partial u}{\partial z} = \frac{\partial v}{\partial z} = 0, \quad w = 0 \quad \text{everywhere}$$

Therefore the flow is entirely two dimensional in planes perpendicular to the axis of rotation. This has striking consequences when an obstacle is placed in the flow. The fluid is deflected past the obstacle and as the flow must be two-dimensional, this deflection also occurs above and below it, leaving a stagnant column of fluid, known as a transverse 'Taylor column', parallel to the rotation axis.

The pioneering experiments of G.I. Taylor (1923) verified the existence of these columns which showed that dye deposited in the region above a sphere placed in a rotating flow remained almost stationary and was not swept away by the flow in which the sphere sat. The interior region of the 'Taylor column' has been the subject of many experimental (a typical experimental set up is shown in figure 5.3) and theoretical studies since then (Long 1952, Ibbetson 1964, Hide and Ibbetson 1966, Hide et al 1968, Davies 1972, Maxworthy 1977, Vaziri and Boyer 1977, Mason and Sykes 1979). It is found in practice that because of viscous and ageostrophic effects the 'Taylor column' can have a complex 3 dimensional structure and the exchange of fluid between the interior and exterior takes place via shear layers. For an isolated obstacle the streamlines in the interior can be interpreted in terms of potential vorticity arguments (Hide 1961, Greenspan 1968) and for

inviscid steady motion the obstacle height must exceed a critical value in order that stagnant fluid appears above the topographic feature i.e.

$$\frac{h}{dR_0} > 1$$

The above description of a 'Taylor column' flow is strictly valid only in the double limit  $(R_0, E) \rightarrow 0$  and so caution must be exercised when applying these ideas to real fluids. As inertial effects become important (i.e. as  $R_0$  increases) it is observed that the 'Taylor columns' slope at an angle  $\psi$  relative to the rotation axis (see figure 5.4), where  $\psi$  is given by

$$\tan \psi = CR_0 \quad \text{where } C = \text{a constant}$$

In a strict sense the Taylor-Proudman theorem is violated either when  $\partial u / \partial z$  (or  $\partial v / \partial z$ )  $\neq 0$  which would cause twisting or tilting of vortex lines (compare with  $\frac{\partial w}{\partial x} \frac{\partial v}{\partial z} - \frac{\partial w}{\partial y} \frac{\partial u}{\partial z}$  term in the vorticity equation, see lecture 1) or when  $\partial w / \partial z \neq 0$  which would cause stretching of vortex lines ( $(\zeta + f) \partial w / \partial z$  term in the vorticity equation, where  $\zeta$  = relative vorticity and  $f = 2\Omega$ ). The latter would occur if an inviscid, homogeneous fluid was forced to flow over a two dimensional obstacle (as shown in figure 5.5) where there can be no flow around it. The deflection of a streamline passing over the ridge can be calculated from the potential vorticity equation ( $\frac{\zeta + f}{\Delta z} = \text{constant}$ ). As the column of fluid rises over the topography it is compressed and the relative vorticity decreases ( $\partial w / \partial z < 0$ ). On moving over the obstacle the column is restored to its original length thus returning to its original relative vorticity (Holton 1972).

#### 5.4 Rotating stratified flow.

When both rotation and stratification are present their relative importance is indicated by the parameter

$$S = \frac{N}{2\Omega} \quad \text{or the Burger number } B = \frac{N^2 d^2}{f^2 L^2}$$

When  $S$  is small, one is dealing essentially with a rotating flow modified by stratification and 'Taylor columns' would be expected to be observed. Davis (1972), using an apparatus in which a sphere is towed slowly through a rotating container filled with a salt stratified fluid, found that the vertical penetration of the 'Taylor column' produced was strong when  $S < 0.1$  and only very weak when  $S > 0.1$ . With relatively large values of  $S$  the column does not penetrate far from the barrier and becomes more of a cone shape than a column. Figure 5.6 shows the length of the 'Taylor cone' non-dimensionalized by the radius of the sphere as a function of  $S$  and figure 5.7 shows the variation of the diameter of the 'Taylor cone' with height for different values of  $S$ .

When  $R \ll 1$  the possibility of a baroclinic flow being unstable can complicate the situation. Currently in Met. O. 21, laboratory experiments in rotating annuli are being undertaken to investigate the interaction between

baroclinic flows and bottom topography and the effect of topography on the total heat transported by the system. The video velocity acquisition system (described in Appendix A) is being used to get horizontal velocity measurements at 5 different levels in the annulus. This unique, modern technique is helping to extend and clarify previous work carried out by Yeh and Chang 1974, Leach 1975, Jonas 1981 and Guo-Qing et al 1985.

Under conditions for which the flow is axisymmetric in the absence of topography, the presence of topography produces a stationary, topographically forced wave, trapped near the base of the annulus, which has a horizontal wavelength the same as the topography. Figure 5.8 and 5.9 show vector plots of the velocity field looking down on the annulus near the top and bottom of the annulus respectively. The topography used in this experiment is a sinusoidal wave 3 in the azimuthal direction with no radial height variation. Its amplitude is 15% of the total depth. This flow is representative of the type of flow observed with all the different pieces of periodic topography used in the present study. It can be seen that at the level where the wave motion is present the jet streams prefer to cross the gap in the vicinity of the peaks and the troughs of the obstacle and that the areas of maximum and minimum relative vorticity are out of phase with the topography.

Figures 5.10 and 5.11 show cross-sections through the annular gap of the mean zonal flow and the wave 3 component of a Fourier analysis of the radial component of the velocity respectively. When these two cross-sections are compared it is observed that the wave is trapped beneath the level of no mean motion which may be acting as a critical layer (where mean flow = phase speed of wave (Pedlosky 1979)). Figures 5.12 and 5.13 show a series of experiments that were carried out to investigate how the vertical penetration of the wave was effected by rotation. In this case a wave 3 topography was used with a half sine radial variation and a sloping lid was incorporated to damp out any instabilities of the baroclinic flow (Mason 1975). As the rotation rate is increased the drag on the fluid by the obstacles lowers the level of no mean motion until it cuts the topography near mid-radius and when  $N/f < 1$  the topographically forced wave penetrates throughout the whole depth of the fluid. It is also noticeable that the amplitude of the wave approaches zero in the vicinity of the level of no mean motion.

To gain some insight into the phase shift of the wave with respect to the topography (see fig. 5.9) it is necessary to consider the influence of the Ekman layers that form on the lid and the base of the annulus. To do this, a simple analytical barotropic model is used. Consider the linearized barotropic vorticity equation on a  $\beta$  plane (a sloping lid approximately simulates a  $\beta$  plane):

$$\left( \frac{\partial}{\partial t} + \bar{u} \frac{\partial}{\partial x} \right) \nabla^2 \psi' + \left( \beta - \frac{\partial^2 \bar{u}}{\partial y^2} \right) \frac{\partial \psi'}{\partial x} = f_0 \frac{\partial w'}{\partial z} \quad \dots 5.1$$

where  $\psi'$  = the perturbation streamfunction.

Assume a) steady flow i.e.  $\frac{\partial}{\partial t} = 0$

b)  $\bar{U} = U_0 = \text{constant}$

c)  $\frac{\partial w'}{\partial z} = \frac{(w_T - w_B)}{d}$

where  $w_T$  and  $w_B$  are the vertical velocities at the top and bottom of the layer due to Ekman suction/pumping.

Thus equation 5.1 becomes:

$$U_0 \frac{\partial}{\partial x} \nabla^2 \psi' + \beta \frac{\partial \psi'}{\partial x} = \frac{f_0}{d} (w_T - w_B) \quad \dots 5.2$$

The vertical velocity associated with the Ekman layers is proportional to the geostrophic relative vorticity in the interior of the fluid, thus on the lid

$$w_T = -e_T \nabla^2 \psi' \quad \dots 5.3$$

On the base the topography will also contribute to the observed vertical velocity

$$w_B = e_B \nabla^2 \psi' + U_0 \frac{\partial h}{\partial x} \quad \dots 5.4$$

where  $e_B = e_T = \left(\frac{\gamma}{2f}\right)^{1/2}$

The topography has the form:  $h(x,y) = h_0 \sin(kx) \sin(ly) \quad \dots 5.5$

Looking for a solution of the form  $\psi' = [S \sin(kx) + C \cos(kx)] \sin(ly) \dots 5.6$

Substituting 5.3, 5.4, 5.5 and 5.6 into 5.2 and comparing coefficients of  $\sin(kx) \sin(ly)$  and  $\cos(kx) \sin(ly)$  values for C and S can be obtained. The solution has the form:

$$\psi' = \frac{h^* U_0}{[(U_0 - \beta^*)^2 + e^2]} [(U_0 - \beta^*) \sin(kx) + e \cos(kx)] \sin(ly)$$

where  $e = \frac{f_0}{dk} (e_B + e_T)$        $h^* = \frac{f_0 h_0}{d(k^2 + l^2)}$        $\beta^* = \frac{\beta}{(k^2 + l^2)}$

Consider the case when there is no Ekman pumping i.e.  $e=0$

for  $U_0 > 0$        $\psi' = \frac{h^* U_0}{(U_0 - \beta^*)} \sin(kx) \sin(ly)$

when  $U_0 < \beta^*$  ( $k < k_c$ )      +ve relative vorticity over the peaks

$U_0 > \beta^*$  ( $k > k_c$ )      -ve relative vorticity over the peaks

$U_0 = \beta^*$  ( $k = k_c$ )      resonance state

for  $U_0 < 0$  -ve relative vorticity always appears over the peaks

Now consider the case with Ekman pumping i.e.  $e > 0$

The inclusion of Ekman dissipation damps out the resonance state

when  $U_0 = \beta^*$       +ve relative vorticity over the peaks

$U_0 \neq \beta^*$       phase shift depends on  $\frac{e}{U_0 - \beta^*}$

Now consider what happens on an f plane i.e.  $\beta^*=0$

The phase shift of the relative vorticity maxima and minima depends on  $e/U_0$  and the phase shift is largest for longest wavelength topography.

This solution suggests that the phase shift can be physically interpreted as the Ekman layers significantly spinning up or spinning down the relative vorticity being generated by stretching or compression of columns of fluid as they move over the topography. Moving up the slope the columns are compressed, producing -ve relative vorticity. If the horizontal advection is small enough this is slowly spun up through Ekman pumping so that on the downslope vortex tubes are stretched to their original length with an extra +ve relative vorticity. The reverse process then occurs as the fluid moves over the trough. For shorter wavelength topography and the same horizontal advection the Ekman pumping is less efficient and so the phase shift is less.

This is a very simple model and is restricted by the fact that it is barotropic whereas the real system is baroclinic. In practice the phase shift observed of the topographically forced wave is more complex, with variation in the vertical as shown in figure 5.14

Experiments carried out on the transition from baroclinically stable (no drifting waves) to baroclinically unstable (drifting waves) flows indicate that the effect of topography is to stabilize the transition (see figure 5.15). In particular, there is a significant effect on the 'knee' and the lower symmetric transition (see lecture 2) which move to higher Taylor numbers. When drifting waves occur, their wavelength is shorter than the waves in the experiments with the same parameters but no topography, and the intransitivity and hysteresis effects generally observed in the annulus are reduced. It is also found that amplitude vacillation is less widely observed when topography is present. At moderately high rotation, rates the topographically forced wave dominates throughout the whole depth of the fluid and this tends to suppress or reduce the amplitude of the drifting baroclinic waves.

## References

- Davies P.A., 1972: Experiments on Taylor columns in rotating stratified fluids. J. Fluid Mech, 54, 691-717
- Davies P.A. and Baines P.G., 1980: Laboratory studies of topographic effects in rotating and/or stratified fluids, GARP publication series no.23.
- Guo-Qing L., Kung R. and Pfeffer R.L. 1985: An experimental study of baroclinic flows with and without two-wave bottom topography. submitted to J. Atmos. Sci.
- Greenspan H.P., 1968: The theory of rotating fluids., Cambridge Univ Press.
- Hide R., 1961: Origin of Jupiter's Great Red Spot., Nature, 190, 895-896.
- Hide R. and Ibbetson A., 1966: An experimental study of Taylor columns. Icarus, 5, 279-290
- Hide R., Ibbetson A. and Lighthill M.J., 1968: On slow transverse flow past obstacles in a rapidly rotating fluid. J Fluid Mech, 32, 251-272
- Hide R., 1971: On geostrophic motion of a non homogeneous fluid., J. Fluid Mech, 49, 745
- Holton J.R., 1972: An introduction to dynamic meteorology. Academic Press.
- Hoskins B.J. and Karoly D.J., 1981: The steady linear response of a spherical atmosphere to thermal and orographic forcing. J. Atmos Sci, 38, 1179-1196
- Houghton D.D. and Kasahara A., 1968: Nonlinear shallow fluid flow over an isolated ridge. Commun Pure Appl Math, 21, 1-23
- Ibbetson A. 1964: PhD dissertation. University of Durham
- Jonas P.R., 1981: Laboratory observations of the effects of topography on baroclinic instability., Q.J.R.Met. Soc., 107, 775-792
- Leach, H.R., 1975: Thermal convection in a rotating fluid: effects due to irregular boundaries. PhD thesis, University of Leeds.
- Long R.R., 1952: The flow of a liquid past a barrier in a rotating spherical shell. J. Meteorol, 9, 187-199
- Long R.R., 1954: Some aspects of the flow of stratified fluids, II Experiments with a two fluid system. Tellus, 6, 97-115
- Long R.R., 1955: Some aspects of the flow of stratified fluids ,III Continuous density gradients. Tellus, 7, 341-357
- Long R.R., 1970: Blocking effects in flow over obstacles. Tellus, 22, 471-480
- Long R.R., 1974: Some experimental observations of upstream disturbances in a two fluid system. Tellus, 26, 313-317
- Mason P.J. 1975: Baroclinic waves in a container with sloping endwalls, Phil. Trans R. Soc. Lond., A278, 397-445
- Mason P.J. and Sykes R.I., 1979: On the net forces produced by surface mounted obstacles., Q.J.R.Meteorol Soc, 105, 829-840
- Maxworthy T., 1977: Topographic effects in rapidly rotating fluids: flow over a

transverse ridge., Z Angew Math Phys, 28, 853-864

Pedlosky J., 1979: Geophysical Fluid Dynamics, Springer-Verlag

Smith R.B., 1976: The generation of lee waves by the Blue Ridge. J.Atmos. Sci, 33, 507-519

Taylor G.I., 1923: Experiments on the motion of solid bodies in rotating fluids. Proc.R. Soc, A, 104, 213-218

Tritton D.J., 1977: Physical fluid dynamics. Van Nostrand Reinhold

Vaziri A. and Boyer D.L., 1977: Topographically induced Rossby waves. Archiv Mech, 27, 3-12

Yeh T.C. and Chang C.C., 1974: A preliminary experimental simulation of the heating effect of the Tibetan plateau on the general circulation over Eastern Asia in summer. Sci. Sin, 17, 397-420

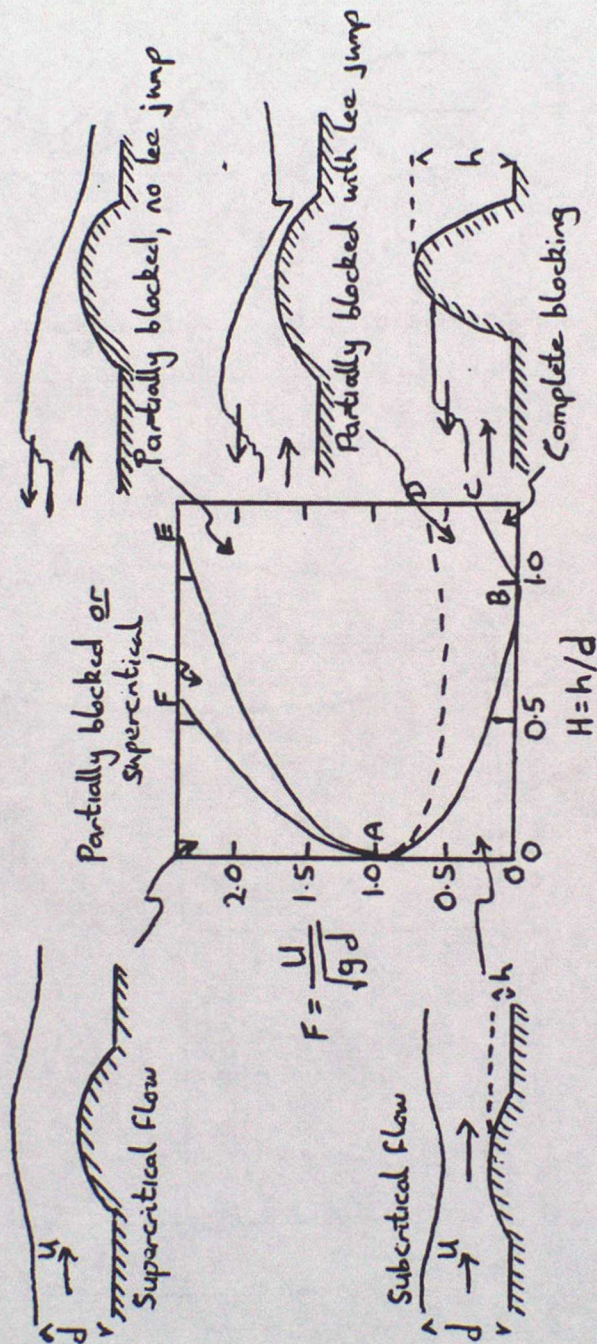


Figure 5.1 A schematic diagram showing the flow regime for hydrostatic, single layer flow over an obstacle.

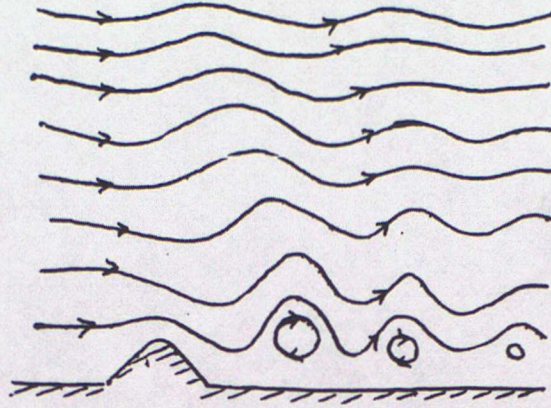


Figure 5.2 A schematic diagram showing a lee wave pattern set up in a stratified fluid as it passes over an obstacle.

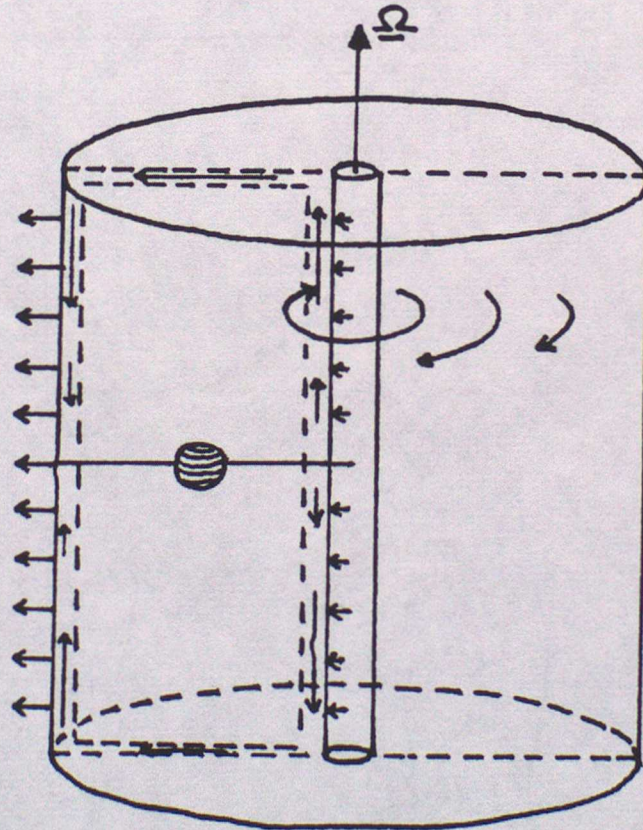


Figure 5.3 A schematic diagram showing the experimental apparatus sometimes used for studying 'Taylor columns'. A source-sink arrangement is used where fluid enters through the inner cylinder and exits through the outer. This produces a geostrophic azimuthal flow in the interior in which a sphere is held stationary in the rotating frame.

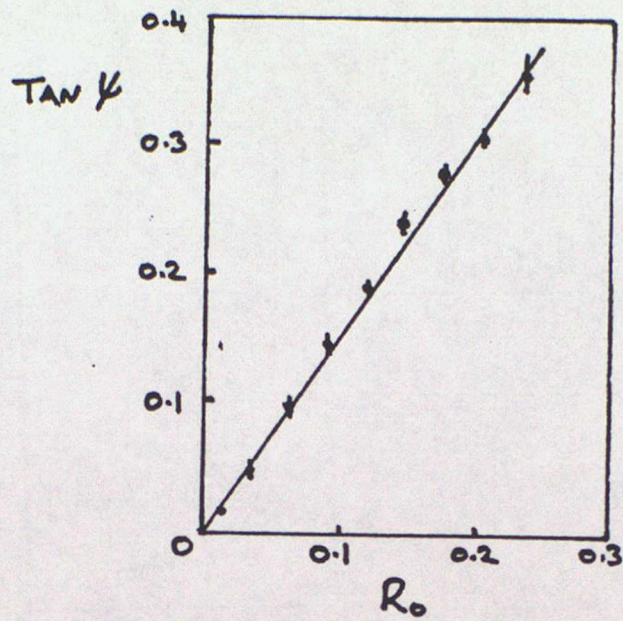


Figure 5.4 A graph showing the measured inclination of a 'Taylor column' as a function of  $R_0$  ( $\phi$ ) and a theoretical comparison (-).

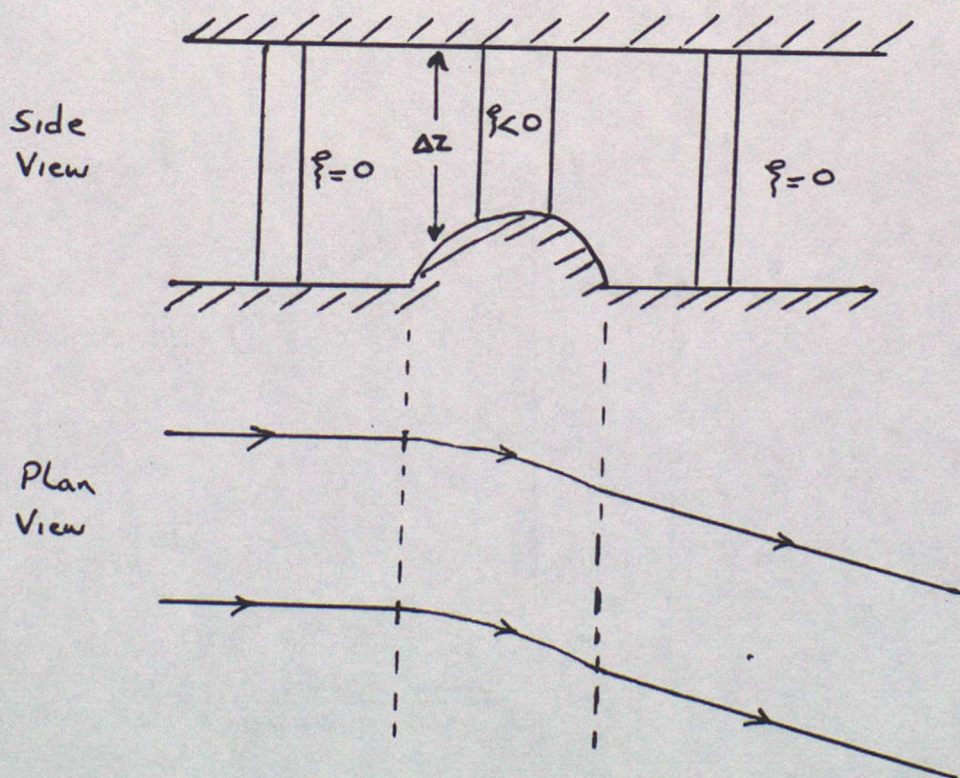


Figure 5.5 A schematic diagram showing an inviscid, homogeneous fluid being forced to rise over an infinite, two dimensional ridge on an  $f$  plane.

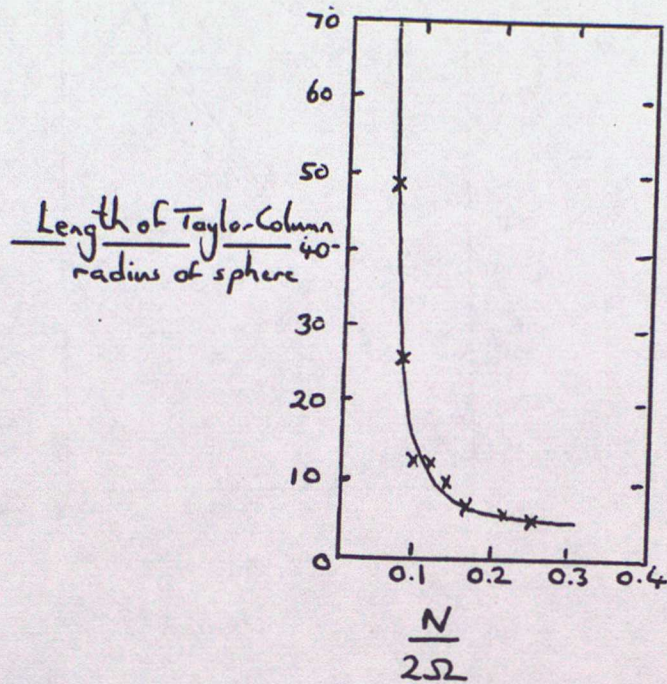


Figure 5.6 A graph of the non-dimensionalized length of a 'Taylor column' as a function of the stratification parameter  $N/2\Omega$ .

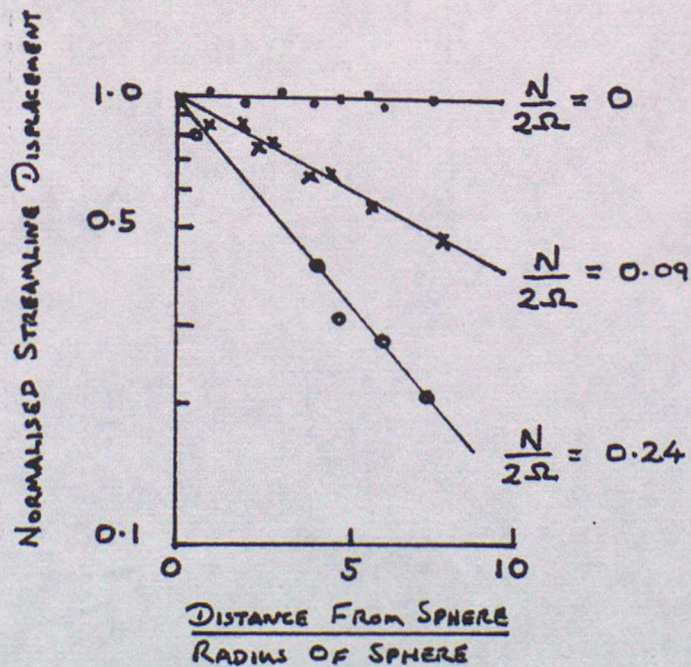


Figure 5.7 A graph of the variation of the diameter of a 'Taylor column' with distance from a sphere in a stratified rotating fluid as a function of  $N/2\Omega$ .

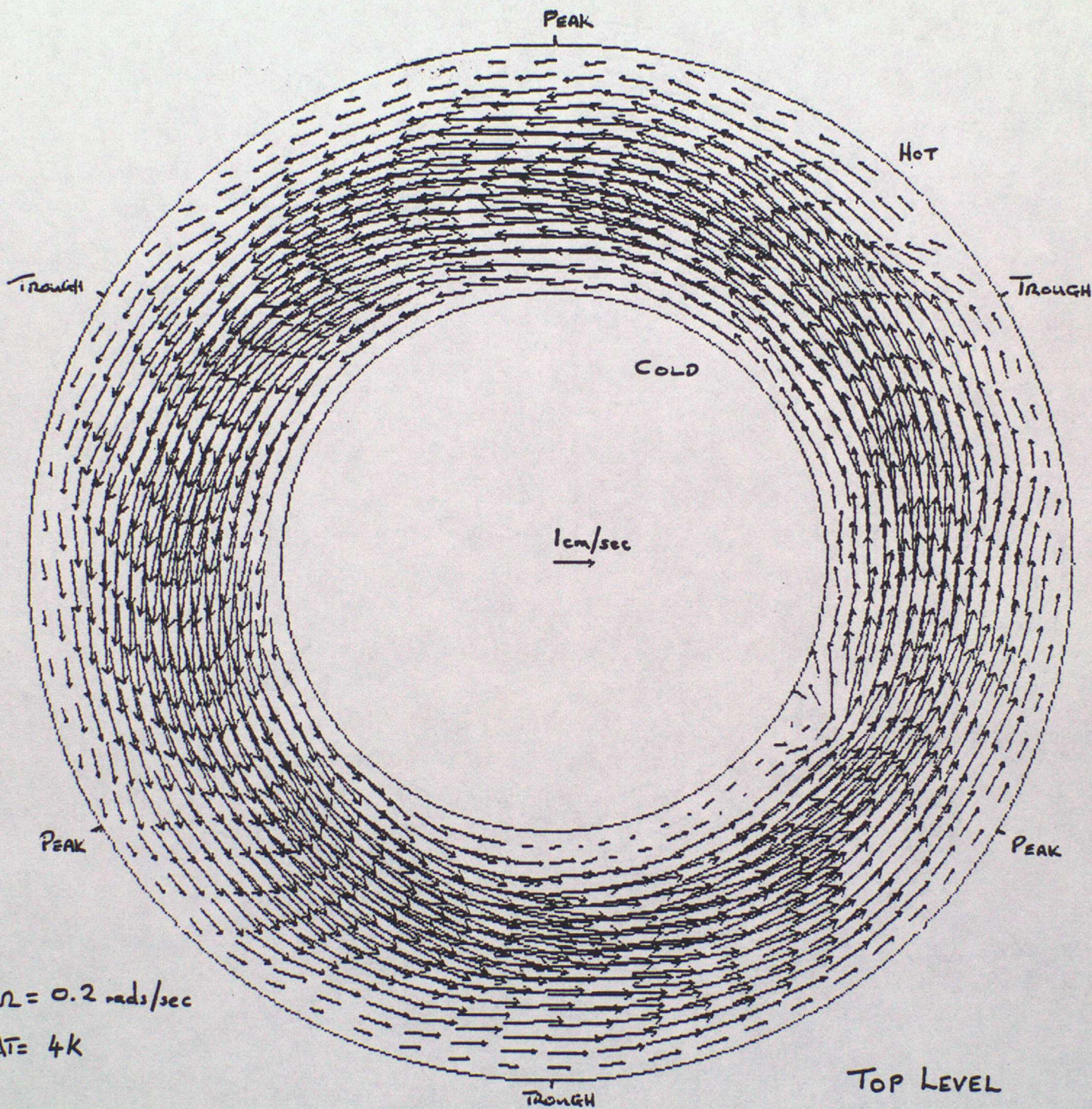


Figure 5.8 A velocity field near the top of the annulus. On the base there is a wave 3 topography with no radial variation and an amplitude 15% of the depth.

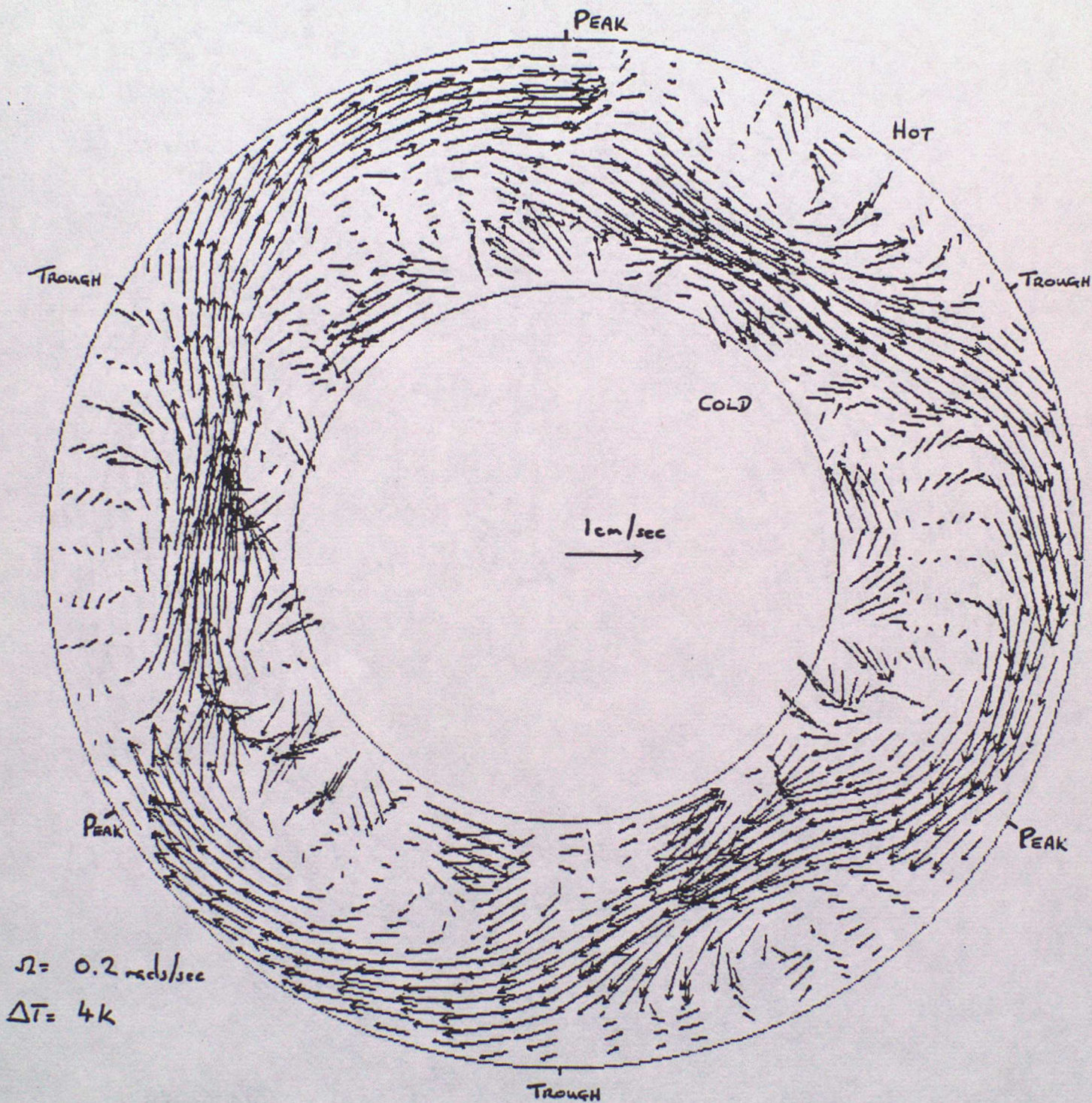
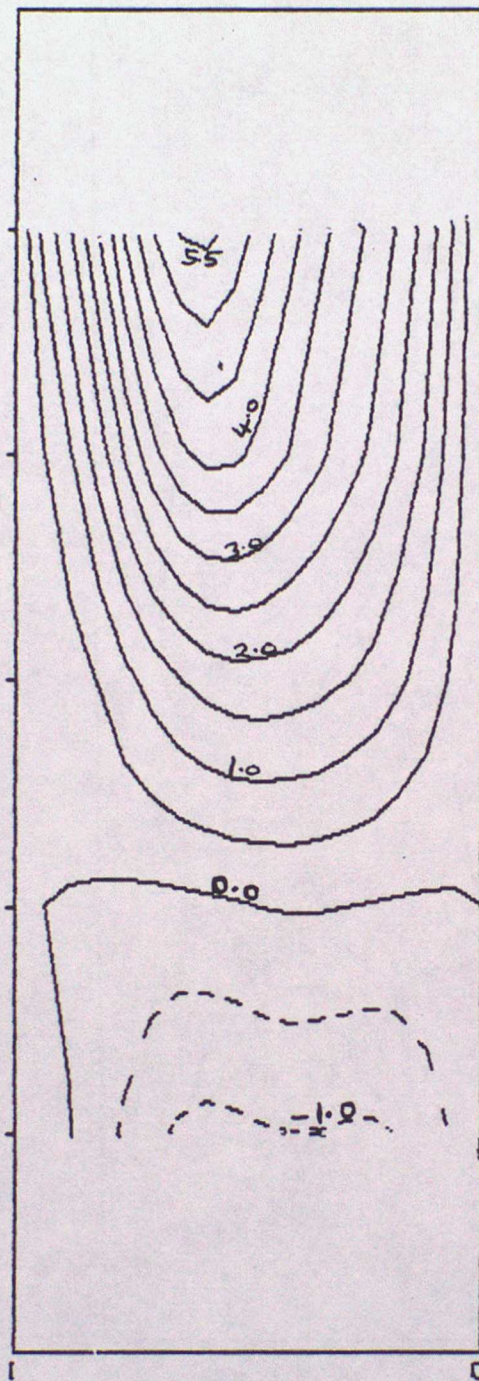


Figure 5.9 A velocity field near the base of the annulus. On the base there is a wave 3 topography with no radial variation and an amplitude 15% of the depth.

# MEAN FLOW (cm/sec)



Run no. 062 Average of all scans.

Inner and outer radii = 75.00, 144.00 mm

Maximum = 0.56E+00 Minimum = -0.11E+00

Contour interval = 0.50E-01

$$\frac{N}{F} \approx 2$$

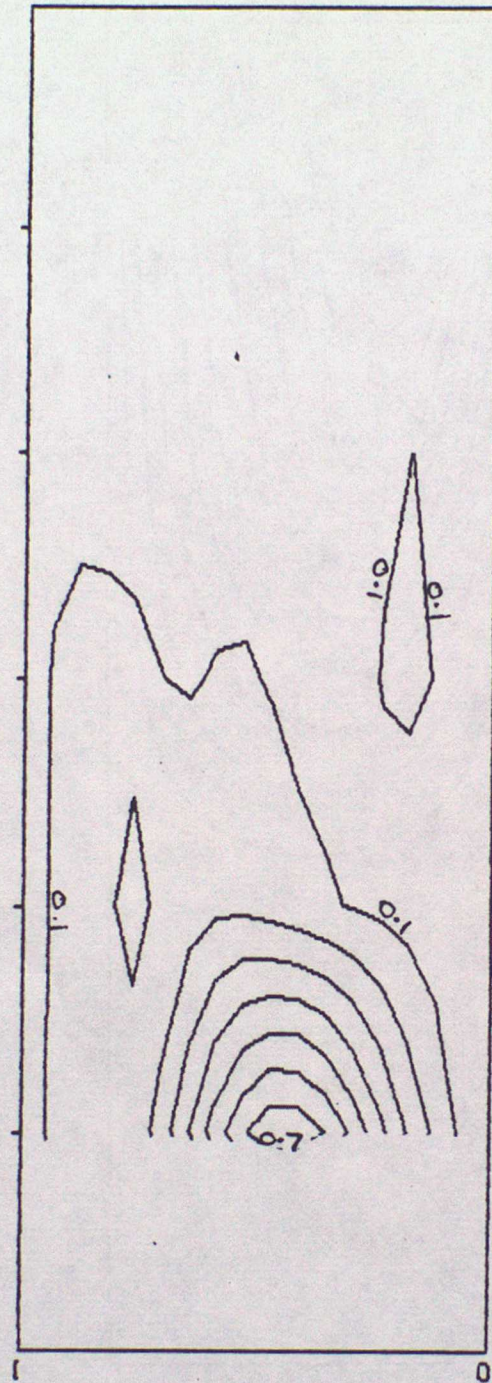
$$\Omega = 0.2 \text{ rad/sec } \Delta T = 4.0K$$

$$\Theta = 12.59 \quad \tau = 3.785 \times 10^{-5}$$

$$\text{Depth} = 200.00 \text{ mm}$$

Figure 5.10 A cross-section of the annulus gap showing the azimuthal mean flow. The experimental parameters are the same as for figs 5.8 and 5.9.

WAVE 3 MEAN RADIAL VELOCITY AMPLITUDE



Run no. 062       $\Omega = 0.2 \text{ rads/s}$        $\Delta T = 4.0k$        $\frac{N}{F} \approx 2$   
 $\Theta = 12.59$        $\tau = 3.785 \times 10^5$   
 Inner and outer radii = 75.00, 144.00 mm      Depth = 200.00 mm  
 Maximum = 0.77E-01      Minimum = 0.00E+00

Contour interval = 0.10E-01

Figure 5.11 A cross-section of the annulus gap showing the wave 3 component of a fourier analysis of the radial component of velocity. The experimental parameters are the same as for figs 5.8 and 5.9.

(cm/s)  
 $\Delta T = 4.0K$

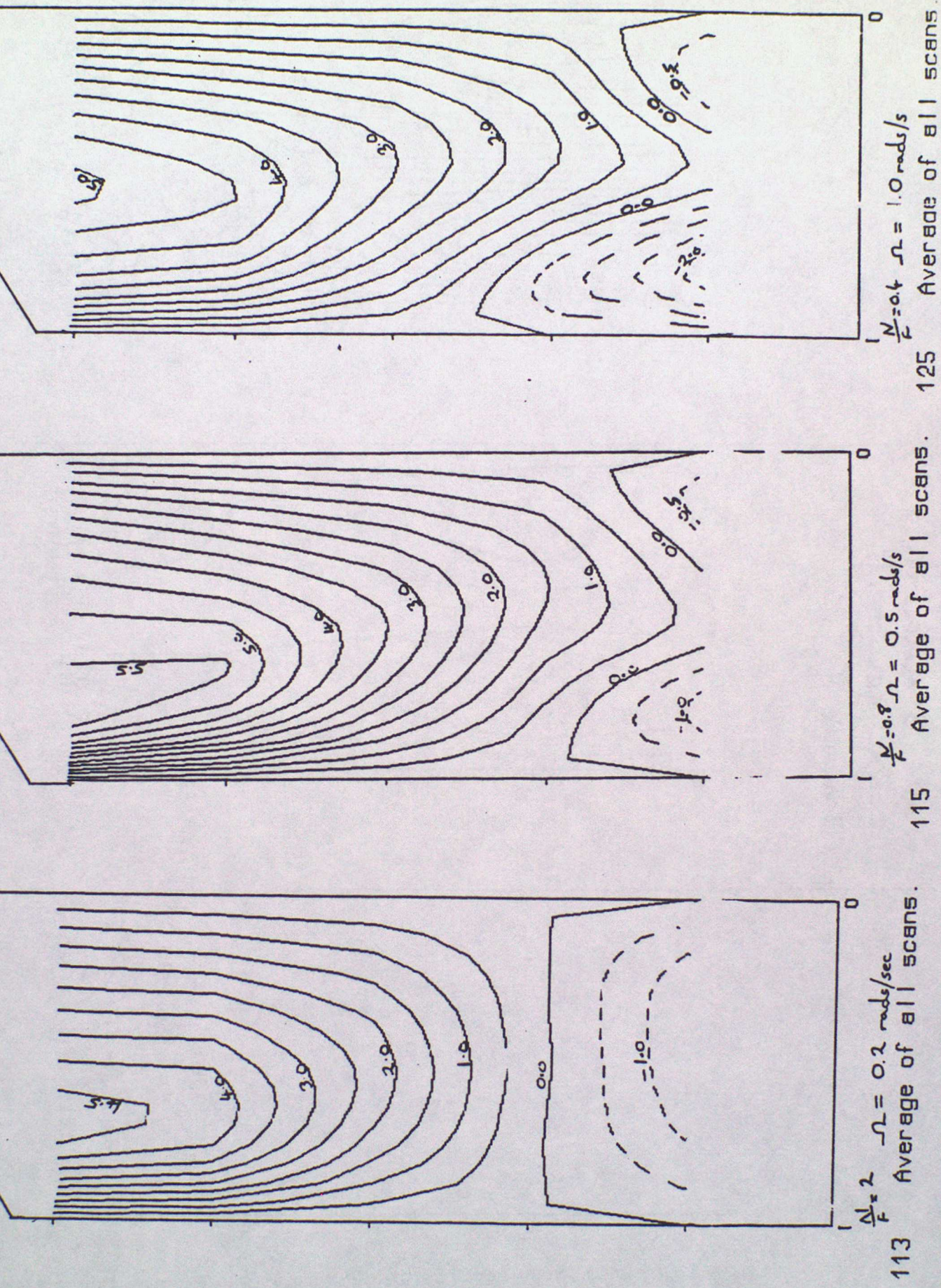


Figure 5.12 Cross-sections of the annulus gap showing the variation of the mean flow at different rotation rates. On the base there is a wave 3 topography with radial variation and an amplitude 15% of the depth.

WAVE 3 AMPLITUDE  
(ZONAL VELOCITY)  
 $\Delta T = 4.0k$

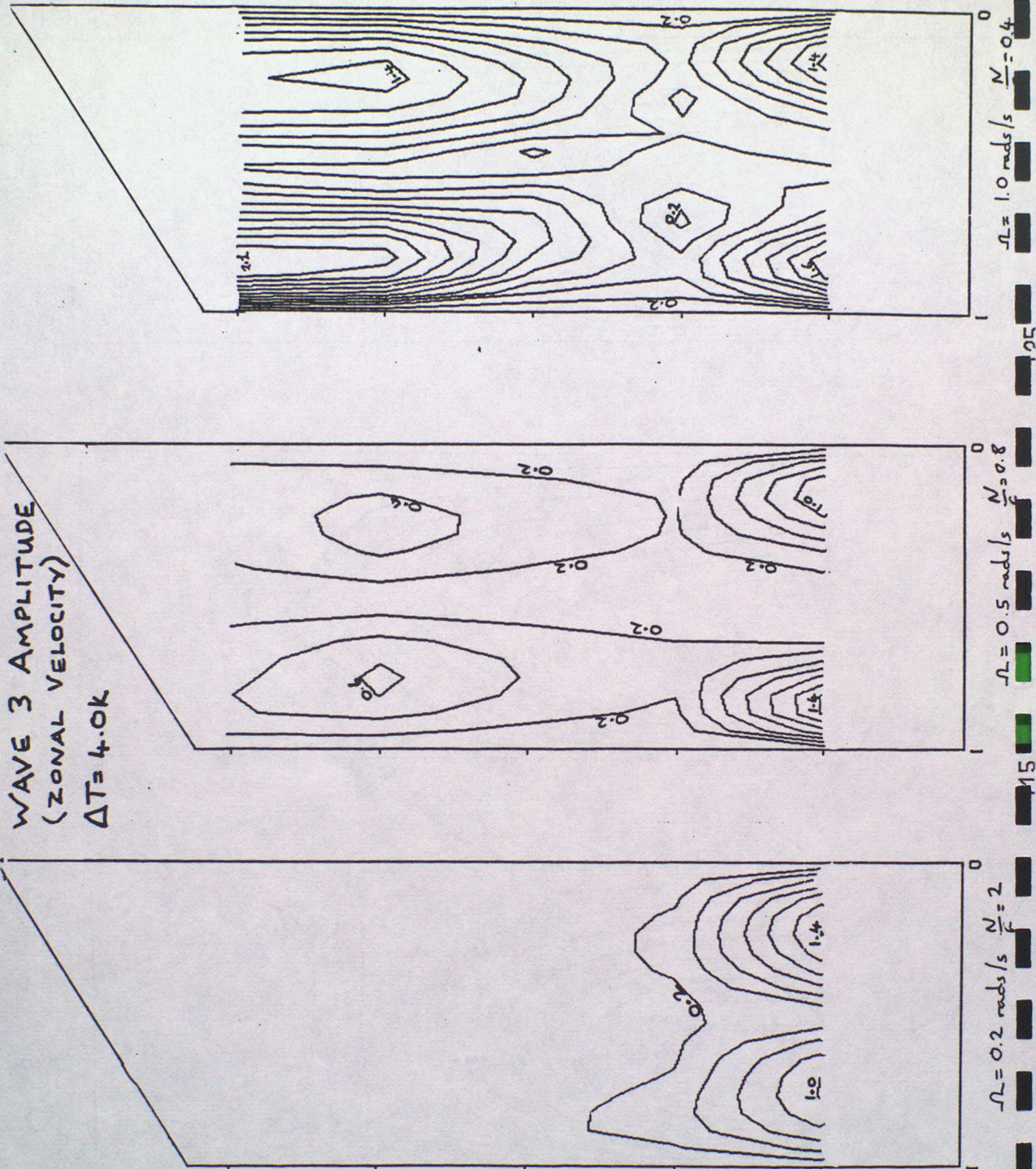


Figure 5.13 Cross-sections of the annulus gap showing the vertical penetration of the topographically forced wave at different rotation rates. On the base there is a wave 3 topography with radial variation and an amplitude 15% of the depth.

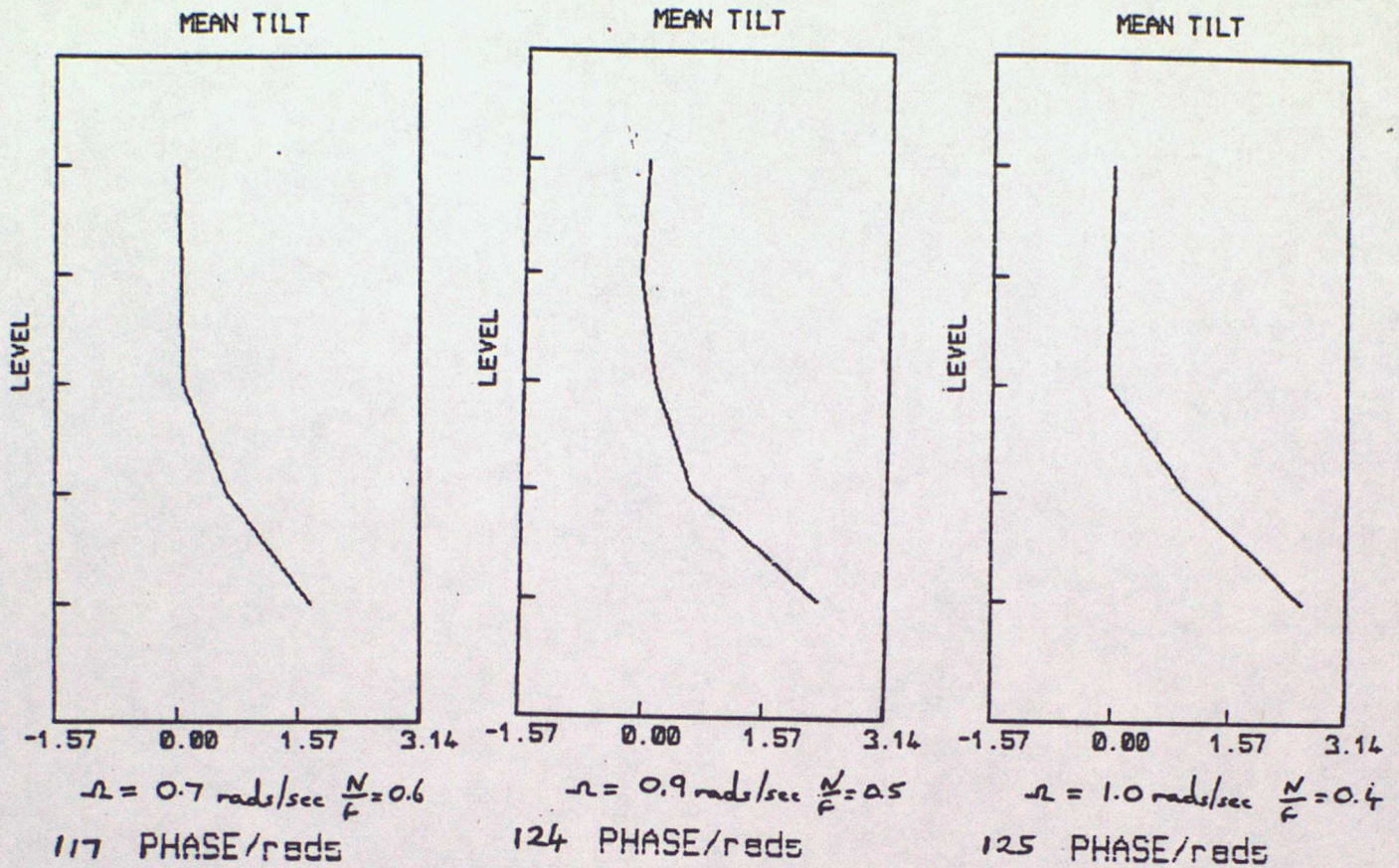


Figure 5.14 A diagram showing the variation of the tilt of the stationary topographically forced wave with height at different rotation rates. On the base there is a wave 3 topography with radial variation and an amplitude 15% of the depth. The lid is sloping.

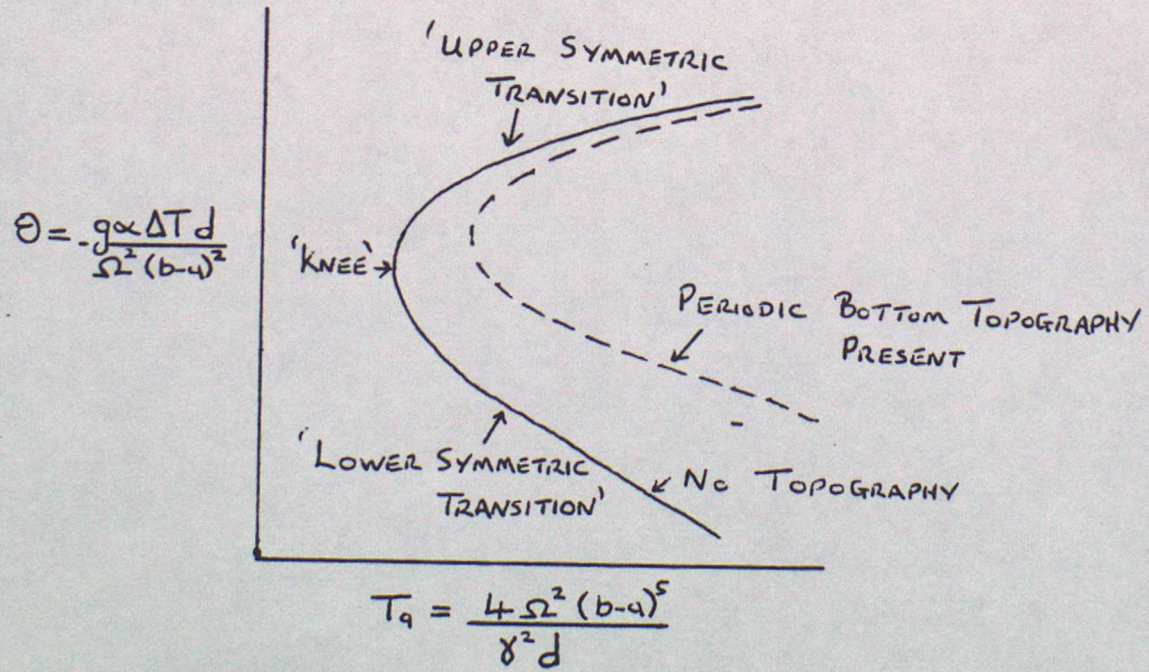


Figure 5.15 A schematic diagram indicating the effect of bottom topography on the regime diagram (see lecture 2).

## APPENDIX A

### The Video Velocity Acquisition System (V.V.A.S.)

An experimental technique for measuring horizontal velocities in a fluid has been developed and widely used in the Met. O. 21 laboratories. In the past, long time exposure photographs of illuminated tracer particles in the fluid have been used for this purpose (Douglas et al 1973, Jonas and Kent 1979, Guo-Qing et al 1985). The resulting tracks or streaks can be analysed (usually by hand which is a very time consuming process) to get the mean velocity at several points in the fluid at a given moment in time. The video velocity acquisition system, shown schematically in figure 1, allows this all to be done automatically in 'real time' using a digitized T.V. signal.

The density of the working fluid used is dictated by the requirement that the tracer particles are neutrally buoyant and are thus advected by the fluid motions. The tracers generally used are spherical polystyrene beads with a density of 1.043 gm/cc and a diameter of 601-710  $\mu\text{m}$ . To obtain a working fluid with this density a water/glycerol solution is used (87% water solution). The fluid is seeded with a bead concentration of  $5 \times 10^{-4}$  gm/cc.

The beads are illuminated by a narrow (3mm in the vertical), horizontal beam of light directed through a perspex window in the outer wall of the annulus. The motion of the beads that pass through this flat beam of light (vertical velocities outside of the boundary layers are an order of magnitude less than the horizontal velocities) is viewed from above using a closed circuit television camera. The signal from the camera is then taken off the rotating turntable via a slip-ring and is analysed by a video digitizer. It is converted into a two level (black/white) signal by comparing its intensity against an adjustable threshold level and the positions of the transitions from black to white (the illuminated beads viewed by the camera appear as white dots on a black background) in a  $512 \times 512$  pixel window are analysed using a PDP 11/34 minicomputer. The position of the centre of each bead in the rotating frame is automatically calculated by comparing it with two reference points (point light sources mounted on the side of the annulus) which are digitized at the same time and whose positions are calibrated beforehand. It is possible to scan the field of view 25 times a second and in this way the position of the beads can be tracked over a short period of time. These tracks can be displayed and updated on a television screen in real time and if necessary be recorded using a video tape recorder allowing a speeded up record of the flow to be viewed at a later date. This facility, known as STREAK, is used extensively and has proved very useful for real time flow visualization.

Alternatively the transitions data from several scans can be stored on a hard disk to be analysed at a later date to extract horizontal velocity

measurements. This analysis is currently carried out on a VAX 11/730 and involves four basic steps:

- a) the position of the centre of each bead in the rotating frame is calculated,
- b) the movement (or track) of each bead from one scan to the next is calculated (strict quality control is used to ensure that the centres and tracks are unambiguous),
- c) the mean radial and azimuthal components of horizontal velocity for each bead is calculated from the time taken to move the distance between the start and end of each track (allowance is made for tracks ending and beginning while the scanning is in progress i.e. beads moving in and out of the beam) and
- d) a least-squares fitting technique is used to fit the velocity component data to the following function (Bell 1984, Bell and Jackson 1985):

$$u = \sum_{m=0}^{15} \sum_{n=1}^6 (b/r)^n \sin(m\pi x) [A_{mn} \cos(m\phi) + B_{mn} \sin(m\phi)]$$

$$\text{where } x = \frac{r-a}{b-a}$$

The coefficients A and B are stored in a permanent record so that the horizontal velocity fields can be reconstructed on a regular grid allowing other diagnostics to be produced.

Five perspex spacers are placed in the outer wall, enabling velocity fields to be obtained at five different depths in the annulus. In general between 100 and 550 irregularly spaced speed measurements can be made at each level, with a minimum sampling time between levels (or another sample of the same level) of approximately 12 seconds. The number of speed measurements taken normally decreases in the lower half of the annulus as it is more difficult to get unambiguous tracks because the beads above that level mask the field of view.

#### References

- Bell M.J., 1984: The least squares method of fourier analysing two dimensional velocity data produced by the Video Velocity Acquisition System., Met. O. 21 internal report.
- Bell M.J. and Jackson W.D.N., 1985: Further analysis of methods of fitting fields to two dimensional velocity data. IBU.
- Douglas H.R., Hide R. and Mason P.J., 1973: An investigation of the structure of baroclinic waves using three level streak photography., Q.J.R.Met. Soc. 98 247-263.

- Guo-Qing, Kung R. and Pfeffer R.L., 1985: An experimental study of baroclinic flows with and without two-wave topography., Submitted to J. Atmos. Sci.
- Jonas and Kent, 1979: Two dimensional velocity measurements by automatic analysis of trace particle motion., J.Phys.E.:Sci Instrum., 12, 604-609.

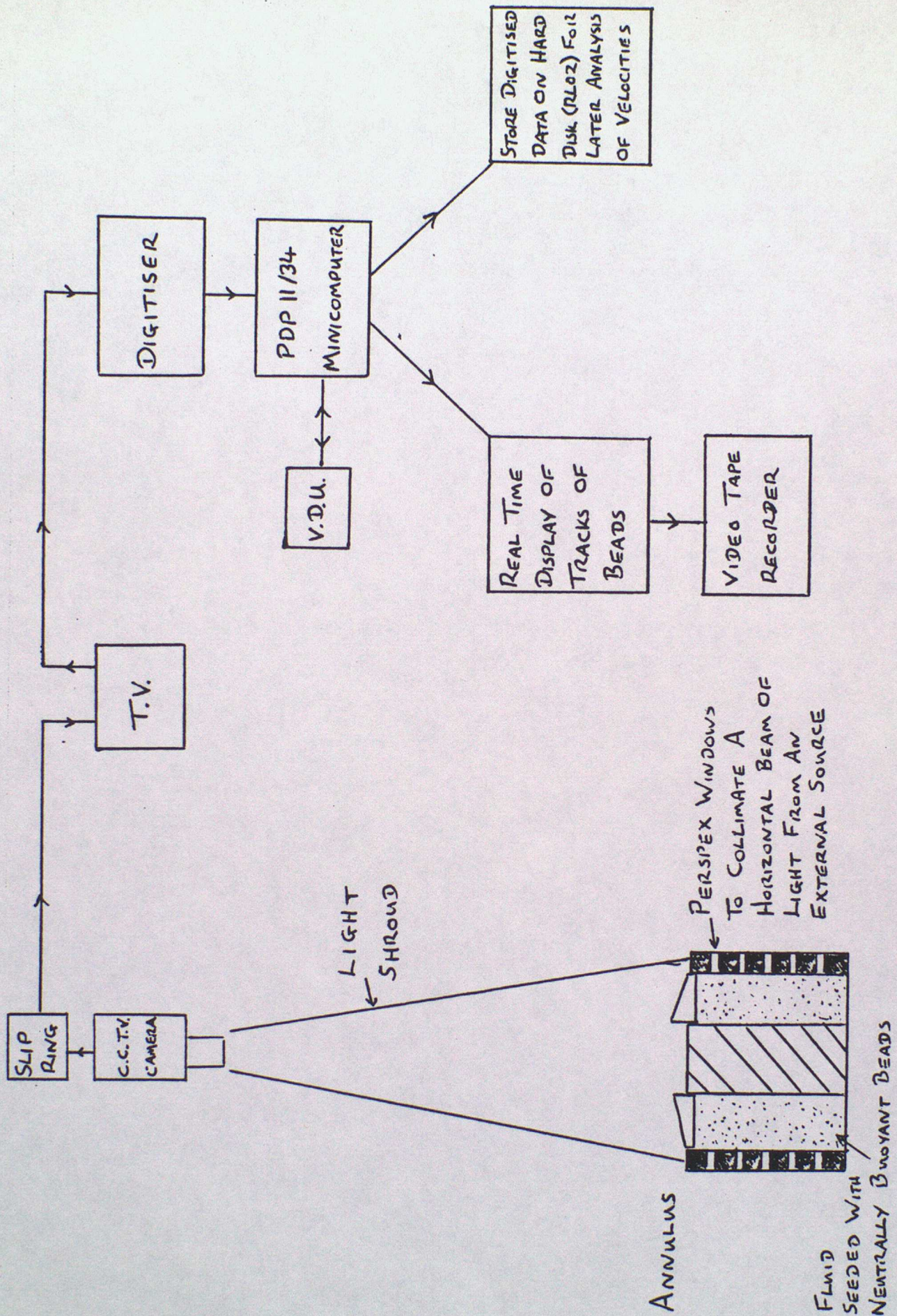


Figure 1. A schematic diagram of the Video Velocity Acquisition System (V.V.A.S.).

## LECTURE 6: THE INTERNALLY-HEATED ANNULUS

1. Introduction

In carrying out experiments in the laboratory on thermal convection in a rotating, baroclinic fluid, it is of great importance to establish which aspects of the flows observed are generally applicable to any fluid system, and which may be more specific to the particular system under study (e.g. dependent on particular means of forcing or boundary conditions). One way in which this may be investigated is by incorporating variations e.g. into the construction of the experiment, the fluid properties, and especially the boundary conditions. Previous lectures have considered variations in the mechanical boundary conditions (using free or rigid upper surfaces, or surface topography). The present lecture will consider some effects of variations in the thermal boundary conditions and the overall distribution of heating and cooling in the annulus. Thus, for example, by using direct internal heating of the working fluid, it is possible to investigate the properties of baroclinic waves in a zonal flow for which the horizontal thermal gradient is non-monotonic, and therefore much removed from the kind of flow considered in 'classical' theoretical analyses.

A further motivation for studying such flows has arisen recently from observations of the atmospheres of other planets, whose composition, scale and means of thermal and mechanical forcing (and its spatial distribution) may be quite different from those of the Earth. The atmospheres of Jupiter and Saturn offer some particularly intriguing phenomena which could be manifestations of sloping convection under conditions more closely similar to those which can be obtained in the internally-heated annulus (e.g. see Hide 1981; Read & Hide 1983, 1984; Read 1986a). This potential application of the annulus experiments will be considered in Section 3 below.

2. Baroclinic waves with internal heating

The laboratory system considered is an annulus of conventional design, but in which heating may be applied internally via ohmic dissipation of an alternating electric current passed through the working fluid (which is a weak electrolyte)

between the (electrically-conducting) sidewalls. Either or both sidewalls can be cooled in the usual way, allowing a wide variation in the effective thermal boundary conditions and distribution of heat sources and sinks (for more details see Hide & Mason 1970, 1975; Read 1986b).

The various regimes of flow obtained in such a system are found to be very similar to those in the conventional (wall-heated) annulus, with transitions between them occurring under comparable experimental conditions (again measured by a stability parameter  $\Theta$  and Taylor number  $T_a$  - see Lecture 2) almost regardless of the distribution of cooling at the boundaries (e.g. see Hide & Mason 1970). Thus, axisymmetric flows occur at the lowest rotation rates  $\Omega$ , regular waves at intermediate  $\Omega$  and irregular waves at the highest values of  $\Omega$ . The most significant difference between the behaviour of internally-heated flows to those in the conventional annulus appears to be in the form of periodic 'vacillations' - recent work suggests that 'amplitude vacillation' rarely occurs in the internally-heated annulus, while 'wavenumber vacillation' is the preferred form of structural vacillation. A selection of regular and irregular wave flows for cases in which both sidewalls are at the same temperature ( $\Delta T = 0$ ) are shown in Fig. 1.

The form of the horizontal flow pattern varies considerably in the axisymmetric and regular wave regimes, depending upon the thermal boundary conditions at the sidewalls (see Fig. 2). Internal heating forces upward motion throughout the interior, which must match onto the horizontal boundary layers via the Ekman suction condition. Thus, the relative vorticity of the axisymmetric or mean zonal flow is anticyclonic at upper levels and cyclonic at lower levels (a more detailed analysis is given by Quon 1977; Read 1986b). In the presence of non-axisymmetric waves, this results in trains of eddies which are predominantly anticyclonic at upper levels, but with an associated meandering jet stream whose location and strength depends upon the thermal boundary conditions at the sidewalls, and hence upon the net inward or outward radial flux of heat. This may be approximately related to the mean zonal flow near the side boundaries (where eddies are weak) by

$$H(r,t) = - (\nu/\Omega)^{1/2} \overline{[T(r,d,t) - T(r,0,t)]} \overline{u(r,d,t)} \quad (1)$$

(see Hide & Mason 1970, 1975; Hide 1981), where  $H$  is the total heat flux through a cylindrical surface of height  $d$  and radius  $r$ ,  $T(r,z,t)$  and  $u(r,z,t)$  are the mean zonal temperature and zonal velocity respectively, and  $\nu$  is the kinematic viscosity. Note that the terms multiplying  $u$  are negative definite, so that  $u$  may be seen to reflect directly the partition of heat flow between the inner and outer sidewalls - the result is summarised schematically in Fig. 3 for comparison with the examples in Fig. 2.

The most striking example occurs when  $\Delta T = 0$ , for which heat is removed at equal rates at both sidewalls. The axisymmetric flow then consists of a temperature maximum at mid-radius on horizontal surfaces, with strong anti-cyclonic shear at upper levels between two opposing jet streams (and cyclonic shear at lower levels). Baroclinic waves take the form of trains of compact, apparently isolated oval eddies, all circulating in the same sense as the shear of the mean zonal flow (i.e. anticyclonic at upper levels). Little motion appears outside the eddies themselves apart from a very weak meandering jet stream. The isolated appearance of the eddies is most obvious for the lowest wavenumbers, which occur at high values of Taylor number and  $\Theta$ . Fig. 1(a) shows the upper level flow for a typical  $m = 1$ , in which the eddy is seen to be concentrated into a narrow range in azimuth. Although the eddy has a 'solitary' appearance, its structure is not consistent with conventional 'soliton' or 'modon' solutions, but rather has the form of a wave packet encompassing little more than a single wavelength in azimuth. Non-linear effects are therefore of great importance in setting up the flow, strongly steepening the basic wave in azimuth. Further details may be found in Read & Hide (1984).

Like the baroclinic waves in the conventional annulus, the eddies in the internally heated system contribute significantly to the transfer of heat in both the horizontal and vertical. Fig. 4 shows the variation of Nusselt number (a dimensionless measure of heat transfer, see Hide & Mason 1975) with rotation rate for the internally-heated system, as measured in the laboratory (note that Nusselt number for an internally heated system is defined slightly differently than for a boundary heated flow - see Hide & Mason 1970; Read 1986b). The Nusselt number which would occur if the flow were to remain axisymmetric is also shown (derived from an axisymmetric numerical model). The presence of regular eddies maintains the heat transfer close to the level in the absence of rotation

until the flow becomes irregular.

Recent (as yet unpublished) studies in Met. O. 21 have incorporated a 'planetary vorticity gradient' (similar to a  $\beta$ -effect) by using sloping endwalls, thereby allowing the depth of the annulus to vary with radius. Similar methods were investigated in the conventional annulus by Mason (1975). The effect of sloping boundaries on the internally-heated flows is found to be very similar to that on other annulus flows, in introducing wave dispersion in a way qualitatively similar to that of Rossby waves - eddies drift with respect to the mean zonal flow at a rate inversely proportional to their wavenumber and proportional to the effective  $\beta$  ( $\propto \Omega$ ). At higher rotation rates, the radial scale of the eddies may be reduced, so that eddies no longer fill the annulus gap. This ultimately results in two independent, parallel trains of waves and eddies adjacent to each sidewall, associated with a series of parallel zonal jet streams.

### 3. Eddies on Jupiter & Saturn

Jupiter and Saturn lie well beyond the Earth's orbit at mean solar distances of 5.2 and 9.6 AU respectively (1 AU = mean Earth-Sun distance =  $1.5 \times 10^{11}$  m). They are giant planets with radii  $\sim 7.14 \times 10^4$  km and  $6.03 \times 10^4$  km respectively, but consist largely of hydrogen (90%) and helium (10%) with small rocky cores. Both planets rotate rapidly (sidereal periods of 9h 55m and 10h 39m respectively) and are shrouded in dense cloud decks consisting mainly of ammonia ice.

Both planets exhibit a variety of eddy-like features at the level of the upper cloud decks, some of which appear to persist for very long periods (from months to many years). The best known examples are the Great Red Spot (GRS) on Jupiter - discovered in the 17th century - and the White Ovals (also on Jupiter) - observed to form in 1939. Some examples are illustrated in Fig. 5. Most long-lived eddies on Jupiter and Saturn take the form of oval spots of various colours, the most common of which are found in regions of anticyclonic mean zonal shear between pairs of opposing mid-latitude jet streams, and are characterised by anticyclonic circulation at the upper cloud levels. They in

include the GRS, the White Ovals and other smaller white spots at higher northern and southern latitudes on Jupiter, and some similar brown spots on Saturn. Cyclonic examples (occurring in regions of cyclonic mean zonal shear) include the brown 'barges' on Jupiter. An intriguing property of many of the smaller anticyclonic ovals on Jupiter is that they appear in almost regularly spaced trains in longitude, often interspersed with weaker cyclonic circulations.

Such features do not bear much resemblance to the more familiar baroclinic eddies in the Earth's atmosphere and in the conventional annulus experiments, and accordingly, many different suggestions have been made to account for their nature and various properties (see Ingersoll 1981; Ingersoll et al. 1984; Read 1986a; Williams 1986 for reviews). The resemblance between these features and the baroclinic eddies obtained in the internally-heated annulus, however, would suggest that sloping convection was a strong candidate to account for their nature and origin. Unfortunately, for various reasons the eddy-like features in all these different models are difficult to compare dynamically with the Jovian and Saturnian eddies:-

- a) The appropriate boundary conditions and background distributions of wind and temperature are probably rather different for Jupiter and Saturn than for the Earth. Both major planets are almost certainly entirely fluid throughout, with no solid surface beneath the clouds. Both generate at least as much heat in their deep interiors as they receive from the Sun. This has the consequence that the deep interior is likely to be nearly isentropic and very weakly stratified, also causing large-scale horizontal thermal contrasts to be very small (see Flasar 1986 for a review). The observed thermal contrast between the equator and poles on Jupiter and Saturn at the cloud tops is very small. At least near the cloud tops (and probably some distance below - see Flasar 1986) the large-scale thermal contrasts which are observed are associated with the banded structure of the zonal winds and clouds. The pattern of zonal winds are consistent with an application of the thermal wind equation to the observed thermal contrasts with latitude, which are actually non-monotonic (i.e. the horizontal thermal gradient reverses several times between equator and poles - cf the laboratory experiments above). More recent analyses of spacecraft infrared data by Gierasch et al. (1986) confirm an association between the pattern of zonal winds and clouds and a

thermally-driven meridional circulation with upwelling in regions of anti-cyclonic shear (again cf the internally-heated experiments above). Many aspects of the deep structure of the flow and the effective lower boundary conditions remain uncertain, however, so that any hypothesis for the Jovian and Saturnian eddies must continue to be controversial.

- b) The available atmospheric data refer only to a thin layer around the cloud tops. It is not possible, therefore, to determine many useful dynamical diagnostics with which to test theories (indeed this is one of the major challenges posed by Jupiter and Saturn to dynamicists - to design an observational strategy which could yield conclusive results).

#### 4. Long-lived eddies on Jupiter & Saturn as sloping convection?

Given that the relevant similarity parameters (e.g. Rossby, Richardson and Burger numbers) are of comparable magnitude for the long-lived Jovian and Saturnian eddies and the baroclinic eddies in the laboratory (although disputes continue concerning the Burger number, e.g. see Read 1986a), it is plausible that the atmospheric features may indeed represent a form of sloping convection similar to that obtained in the internally-heated annulus. The detailed resemblance between the mean flow structures, eddy flow patterns and thermal structures (so far as they can be determined for the major planets) serve to support such an analogy, although these factors are not entirely conclusive in themselves. The relevance of quasi-geostrophic 'free modes' to the laboratory flows, as discussed in Lecture 4, may also be of importance in this context, since similar theoretical solutions form significant components of many competing theories of the Jovian features (see Read 1986a). Further observations tailored towards answering the many questions which arise from this hypothesis are clearly required, almost certainly necessitating data from new spacecraft missions in due course (currently planned missions include 'Galileo' orbiter and probe to Jupiter and the Hubble Space Telescope - both seriously delayed by the recent Space Shuttle disaster!).

Nonetheless, the available observations do demonstrate that eddies occur in the atmospheres of the major planets which are characterised by a high degree

of symmetry in the spatial organisation of the flow, and long persistence times despite the presence of chaotic small-scale features in the background flow. Laboratory studies have indicated the importance of non-linear advection in helping to sustain the regular flows, which would seem to contradict the conclusions of some theories of atmospheric predictability concerning the role of advection in promoting the breakdown of an initial pattern of flow into irregular chaotic motion. Should it ultimately be demonstrated that the long-lived eddies on Jupiter and Saturn are manifestations of sloping convection, it would serve to confirm the latter process as an important paradigm for large-scale flows in planetary atmospheres.

#### REFERENCES

- Flasar, F. M., 1986. 'Global dynamics and thermal structure of Jupiter's atmosphere', Icarus, **65**, 280-303.
- Gierasch, P. J., Conrath, B. J. & Magalhaes, J. A., 1986. 'Zonal mean properties of Jupiter's upper troposphere from Voyager infrared observations', Icarus, in press.
- Hide, R., 1981. 'High vorticity regions in rotating thermally-driven flows', Met. Mag., **110**, 335-344.
- Hide, R. & Mason, P. J., 1970. 'Baroclinic waves in a rotating fluid subject to internal heating', Phil. Trans. R. Soc. Lond., **A268**, 201-232.
- Hide, R. & Mason, P. J., 1975. 'Sloping convection in a rotating fluid', Adv. Phys., **24**, 47-100.
- Ingersoll, A. P., 1981. 'Jupiter and Saturn', Sci. American, **245**, 66-80.
- Ingersoll, A. P., Beebe, R. F., Conrath, B. J. & Hunt, G. E., 1984. 'Structure and dynamics of Saturn's atmosphere', in Saturn (T. Gehrels & M. S. Matthews eds.), pp. 195-238. University of Arizona Press, Tucson.

- Mason, P. J., 1975. 'Baroclinic waves in a container with sloping endwalls', Phil. Trans. R. Soc. Lond., **A278**, 397-445.
- Quon, C., 1977. 'Axisymmetric states of an internally-heated rotating annulus', Tellus, **29**, 83-96.
- Read, P. L., 1986a. 'Stable, baroclinic eddies on Jupiter and Saturn: a laboratory analog and some observational tests', Icarus, **65**, 304-334.
- Read, P. L., 1986b. 'Regimes of axisymmetric flow in an internally-heated, rotating fluid', J. Fluid Mech., **168**, 255-289.
- Read, P. L. & Hide, R., 1983. 'Long-lived eddies in the laboratory and in the atmospheres of Jupiter and Saturn', Nature, **302**, 126-129.
- Read, P. L. & Hide, R., 1984. 'An isolated baroclinic eddy as an analogue of the Great Red Spot on Jupiter', Nature, **308**, 45-48.
- Williams, G. P., 1986. 'Jovian and comparative atmospheric modelling', Adv. in Geophys., **28A**, 381-429.

P. L. Read  
Met. O. 21  
August 1986

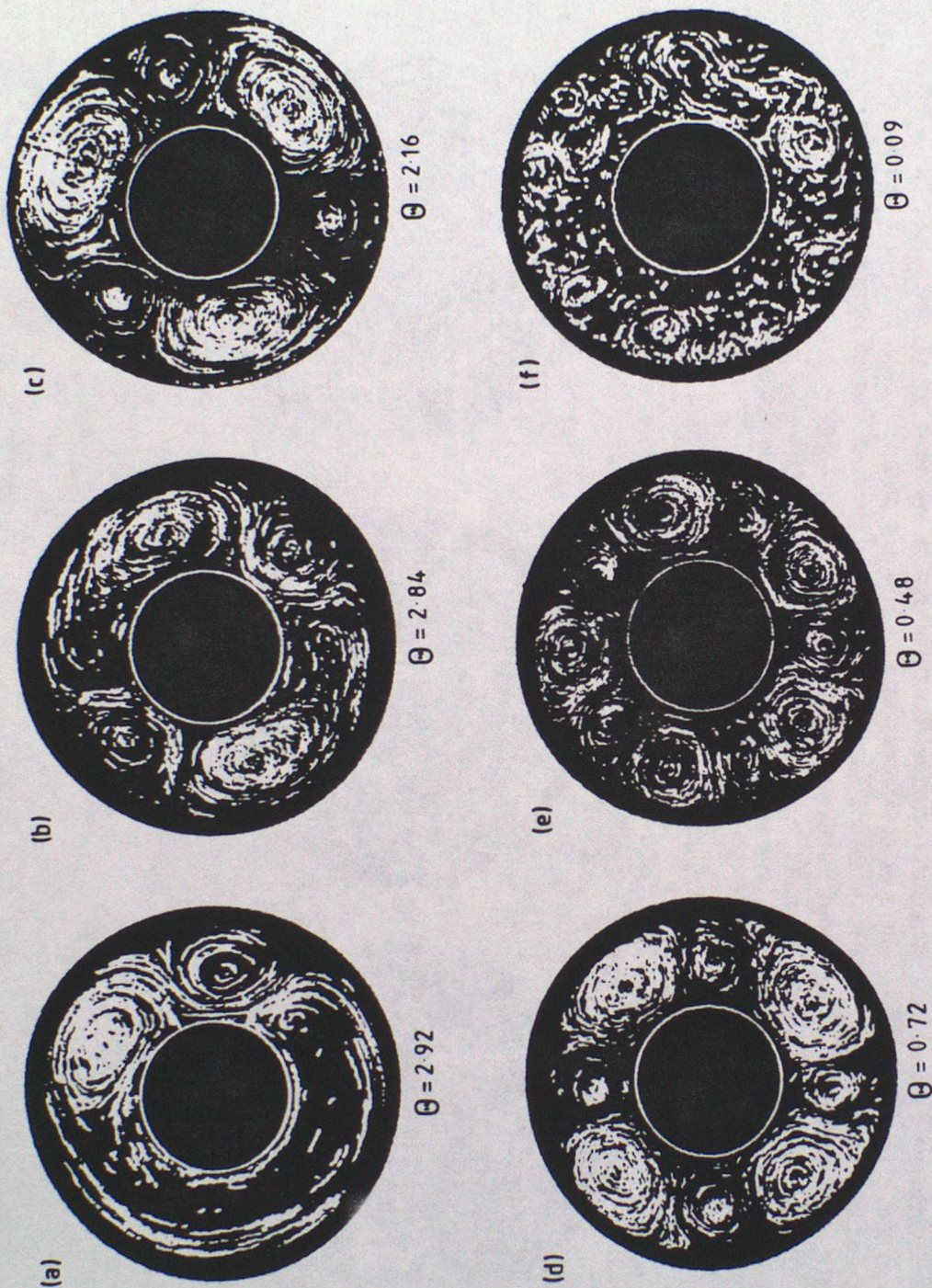
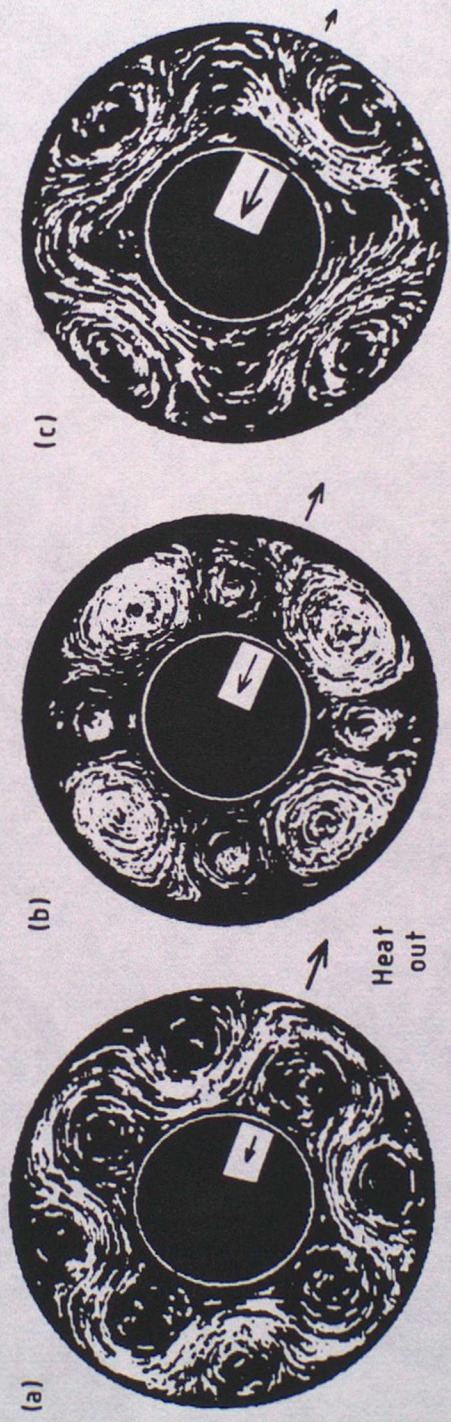


Figure 1

**REGULAR & IRREGULAR WAVES IN AN INTERNALLY-HEATED ROTATING ANNULUS**  
 AS WITH THE BOUNDARY-HEATED ANNULUS, THE ZONAL WAVELENGTH  $m$  OF THE FLOW IN AN INTERNALLY-HEATED ANNULUS (WITH  $T = T_1$ ) DEPENDS ON  $\Omega$ . LOWER ROTATION RATES TEND TO FAVOUR SMALLER WAVELENGTHS, BUT  $m = 2$  [(b)] AND THE NEARLY-ISOLATED  $m = 1$  [(a)] FLOWS OCCUR ONLY AT HIGH TAYLOR NUMBER WITH STRONG HEATING. FOR MODERATE  $\Omega$ , THE FLOW IS REGULAR AND STEADY. AT HIGHER ROTATION RATES AND FOR  $m > 5$ , THE FLOW BECOMES TIME-DEPENDENT WITH THE ONSET OF QUASI-PERIODIC OR APERIODIC 'WAVELENGTH VARIATION', PROGRESSING TO FULLY IRREGULAR, CHAOTIC FLOW AT THE LARGEST VALUES OF  $\Omega$  (E.G. (f)).

Figure 2

DEPENDENCE OF UPPER LEVEL FLOW PATTERN ON IMPRESSED TEMPERATURE GRADIENT BY HEATING/COOLING THE FLUID DIRECTLY (E.G. WITH OHMIC HEATING, USING A WEAK ELECTROLYTE AS WORKING FLUID AND PASSING AN ELECTRIC CURRENT BETWEEN THE SIDE-WALLS), AS WELL AS AT THE BOUNDARIES, A WIDE VARIETY OF DIFFERENT FLOW PATTERNS CAN BE OBTAINED (THE VARIOUS POSSIBLE FLOWS ARE ILLUSTRATED SCHEMATICALLY LEFT). SUCH FLOWS CAN ALSO TRANSFER HEAT BY SLOPING CONVECTION. INTERNAL HEATING IN A ROTATING FLUID GENERATES UPPER LEVEL FLOWS CHARACTERISED BY ANTI-CYCLONIC LATERAL SHEAR. THE RELATIVE STRENGTHS OF CLOSED EDDIES AND MEANDERING JET STREAMS THEN DEPENDS UPON THE LOCATION AND INTENSITY OF THE HEAT SINKS, WHICH CAN BE CONTROLLED BY THE SIDE-WALL THERMAL BOUNDARY CONDITIONS (I.E.  $(T_b - T_a)$  OR  $dt/dr$ ). IF  $T_b = T_a$  EQUAL AMOUNTS OF HEAT ARE EXTRACTED AT BOTH BOUNDARIES, AND THE FLOW IS DOMINATED BY CLOSED EDDIES. IF  $T_b > ( ) T_a$ , MORE (LESS) HEAT IS EXTRACTED AT THE INNER SIDEWALL (THE EXTREME CASE BEING WHEN  $dt/dr$  OR  $dt/dt = 0$ , SEE ABOVE) AND THE MEANDERING JET STREAM ADJACENT TO THE MORE STRONGLY COOLED SIDE-WALL IS STRENGTHENED. SOME STREAK PHOTOGRAPHS ILLUSTRATING CASES FOR DIFFERENT VALUES OF  $(T_b - T_a)$  ARE SHOWN BELOW.



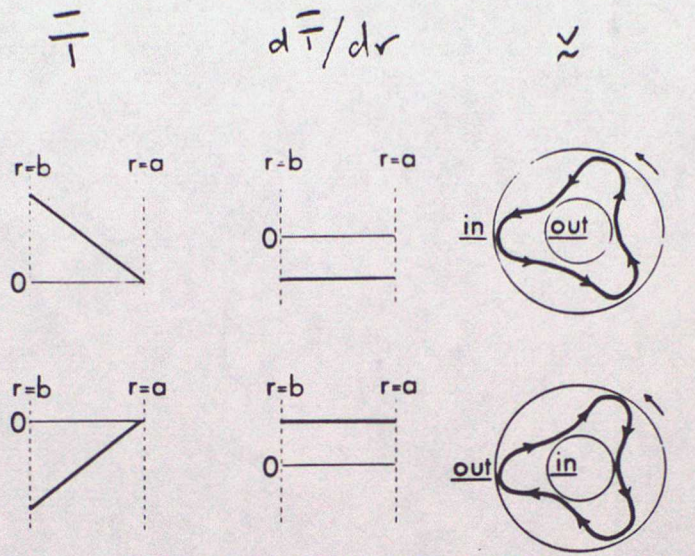
$(T_b - T_a)/K$

-3

0

+3

Wall Heating



Internal Heating

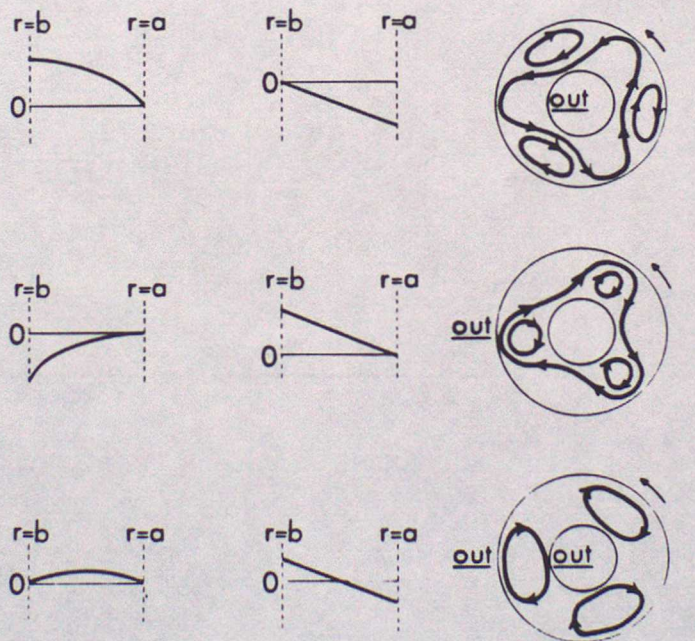
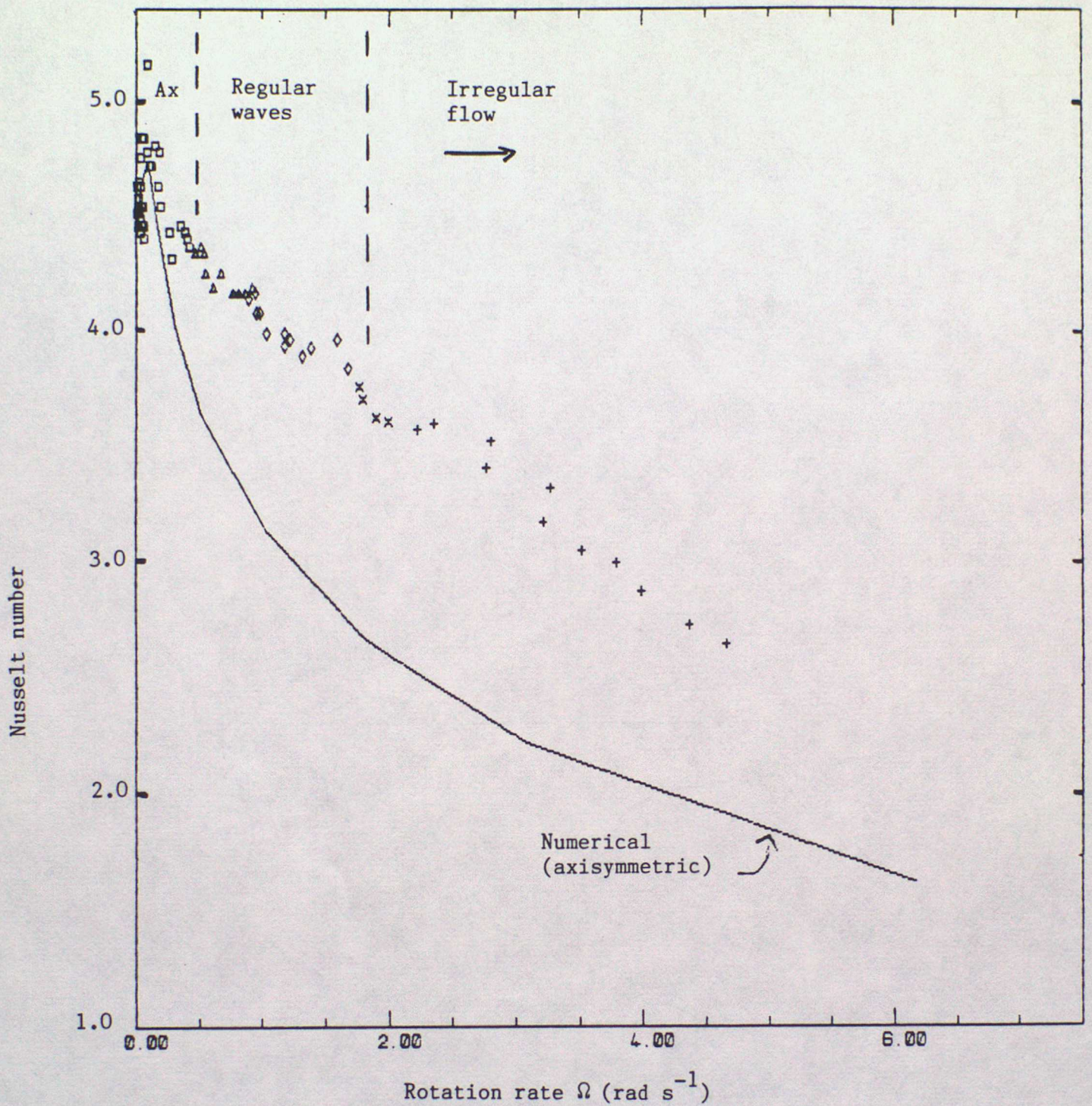


Figure 3: Schematic illustrations of the variations of the impressed temperature gradient with radius  $r$  (left column);  $dT/dr$ , proportional to minus the top surface zonal velocity (see Eq (1)) (centre column); and the main characteristics of the top surface flow pattern in the steady wave regime based on the integral constraints expressed in Eq (1) (right column) - see text and Hide & Mason (1970, 1975).



KEY

- ---- Numerical (axisymm.)
- ---- Lab. (axisymm.)
- △ ---- Lab. (m=3)
- ◇ ---- Lab. (m=4)
- × ---- Lab. (m=4-6 wnv)
- + ---- Lab. (irr.)

Figure 4: Variation of Nusselt number (a measure of the total heat transfer with respect to that due to conduction alone) for an internally-heated annulus as a function of rotation rate  $\Omega$ . Results shown are laboratory measurements by Read (1986b and unpublished) for various baroclinic wavenumbers (denoted  $m$ ), compared with the axisymmetric heat transfer over the same range of  $\Omega$ , obtained from an axisymmetric numerical model (Read 1986b). The terms 'wnv' and 'irr.' denote wavenumber vacillation (a form of structural vacillation) and irregular flows respectively.

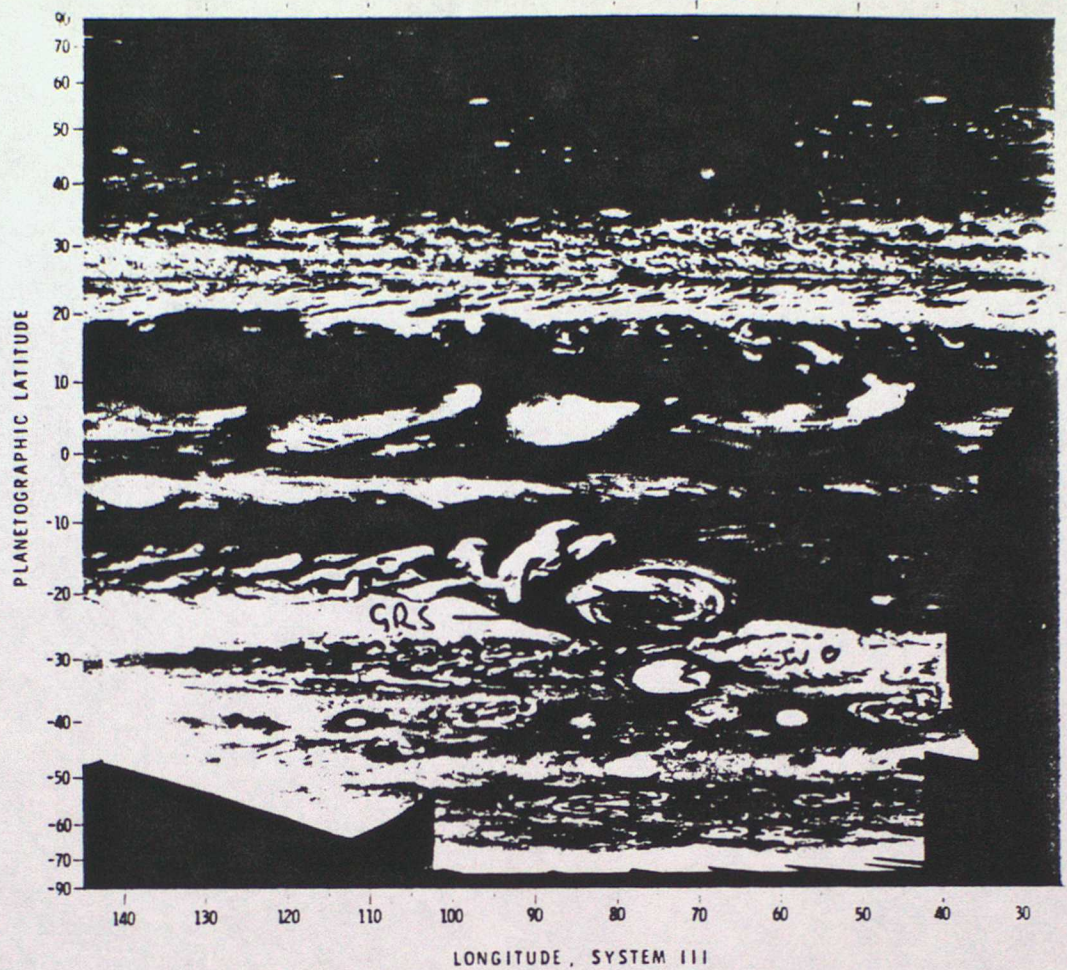
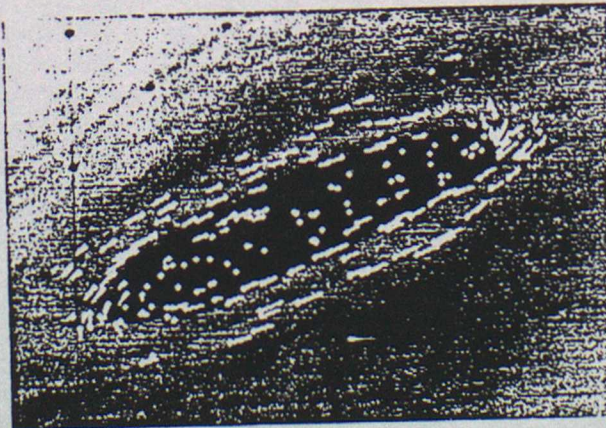


Figure 5: Some examples of long-lived oval eddies in the atmospheres of Jupiter and Saturn: a) Jupiter in a cylindrical projection (from Voyager spacecraft images), showing the Great Red Spot (GRS), White Oval (WO) and other smaller features.



(b) Brown Spot 1 on two successive Saturn rotations, showing anticyclonic (clockwise in the northern hemisphere) rotation around its periphery. North is to the upper right. The spot's latitude is  $42.5^{\circ}\text{N}$  and it drifts to the east at  $5 \text{ m sec}^{-1}$ . The major diameter of the spot is 5000 km. A green filter was used in these narrow-angle images taken about 2 days before Voyager 2's encounter with Saturn.



(c) Velocity vectors superimposed onto an image of a long-lived cyclonic «barge» on Jupiter, obtained from «Voyager» data by Hatzes et al. (1981). The tails on the vectors point in the direction of the flow.

Lecture 7: Numerical modelling of annulus flows

There are two main reasons why numerical modelling of annulus flows is important:

(i) through comparisons of model results with good laboratory measurements it is possible to test numerical models of rotating baroclinic flow in a unique way;

(ii) good simulations provide extensive data which are invaluable in understanding the flows and in constructing simplified mathematical and conceptual models.

In this lecture both (i) and (ii) will be discussed, but the emphasis will be on (i). The annulus system we shall consider is the familiar 'wall-heated' one in which concentric cylinders are maintained at different temperatures. (The upper and lower bounding surfaces are horizontal and rigid.) The numerical model - the 'Met 0 21 model' - is a grid point formulation based on the (nonhydrostatic) Navier-Stokes equations for the motion of an incompressible baroclinic fluid; a typical resolution is 16 (vertical) x 16 (radial) x 64 (zonal) points. Details are given by James et al (1981) and Hignett et al (1985), and a similar - though slightly less comprehensive - model was used by Williams (1969),(1971).

In the atmosphere the forcing processes are many and various. Momentum sources and sinks arise from sub-grid-scale motions of several different types: small-scale turbulence, cumulus convection, cumulonimbus, gravity wave motion &c. Diabatic heating and cooling occur as a result of radiative effects, sub-grid-scale motion (see above), latent heat release/absorption in condensation/evaporation &c. All these processes are highly variable in space and time, and their representation or 'parametrization' in atmospheric numerical models is a matter of considerable complexity and uncertainty.

On the other hand, in laboratory systems such as the rotating baroclinic annulus the only significant forcing processes are molecular viscosity and conductivity (which can be represented to high accuracy using established formulae), and over wide ranges of conditions all flow scales can be resolved by tractable grids. Thus no "parametrizations" are required in numerical simulations of these systems; and comparison with experimental measurements enables the dynamical formulation of numerical models to be tested ('verified') to an extent which is virtually impossible for atmospheric models through direct comparison with meteorological data.

Comparisons with laboratory measurements can be made at a qualitative and a quantitative level.

#### Qualitative

The main flow phenomena of the wall-heated rotating annulus are axisymmetric flow, steady waves, intransitivity, wavenumber transitions, hysteresis, amplitude vacillation, structural vacillation and irregular flow. All of these have been qualitatively simulated using the Met 0 21 model (though little attention has been paid as yet to structural vacillation and irregular flow). See Hignett et al for a detailed description.

#### Quantitative: non-axisymmetric flow

Hignett et al also describe a quantitative comparison of a steady wave 3 flow in the 'small annulus' system (inner and outer radii 2.5 and 8.0 cm, depth 14.0cm) for a temperature difference of 4 deg C and a rotation rate of 1.0 rad s<sup>-4</sup>.

Temperatures are measured at mid-radius and mid-depth using a ring of 32 thermocouple junctions. Total heat flux by the working fluid is calculated from the inflow and outflow temperatures of the water circulating in the inner (cool) wall. In a physically separate apparatus having the same dimensions, horizontal velocity components are obtained at 5 levels using a particle tracking technique.

Table 1 and Figure 1 show some of the experimentally measured quantities and the corresponding numerical model values. Note that the simulated main-wave phase speed is in better agreement with the value determined from the temperature

	LABORATORY EXPERIMENT	NUMERICAL MODEL
MAIN-WAVE TEMPERATURE AMPLITUDE *	0.27 deg C	0.28 deg C
NUSSELT NUMBER	9.2	10.4
MAIN-WAVE PHASE SPEED (i) FROM T (ii) FROM $V^\ddagger$	$3.54 \times 10^{-3} \text{ rad s}^{-1}$ $7.80 \times 10^{-3} \text{ rad s}^{-1}$	$7.90 \times 10^{-3} \text{ rad s}^{-1}$
ZONAL MEAN FLOW (MAXIMUM)	$0.26 \text{ cm s}^{-1}$	$0.23 \text{ cm s}^{-1}$

\* Fourier wave 3 at mid-radius and mid-height

‡ No thermocouple ring present in fluid

TABLE 1 Comparison of laboratory measurements and numerical simulation. For annulus dimensions and external conditions see text. The Nusselt Number is a non-dimensional measure of the total heat transport between the warm and cool bounding cylinders of the annulus.

field. This is encouraging because the particle tracking system disturbs the flow less than the ring of thermocouple junctions does - and the numerical model assumes no disturbance by any measuring system. Total heat fluxes are in agreement to within 15% and main-wave temperature amplitudes to better than 5%. The agreement between the measured and simulated zonal mean flow (Figure 1) is very good at all 5 levels. A marked 'double-jet' structure is present. This feature is typical of steady wave flows and is important theoretically (see below): Figure 2 compares the numerical results for steady wave and axisymmetric flow.

#### Quantitative: axisymmetric flow

Recent work in Met 0 21 has focussed on comparisons of simulated and measured axisymmetric flow. High resolution integrations are fairly economical in the axisymmetric case and so it is easy to examine resolution effects. Figure 3 shows results from a series of such comparisons. There is very good agreement between the measured and simulated fluxes; in fact, the lower resolution (16x16) numerical results are closer to the measured fluxes than the high resolution (32x32) results are - although both are within the the estimated error of the measurements.

These comparisons revealed an unexpected weakness in the Dufort-Frankel viscous scheme. At low rotation rates and high resolution (but not otherwise) the model produced spurious circulations near the inner cylinder and heat fluxes which were too high by 5 to 10%. These numerical phenomena were traced to the Dufort-Frankel representation of the viscous terms after a long series of model reformulations. Use of a simpler (and less numerically robust!) viscous scheme cured the problem and led to the quantitatively pleasing results shown in Figure 3 for  $\Omega = 0.1 \text{ rad s}^{-1}$ . This is a good illustration of the use of annulus flows to test numerical schemes.

#### Theoretical models of annulus flows

The transition from axisymmetric to non-axisymmetric flow is quite well explained by the short-wave cut-off which is found in the Eady problem (lecture 3). Eady waves are unstable only for nondimensional wavenumbers  $p < 2.399$ . Thus, in a given annulus, the minimum allowable value of  $p$  may be greater than 2.399 and so no instability occur: the unstable waves may be too big to fit into

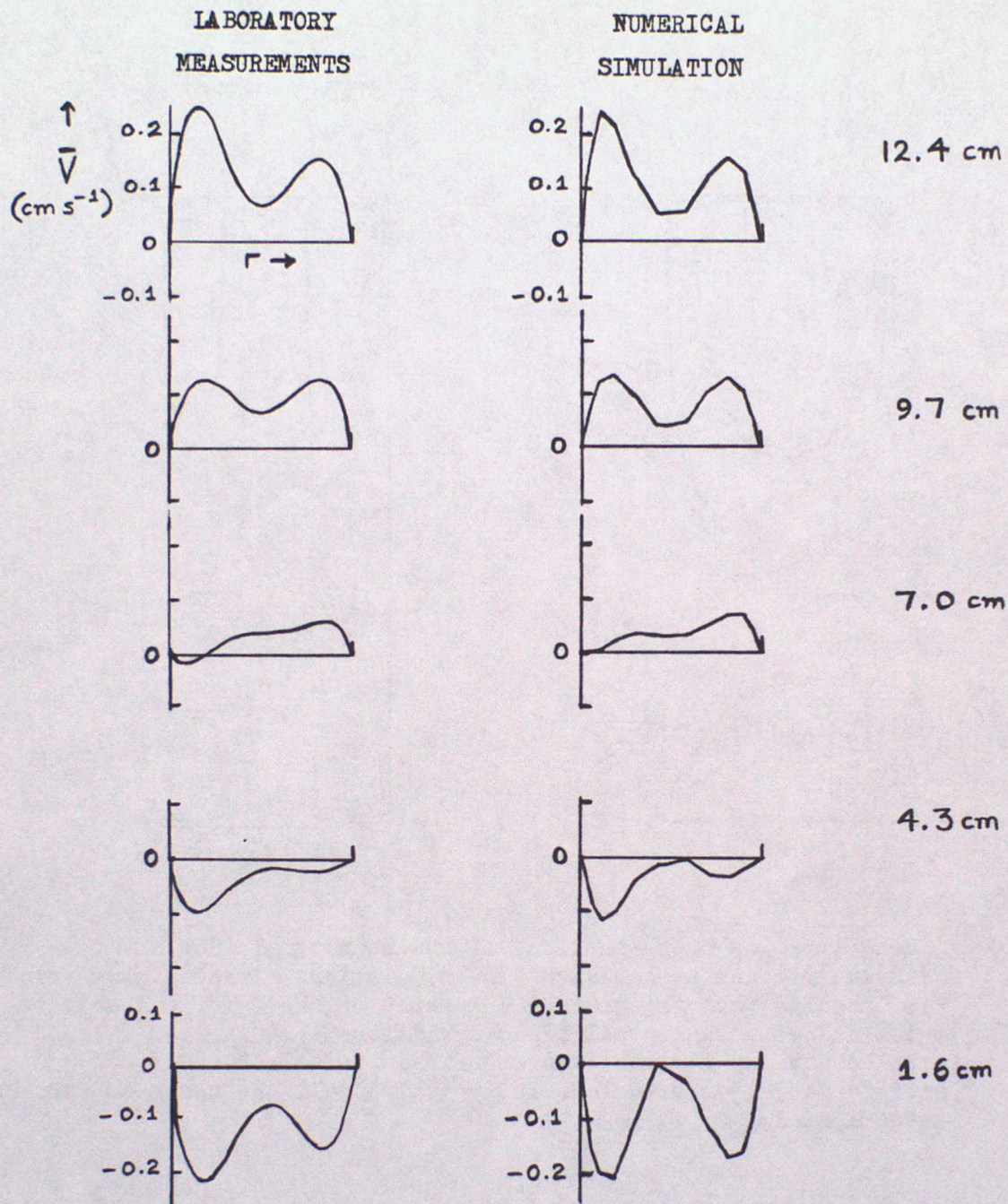
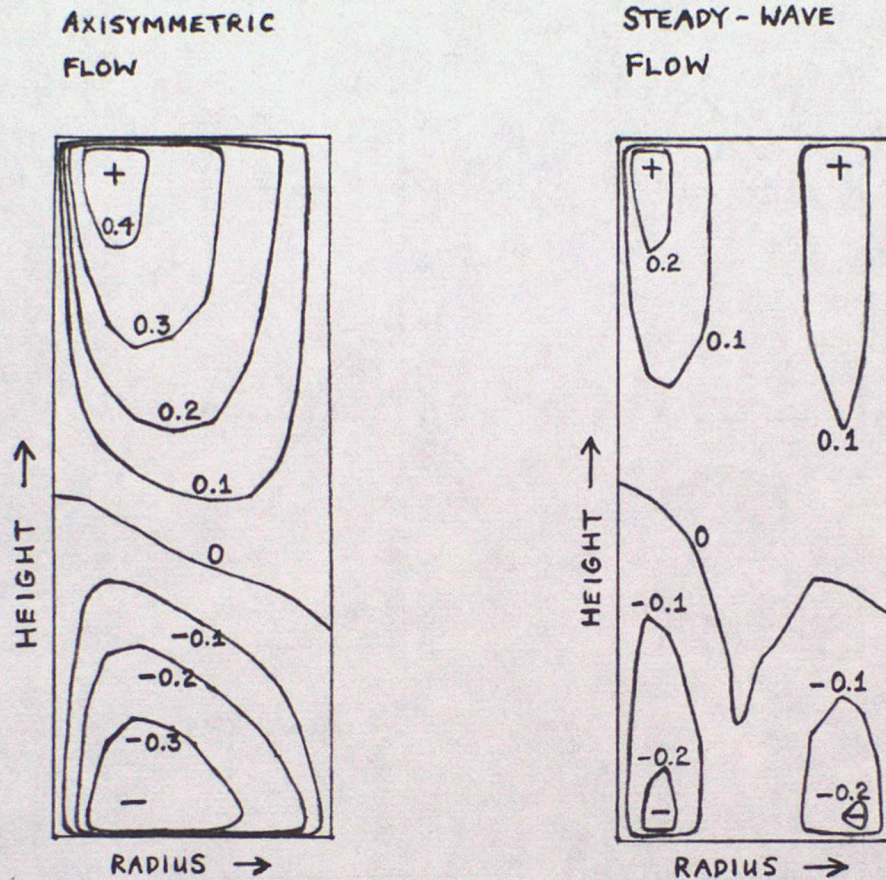


FIG 1 Radial variation of mean zonal flow at 5 equally spaced levels according to laboratory measurements and numerical simulation. See text for annulus dimensions and applied external conditions.



**FIG 2** Height/radius cross-sections of the mean zonal flow in axisymmetric and steady-wave flow simulations. The axisymmetric flow results from integrating a version of the numerical model which allows no azimuthal field variations. Parameter values are the same as for the case described in Table 1. The difference in jet structure is typical of all the cases so far investigated. Units  $\text{cm s}^{-1}$ .

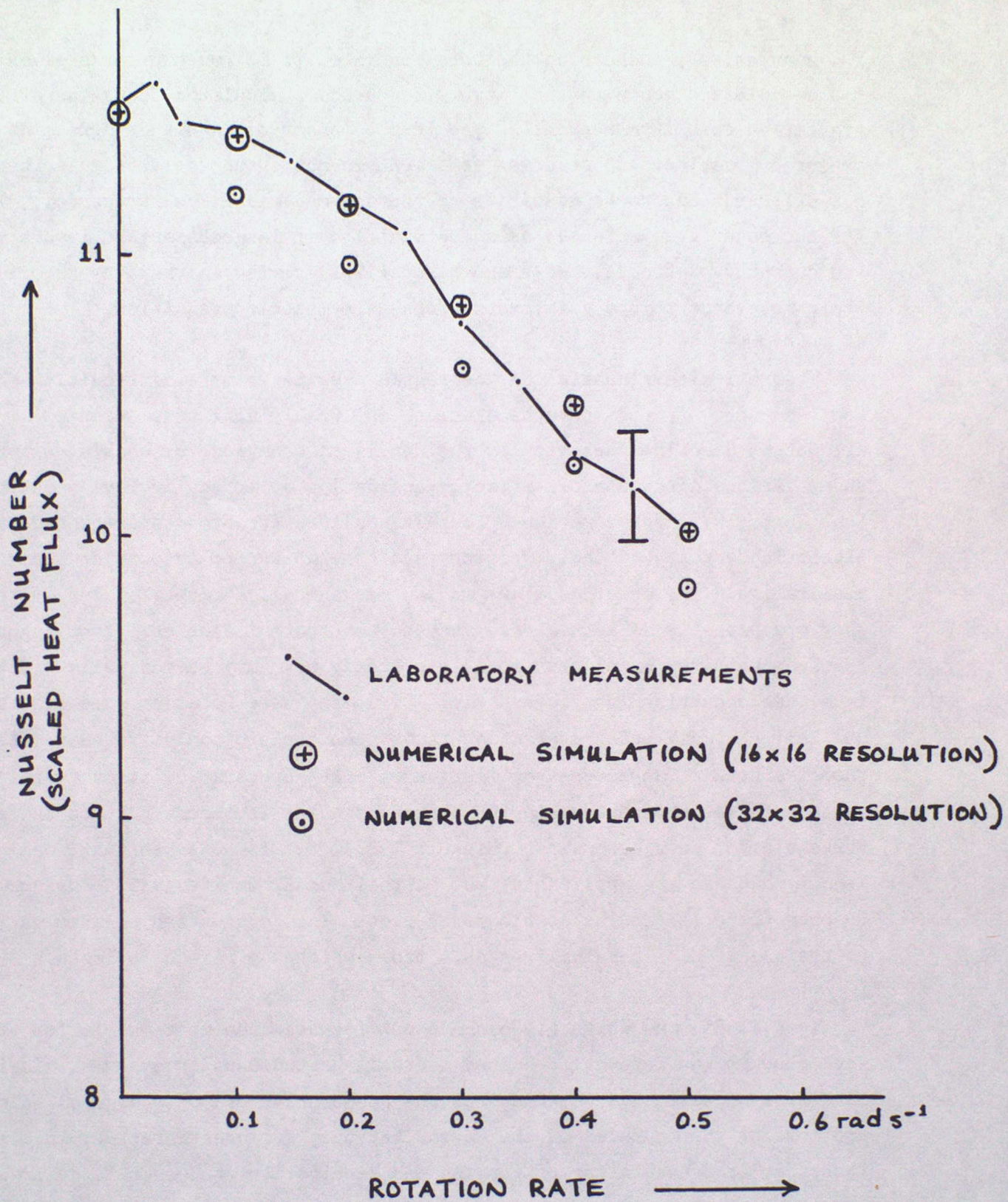


FIG 3 Measured and numerically simulated total heat fluxes in the 'small annulus' system at rotation rates up to  $0.5 \text{ rad s}^{-1}$  (beyond which non-axisymmetric motion occurs). The error bar indicates the uncertainty in the heat flux measurements.

the annulus. By increasing the rotation rate,  $\rho$  is reduced for a given true space scale and hence instability is favoured. Calculated locations of the upper transition to axisymmetric flow are in good order-of-magnitude agreement with the measured location. (A stronger statement is not supportable because the theoretical cut-off turns out to be sensitive to the assumed mean flow structure.) To account for the lower transition to axisymmetric flow it is necessary to invoke viscous and conductive effects. Hide and Mason (1975) review instability theories and their relevance to the axisymmetric/non-axisymmetric transition.

Theoretical explanation of the regular regime is more difficult. Much work has been done by applied mathematicians on 'weakly nonlinear theories'. These attempt to describe analytically the nonlinear behaviour of weakly unstable waves: under various circumstances steady, vacillating or irregular wave solutions occur (see Hart (1979) for a review). Weakly nonlinear treatments are monuments to the algebraic tenacity of their creators and they appear to account at least qualitatively for observed flows in the mechanically-driven 2-layer system; but they are probably of little relevance to the thermal annulus. From Figure 2 it is clear that the zonal mean flow in a steady wave may be radically different from that occurring in axisymmetric flow at the same rotation rate and it seems unlikely that any weak interaction theory can explain the difference. Also, the theories predict amplitude vacillation at high supercriticalities (within their assumed framework) whereas in the thermal annulus it occurs next to the stability threshold for each wavenumber (Hignett 1985). It is possible that weakly nonlinear theories are applicable, but in their usual manifestations assume an inappropriate marginally stable zonal flow. This suggestion relates very much to the question of marginally-stable flows which was raised in lecture 3.

Read (1985) and White (1986) have put forward free-mode models for steady wave flow in the internally-heated and wall-heated annulus systems. Their models have some success in accounting for the gross structure of the zonal mean flow and some of the features of the waves, but they are unsatisfactory in some respects; representation of forcing and dissipative processes is desirable but mathematically unsavoury.

The transition to irregular flow is broadly accounted for by the theory of Rossby wave instability (see Grotjahn (1984) for references). Behaviour in

irregular flow should be comparable with theories of geostrophic turbulence (see Charney (1971)) but little work has yet been done on this comparison. A practical difficulty is that irregular flow is attainable in Met O 21's present laboratory systems only under extreme experimental conditions.

### References

- Charney, J.G. 1971 J.Atmos.Sci., 28, 1087-1095
- Grotjahn, R. 1984 Quart.J.R.Met.Soc., 110, 663-668
- Hart, J.E. 1979 Ann.Rev.Fluid Mechanics, 11, 147-172
- Hide, R. and Mason, P.J. 1975 Advances in Physics, 24, 47-100
- Hignett, P., White, A.A., 1985 Quart.J.R.Met.Soc., 111, 131-154
- Carter, R.D., Jackson, W.D.N.  
and Small, R.M.
- James, I.N., Jonas, P.R. 1981 Ibid., 107, 51-78  
and Farnell, L.
- Read, P.L. 1985 Dyn.Atmos.Oceans, 9, 135-207
- White, A.A. 1986 Quart.J.R.Met.Soc., 112, 749-773
- Williams, G.P. 1969 J.Fluid Mech., 37, 727-750
- 1971 Ibid., 49, 417-449

QUARTERLY JOURNAL  
OF THE  
ROYAL METEOROLOGICAL SOCIETY

Vol. 103

JANUARY 1977

No. 435

*Quart. J. R. Met. Soc.* (1977), 103, pp. 1-28

551.511.32: 532.5

Experiments with rotating fluids

By R. HIDE

(Presidential Address: 21 April 1976)

1. INTRODUCTION

At the turn of the present century an eminent physicist expressed the firm opinion that perfectly accurate weather forecasts would be available by the year 1950. He did not consider it necessary to explain how this development would come about, presumably because he shared the view of many of his contemporaries that further work on macroscopic systems satisfying the laws of classical physics would be a matter of mere routine, requiring no more than the diligent efforts of a sufficient number of dedicated but not necessarily inspired investigators. This attitude led to the neglect of important areas of physics, so it is hardly surprising to find today, with three-quarters of the twentieth century gone, that insufficient knowledge of various hydrodynamical processes still constitutes a major difficulty not only in meteorology, but also in oceanography and other geophysical sciences.

In this address I propose to discuss one area of 'geophysical fluid dynamics' in which I have been engaged with various colleagues over a number of years, namely the study of rapidly-rotating fluids. Our work has, by choice, centred largely on laboratory investigations, but mathematical studies are found necessary in the formulation of crucial experiments and the interpretation of their results. Numerical studies employing high-speed electronic computers are becoming increasingly important in our work, but in spite of their many attractions computers are still comparatively very expensive to use and to date they have been employed successfully only in detailed investigations of the less complex types of flow encountered in laboratory work.

It is unnecessary to apologize for discussing simple systems that can be realized in the laboratory, and asserting their relevance to the science of atmospheres and oceans, since the essence of basic science, upon which all applied science depends, is the obtaining of general results concerning well-defined problems, not limited results concerning only vaguely-defined problems. A critical review of recent progress made with the study of rotating fluids would, however, take much more than an hour to present and interest only specialists in dynamics, so in preparing this address to a wider audience I considered it preferable to take a didactic approach, with a view to showing that a few theorems and other basic theoretical results (see section 2) suffice to provide considerable insight into the behaviour of a variety of mechanically and thermally-driven systems, such as those few selected for discussion under the various section headings of this paper, namely flows due to oscillatory mechanical forcing (section 3), steady source-sink flows (section 4) and thermal convection due to an impressed horizontal temperature gradient (section 5).

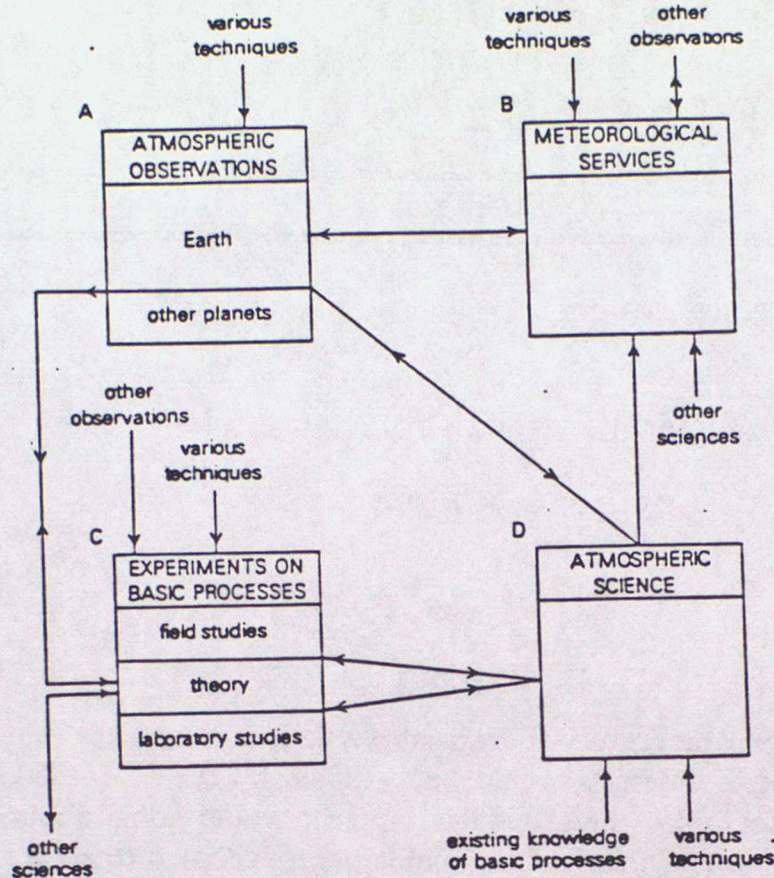


Figure 1. An attempt to illustrate the relationship between atmospheric science, applied meteorology and research on basic processes (see text).

But with an audience consisting mainly of meteorologists it is necessary before going into details to consider how the study of basic processes bears on atmospheric science generally and is thus able to contribute, at least potentially, to practical meteorology. A rough and inevitably over-simplified attempt to portray the complex relationships involved is illustrated in Fig. 1. Box B at the top right-hand corner represents meteorological services, the provision of which to the public and to other scientists involves the application of meteorological knowledge to a wide range of practical problems. Box A at the top left represents the routine acquisition and analysis of (a) observations of the earth's atmosphere, which are made largely to meet the needs of meteorological services, and (b) observations of the atmospheres of other planets, the collection of which was initiated over a century ago by amateur astronomers but is now undertaken in collaboration with observatories staffed with professional workers. Box D at the bottom right represents the development of a body of knowledge known as atmospheric science, which comprises the systematic description or interpretation of atmospheric phenomena, as revealed by observations, in terms of basic physical\* and chemical processes. Box C at the bottom left represents research on basic processes, involving experimental field or laboratory (including numerical) investigations rendered crucial through close contact with appropriate theory. Box C would not, of course, be needed if the textbooks of physics and chemistry contained all the information and ideas required for the purposes of atmospheric science.

Theory without contact with experiments is an uncertain and often pointless venture and the direct link AD between observations and atmospheric science is weaker than the indirect link through the intermediary of experiments on basic processes (box C). The link AC involves speculation, but when this is followed by well-formulated theories fully tested

\* Here 'physics' is taken in the generally accepted sense and not as implied by unfortunate jargon employed by some dynamical meteorologists when, in their descriptions of numerical models of large-scale motions in the atmosphere, they use the term to refer to processes not explicitly represented in the models, such as small-scale dynamical processes, radiation, clouds, etc.

by crucial field or laboratory studies, true scientific advances are made and, what is equally important, practical meteorologists are presented with opportunities to improve the services they are asked to provide. Laboratory experiments with rotating fluids fall within the middle and lower subdivisions of box C. They are comparatively cheap to carry out and could easily be pursued without reference to observational studies in meteorology, oceanography, etc. Indeed, in retrospect one can see that some of the most relevant work has been motivated not by the direct demands of atmospheric science and practical meteorology but by sheer scientific curiosity. This state of affairs is by no means unusual when seen in the context of the development of ideas in other fields of science, and a few leading meteorologists have been quick to appreciate and exploit the results of laboratory work. Others, however, including several prominent workers, have evidently misunderstood the role of laboratory experiments by supposing, unjustifiably in my opinion, that the objective of the laboratory work should be the construction of purblind models merely for the purpose of improving the direct link AB or AD in Fig. 1. Much has been said by these critics about the differences between laboratory systems and the real atmosphere, and it is true that without a method of simulating a radially-symmetric gravitational field it will never be possible to construct a perfect laboratory 'model' in the engineering sense. But surely the very essence of the problem of understanding the circulation of the atmosphere is not just to create a replica but to study a hierarchy of related but different systems; it is a matter for investigation whether or not the shape of the boundary, for example, is important, not for *a priori* assessment (see e.g. Hide 1969, Monin 1972).

## 2. SOME USEFUL THEORETICAL RESULTS

(i) *Equations of motion of an incompressible Boussinesq fluid.* When dealing with most geophysical and laboratory systems it is sufficient to consider the behaviour of a fluid in which (a) the velocities are so small in comparison with the speed of sound that the assumption of incompressibility is valid, and (b) the accelerations are so small in comparison with gravity that the Boussinesq approximation (which takes density variations into account in the buoyancy term in the equations of motion but not in the other terms) can be used. When referred to a system that rotates with steady angular velocity  $\Omega$  relative to an inertial frame, the equations of continuity and momentum of such a fluid of uniform kinematic viscosity  $\nu$  and variable density  $\bar{\rho}(1 + \theta)$ , where  $\bar{\rho}$  is the mean density and  $\theta \ll 1$ , are:

$$\nabla \cdot \mathbf{u} = 0 \quad (2.1)$$

$$\text{and} \quad \partial \mathbf{u} / \partial t + (2\Omega + \xi) \times \mathbf{u} = -\nabla(P + \frac{1}{2}\mathbf{u} \cdot \mathbf{u}) + \mathbf{g}\theta + \nu \nabla^2 \mathbf{u} \quad (2.2)$$

Here  $\mathbf{u}$  is the Eulerian flow velocity relative to the rotating frame and  $\xi \equiv \nabla \times \mathbf{u}$  is the corresponding vorticity vector,  $t$  denotes time,  $\mathbf{g}$  the acceleration due to gravity plus centrifugal effects, and  $\bar{\rho} \nabla P$  is equal to the pressure gradient minus  $\mathbf{g}\bar{\rho}$ .

Variations in density may be due to changes in temperature, salinity, etc., and in general  $\theta$  satisfies an equation of the form

$$\partial \theta / \partial t + (\mathbf{u} \cdot \nabla) \theta = \chi \nabla^2 \theta + \bar{Q} \quad (2.3)$$

where  $\chi$  is a diffusion coefficient and  $\bar{Q}$  represents effects due to internal sources; in the case of thermally-driven flows  $\bar{Q}$  is proportional to the rate of internal heating per unit mass. When the r.h.s. of Eq. (2.3) vanishes we have

$$D\theta/Dt = 0 \quad (2.4)$$

(where  $D/Dt \equiv \partial/\partial t + \mathbf{u} \cdot \nabla$ ), implying that the value of  $\theta$  of an individual fluid element then remains constant throughout the motion.

(ii) *Energetics*. An energy equation follows from Eq. (2.2) when that equation is multiplied scalarly by  $\mathbf{u}$  (noting that the second term on the l.h.s. vanishes because it represents a force acting at right-angles to  $\mathbf{u}$  and therefore does no work); whence

$$\partial(\frac{1}{2}\mathbf{u}\cdot\mathbf{u})/\partial t = -\nu\xi\cdot\xi + \mathbf{u}\cdot\mathbf{g}\theta - \nabla\cdot[\frac{1}{2}\mathbf{u}(\mathbf{u}\cdot\mathbf{u}) + \mathbf{u}P + \nu(\xi\times\mathbf{u})]. \quad (2.5)$$

When integrated over a given volume, the l.h.s. represents the rate of change of total kinetic energy and the first term on the r.h.s. (which is essentially negative) represents viscous dissipation of kinetic energy. The second term on the r.h.s. represents the rate at which buoyancy forces convert into kinetic energy the potential energy of gravity acting on the density field. It can in general take either sign, depending on the sign of the average correlation between density variations, proportional to  $\theta$ , and the vertical component of velocity, proportional to  $\mathbf{u}\cdot\mathbf{g}$ , but in the case of thermally-driven motions (see e.g. Dutton and Johnson 1967; Van Mieghem 1973; also section 5 below) this buoyancy term is essentially positive when integrated over the whole system.

The last term on the r.h.s. represents mechanical forcing. When integrated, this term can be converted into a surface integral comprising three contributions representing, respectively, the advection of kinetic energy over the surface, the rate of working of normal pressure forces, and the rate of working of tangential viscous forces. Each contribution can take either sign but their sum when integrated over the whole system must be positive in cases of mechanically-driven flows (see sections 3 and 4).

(iii) *Vorticity equation; Jeffreys' theorem and Ertel's theorem*. Equation (2.2) expresses the balance of *forces* acting on individual fluid elements. The corresponding *torque* balance is expressed by the vorticity equation obtained by taking the curl of Eq. (2.2); thus

$$\partial\xi/\partial t + (\mathbf{u}\cdot\nabla)\xi - [(2\Omega + \xi)\cdot\nabla]\mathbf{u} = -\mathbf{g}\times\nabla\theta + \nu\nabla^2\xi. \quad (2.6)$$

This equation leads directly to a general result which goes under several names but is conveniently referred to as 'Jeffreys' theorem' and concerns the conditions under which hydrostatic equilibrium obtains, defined as  $\mathbf{u} = 0$  everywhere. By Eq. (2.6),  $\mathbf{u} = 0$  when  $\mathbf{g}\times\nabla\theta = 0$ , implying that *hydrostatic equilibrium is impossible if density variations occur on level surfaces*. Jeffreys' theorem is a direct corollary of Bjerknes' well-known circulation theorem (see Eliassen and Kleinschmidt 1957); it provides the most direct demonstration that the atmosphere *must* circulate under the influence of solar heating, which maintains a generally north-south density gradient on level surfaces.

We now introduce a quantity known as 'potential vorticity' and defined as

$$(2\Omega + \xi)\cdot\nabla\Lambda, \quad (2.7)$$

where  $\Lambda$  is any quantity satisfying

$$D\Lambda/Dt = 0 \quad (2.8)$$

(cf. Eq. (2.4)). By Eq. (2.6)

$$D[(2\Omega + \xi)\cdot\nabla\Lambda]/Dt = -(\mathbf{g}\times\nabla\theta)\cdot\nabla\Lambda + \nu\nabla\Lambda\cdot\nabla^2\xi \quad (2.9)$$

and therefore

$$D[(2\Omega + \xi)\cdot\nabla\Lambda]/Dt = 0 \quad (2.10)$$

when the fluid is homogeneous ( $\nabla\theta = 0$ ) and inviscid. This is Ertel's particularly useful theorem (see e.g. Charney 1973; Eliassen and Kleinschmidt 1957; Greenspan 1968; Krauss 1973; Pedlosky 1971) for an incompressible Boussinesq fluid.

(iv) *Two-dimensional flows: Taylor's theorem and Fjørtoft's theorem*. When the fluid is homogeneous ( $\nabla\theta = 0$ ) and, in virtue of the boundary conditions,  $\mathbf{u} = (u, v, w)$  is independent of the coordinate  $z$  parallel to the rotation axis, the relative vorticity has no (transverse)

components in the  $(x, y)$  directions (i.e.  $\xi = (\xi, \eta, \zeta) = (0, 0, \zeta)$ ) and the axial component of  $\xi$  satisfies

$$\partial\zeta/\partial t + u \partial\zeta/\partial x + v \partial\zeta/\partial y = \nu(\partial^2\zeta/\partial x^2 + \partial^2\zeta/\partial y^2). \quad (2.11)$$

The angular velocity vector  $\Omega$  does not appear in this equation, implying that *if  $\mathbf{u}$  is independent of  $z$  and the boundary conditions on  $\mathbf{u}$  are independent of  $\Omega$ , then  $\mathbf{u}$  is independent of  $\Omega$*  (see Taylor 1917). The pressure field, on the other hand, is *not* unaffected by rotation; by Eq. (2.2)  $P$  exceeds its value for  $\Omega = 0$  by an amount  $\hat{P}$  where

$$\nabla\hat{P} + 2\Omega \times \mathbf{u} = 0. \quad (2.12),$$

Laboratory experiments bearing on this theorem have been carried out by Taylor (1917) who demonstrated the existence of the  $\Omega$ -dependent part of the pressure field by determining the trajectories of moving objects, and by Hide (1968), who investigated flows due to various distributions of sources and sinks and demonstrated that  $\mathbf{u}$  is independent of  $\Omega$  when sources and sinks of the monopole (but not dipole) type are absent but not when they are present (see section 4).

The vanishing of the r.h.s. of Eq. (2.11) when viscous effects are negligible shows that in two-dimensional flow of an inviscid homogeneous fluid the vorticity remains constant throughout the motion (cf. Eq. (2.23) below), so that the total enstrophy (per unit length in the  $z$ -direction)

$$\mathcal{E} \equiv \iint \zeta^2 dx dy, \quad (2.13)$$

where the integral is taken over the whole system, remains fixed (i.e.  $d\mathcal{E}/dt = 0$ ). This result represents a powerful constraint on non-linear interactions between different scales of motion, for in order to conserve both total enstrophy and total kinetic energy (per unit length in the  $z$ -direction)

$$\mathcal{K} \equiv \iint \frac{1}{2}\bar{\rho}(u^2 + v^2) dx dy \quad (2.14)$$

(cf. Eq. (2.5)), *the transfer of energy from one scale to a smaller (larger) scale must be accompanied by the simultaneous transfer to a larger (smaller) scale*. Such behaviour of two-dimensional systems, as expressed by this 'anti-cascade' theorem of Fjørtoft and others (Fjørtoft 1953; for additional references see Charney 1973 and Lilly 1973) contrasts strongly with isotropic homogeneous three-dimensional turbulence, where the energy cascade from larger to smaller scales involves a rapid increase in enstrophy, associated with the three-dimensional stretching and twisting terms in the vorticity equation. Whereas the energy spectrum of three-dimensional turbulence follows Kolmogoroff's celebrated (wavenumber)<sup>-5/3</sup> (energy-dissipation rate)<sup>2/3</sup> law, that of two-dimensional turbulence satisfies a (wavenumber)<sup>-3</sup>(enstrophy-dissipation rate)<sup>2/3</sup> law.

(v) *Geostrophic flow; thermal wind equation and Proudman's theorem*. Geostrophic flow occurs in regions where the relative acceleration term  $D\mathbf{u}/Dt (= \partial\mathbf{u}/\partial t + \xi \times \mathbf{u} + \nabla(\frac{1}{2}\mathbf{u}\cdot\mathbf{u}))$  in Eq. (2.2) and the viscous term  $\nu\nabla^2\mathbf{u}$  can be neglected in comparison with the Coriolis term  $2\Omega \times \mathbf{u}$ . The Coriolis force then balances the non-hydrostatic component of the pressure force exactly, so that

$$2\Omega \times \mathbf{u} = -\nabla P + g\theta. \quad (2.15)$$

This equation is mathematically degenerate, being of lower order than the complete equation of motion and consequently incapable of solution under *all* the necessary boundary conditions and initial conditions, and it follows that *regions of highly ageostrophic flow (occurring not only on the boundaries of the system but also in the localized regions of the main body of fluid) are necessary concomitants of geostrophic motion*. The geostrophic equation nevertheless expresses with good accuracy various important properties that slow, steady hydrodynamical

flows in a rapidly-rotating fluid must possess nearly everywhere, and when judiciously applied the equation usually indicates the nature and location of essentially ageostrophic features.

A rapidly rotating fluid can be defined as one for which the Rossby number

$$\varepsilon \equiv \langle Du/Dt \rangle / \langle 2\Omega \times u \rangle \quad (2.16)$$

and the Ekman number

$$E \equiv \langle \nu \nabla^2 u \rangle / \langle 2\Omega \times u \rangle \quad (2.17)$$

are both very much less than unity, the symbol  $\langle \rangle$  meaning the root mean square value taken over the whole volume occupied by the fluid, so that  $\varepsilon = U/\tilde{L}\Omega$  and  $E = \nu/\tilde{L}^2\Omega$  if  $U$  is a typical relative flow speed and  $\tilde{L}$  a characteristic length scale. From a mathematical point of view, geostrophic flow occurs in the limit when  $\varepsilon \rightarrow 0$  and  $E \rightarrow 0$ . The vorticity equation (2.6) then simplifies to

$$(2\Omega \cdot \nabla)u = g \times \nabla\theta \quad (2.18)$$

expressing a balance between the gyroscopic torque and the gravitational torque.

When  $\nabla\theta = 0$  Eq. (2.18) reduces to

$$2\Omega \partial u / \partial z = 0, \quad (2.19)$$

a result first proved by Proudman (1916) and later by others and which goes under various names (e.g. Proudman's theorem, Proudman-Taylor theorem, Taylor-Proudman theorem). In words, Proudman's 'two-dimensional' theorem states that *geostrophic motion of a homogeneous fluid will be the same in all planes perpendicular to the axis of rotation*. This fundamental result underlies the interpretation of a very wide range of phenomena in mechanically-driven flows (see sections 3 and 4 below).

Suppose that  $(U, V, W)$  are the  $(X, Y, Z)$  components of  $u$ , where  $Z$  is the downward vertical coordinate, so that in these coordinates  $g = (0, 0, g)$ ,  $W$  is the corresponding vertical component of motion, and  $(U, V)$  are the horizontal components. When  $\nabla\theta \neq 0$  we have, by Eq. (2.18),

$$(2\Omega \cdot \nabla)(U, V, W) = g(-\partial\theta/\partial Y, \partial\theta/\partial X, 0). \quad (2.20)$$

In cases when the horizontal component of  $\Omega$  is negligible, the first two components of Eq. (2.20) give the familiar thermal wind equation, which expresses the relationship between the vertical rate of change of horizontal geostrophic motion and the horizontal density gradient. It may be shown (Hide 1971) by combining Eq. (2.20) with Eq. (2.4) and setting  $\partial\theta/\partial t = 0$  that under steady isentropic conditions

$$(2\Omega \cdot \nabla)(V/U) = -g \frac{W \partial\theta/\partial Z}{U^2 + V^2}, \quad (2.21)$$

implying that even when, as a result of strong density inhomogeneities, the *speed* of horizontal flow varies rapidly with respect to the axial coordinate  $z$ , the corresponding rate of change of the *direction* of horizontal flow may be quite slow and even vanish altogether when  $W \partial\theta/\partial Z = 0$ .

(vi) *Quasi-geostrophic flow of an inviscid fluid.* Quasi-geostrophic flow occurs when  $E \ll 1$  and  $\varepsilon \ll 1$ , and if  $E \ll \varepsilon$  the dominant ageostrophic contributions in the equations of quasi-geostrophic motion are provided by advective effects, not viscosity. Then

$$\partial u / \partial t + (u_1 \cdot \nabla_1)u + 2\Omega \times u = -\nabla P + g\theta \quad (2.22)$$

where  $\mathbf{u}_1 \cdot \nabla_1 \equiv u \partial / \partial x + v \partial / \partial y$ , and the corresponding equation for  $\zeta$  is

$$\partial \zeta / \partial t + (\mathbf{u}_1 \cdot \nabla_1) \zeta \doteq 2\Omega \partial w / \partial z - (\mathbf{g} \times \nabla \theta)_z \quad (2.23)$$

(see Eqs. (2.2), (2.6), (2.11), (2.16) and (2.17)). Equation (2.23) shows that *in quasi-geostrophic motion of a homogeneous (i.e.  $(\mathbf{g} \times \nabla \theta)_z = 0$ ) incompressible fluid, changes in the relative vorticity of a moving fluid element are brought about largely by axial stretching*, as represented by the term  $2\Omega \partial w / \partial z$  on the right-hand side.

Suppose for the moment that the buoyancy term can be neglected and that the fluid is bounded by rigid end-walls in  $z = z_l(x, y)$  and  $z = z_u(x, y)$  where  $z_u > z_l$ . When effects due to viscous boundary layers are negligible (see section 4), the term  $2\Omega \partial w / \partial z$  equals  $2\Omega \mathbf{u}_1 \cdot \nabla_1 \ln(z_u - z_l)$  (to sufficient accuracy) and the equation (2.23) reduces to an expression for the conservation of potential vorticity  $(2\Omega + \zeta) / (z_u - z_l)$ , namely

$$\{\partial / \partial t + \mathbf{u}_1 \cdot \nabla_1\} \{(2\Omega + \zeta) / (z_u - z_l)\} = 0. \quad (2.24)$$

(Equation (2.24) follows directly from Ertel's potential vorticity theorem given by Eq. (2.10) when  $\mathbf{u} \cdot \nabla$  is approximated by its transverse part  $\mathbf{u}_1 \cdot \nabla_1$  and  $\Lambda = (z - z_l) / (z_u - z_l)$  or  $\Lambda = (z_u - z) / (z_u - z_l)$ .)

If  $\theta$  satisfies Eq. (2.4) we can set  $\Lambda = \theta$  (cf. Eq. (2.8)) in Eq. (2.9), and if we further assume that  $v = 0$  the r.h.s. vanishes, giving

$$D[(2\Omega + \zeta) \cdot \nabla \theta] / Dt = 0. \quad (2.25)$$

In the geostrophic limit, this potential vorticity equation for a non-homogeneous fluid has no general form analogous to Eq. (2.24), but for a shallow system, such as the earth's atmosphere (see e.g. Charney 1973; Obukhov 1974; Pedlosky 1971; Phillips 1963), in which  $\varepsilon \ll 1$  (but  $> E$ ),  $\theta = \theta_0(Z) + \delta\theta$  with  $\delta\theta \ll \theta_0$ ,  $P = P_0(Z) + \delta P$  with  $\delta P \ll P_0$  and  $f$  is the vertical component of  $2\Omega$ , so that by Eq. (2.15)

$$(\xi)_z = -f^{-1}(\partial^2 / \partial X^2 + \partial^2 / \partial Y^2) \delta P \text{ and } \delta\theta = g^{-1} \partial(\delta P) / \partial Z, \quad (2.26)$$

Eq. (2.25) reduces to

$$\left( \frac{\partial}{\partial t} + U \frac{\partial}{\partial X} + V \frac{\partial}{\partial Y} \right) \left\{ \left( \frac{\partial \theta_0}{\partial Z} \right) \left[ f + \frac{1}{f} \left( \frac{\partial^2}{\partial X^2} + \frac{\partial^2}{\partial Y^2} + \frac{f^2 \partial^2 / \partial Z^2}{g \partial \theta_0 / \partial Z} \right) \right] \delta P \right\} = 0. \quad (2.27)$$

Equation (2.27) is of central importance in a wide range of theoretical investigations in dynamical meteorology and oceanography, including the study of 'geostrophic turbulence' (see section 5), where the constraints on potential vorticity represented by Eq. (2.27) (or (2.24)) place severe restrictions on the types of non-linear interactions that are possible. This results in behaviour (see e.g. Charney 1973; Lilly 1973; Rhines 1976) which is analogous in some respects to that of two-dimensional turbulence in a homogeneous fluid (see e.g. Eqs. (2.12) and (2.13) above and Figs. 10 and 11 below).

### 3. FLOWS DUE TO OSCILLATORY MECHANICAL FORCING

A fluid differs in an essential way from a solid in its inability in the absence of rotation (and of buoyancy forces due to the action of gravity on stable density stratification or magnetohydrodynamic effects) to resist shearing stresses and thereby support shear waves (see e.g. Lighthill 1966). When the fluid rotates relative to an inertial frame the constraints imposed on the system by angular momentum requirements are such as to endow the fluid with pseudo-elastic properties, and a brief account of the so-called 'elastoid-inertial oscillations' or, more briefly, 'inertial oscillations', which these properties make possible provides

a suitable starting point for our discussion of various phenomena encountered in the study of rotating fluids.

Relative to a state of solid-body rotation with angular velocity  $\Omega$ , a weak disturbance  $\mathbf{u}'(\mathbf{r}, t)$ ,  $P'(\mathbf{r}, t)$ ,  $\theta'(\mathbf{r}, t)$  ( $\mathbf{r}$  being the position vector) of an incompressible, uniformly and steadily-rotating, inviscid fluid which is stably stratified (i.e.  $\theta = \theta_0(Z)$  in the basic state and  $d\theta_0/dZ > 0$ , see Eqs. (2.1), (2.2) and (2.4)) satisfies the following linear equations

$$\nabla \cdot \mathbf{u}' = 0 \quad (3.1)$$

$$\partial \mathbf{u}' / \partial t + 2\Omega \times \mathbf{u}' = -\nabla P' + g\theta' \quad (3.2)$$

$$\partial \theta' / \partial t + W' d\theta_0/dZ = 0. \quad (3.3)$$

We can satisfy Eq. (3.1) by taking  $\mathbf{u}' = \nabla \times \mathbf{A}$ . The vorticity equation obtained by taking the curl of Eq. (3.2) (see Eq. (2.6)), namely

$$\partial \xi' / \partial t = (2\Omega \cdot \nabla) \mathbf{u}' - \mathbf{g} \times \nabla \theta' \quad (3.4)$$

(where  $\xi' = \text{curl } \mathbf{u}'$ ) then takes the form

$$\partial^2 (\nabla^2 \mathbf{A}) / \partial t^2 + (2\Omega \cdot \nabla) \partial (\nabla \times \mathbf{A}) / \partial t + (d\theta_0/dZ) \mathbf{g} \times \nabla (\nabla \times \mathbf{A})_z = 0 \quad (3.5)$$

when  $d\theta_0/dZ$  is constant.

There have been many studies of the highly anisotropic oscillations satisfying the wave-equation (3.5). It is instructive to consider disturbances on a scale much less than the dimensions of the container (but large enough to ensure that viscous dissipation is negligible). Such disturbances propagate as highly-dispersive elliptically-polarized shear waves – the ‘inertial-gravity waves’ – with Fourier components  $\exp i(\omega t - \boldsymbol{\kappa} \cdot \mathbf{r})$  where the angular frequency  $\omega$  is related to the wavenumber vector  $\boldsymbol{\kappa}$  through the dispersion relationship

$$\omega^2 = [(2\Omega \cdot \boldsymbol{\kappa})^2 + (\mathbf{N} \times \boldsymbol{\kappa})^2] / \boldsymbol{\kappa} \cdot \boldsymbol{\kappa}; \quad (3.6)$$

here  $\mathbf{N} \equiv gN/|g|$ ,  $N$  being the Brunt-Väisälä frequency ( $g d\theta_0/dZ$ )<sup>1/2</sup> (see Eckart 1960). Disturbances on larger scales, comparable with the dimensions of the boundaries of the system, such as the familiar Rossby-Haurwitz waves (see e.g. Greenspan 1968; Pedlosky 1971; Platzman 1968; Thompson 1961) behave in a more complicated way but, in common with plane waves, when  $N = 0$  the angular frequency  $\omega$  never exceeds  $2\Omega$  in magnitude. This maximum value is attained in inertial waves, for which by Eq. (3.6)

$$\omega^2 = (2\Omega \cdot \boldsymbol{\kappa})^2 / \boldsymbol{\kappa} \cdot \boldsymbol{\kappa}, \quad (3.7)$$

when the wavefronts and displacements of particles, which now move in circular orbits, are everywhere perpendicular to  $\Omega$ . In accordance with Proudman's theorem (see Eq. (2.19) we have the other extreme  $\omega = 0$ , corresponding to steady flow, when the wavefronts are parallel to  $\Omega$ , i.e.  $2\Omega \cdot \boldsymbol{\kappa} = 0$ .

Several laboratory studies of inertial oscillations are described in the literature (see Greenspan 1968). Aldridge and Toomre (1969) have reported a particularly detailed investigation based on experiments with a rigid fluid-filled spherical cavity whose rotation speed about a fixed axis was forcibly varied in a slight but sinusoidal manner about a non-zero value (see Fig. 2). Their objective was to excite inertial eigen-oscillations within the relatively low viscosity fluid through the mild pumping of the thin viscous boundary layer (see section 4 (ii) below) near the wall – the energy input to the system being represented by the term  $\nu \nabla \cdot (\mathbf{u} \times \boldsymbol{\xi})$  in Eq. (2.5) – and to measure and compare with theory some of the properties of such modes. Several distinct resonances were detected via pressure measurements made along the axis for various ratios of the excitation to the mean rotating frequency. For the three most pronounced of these modes, the observed frequency ratios  $\Omega/\omega$  were found to

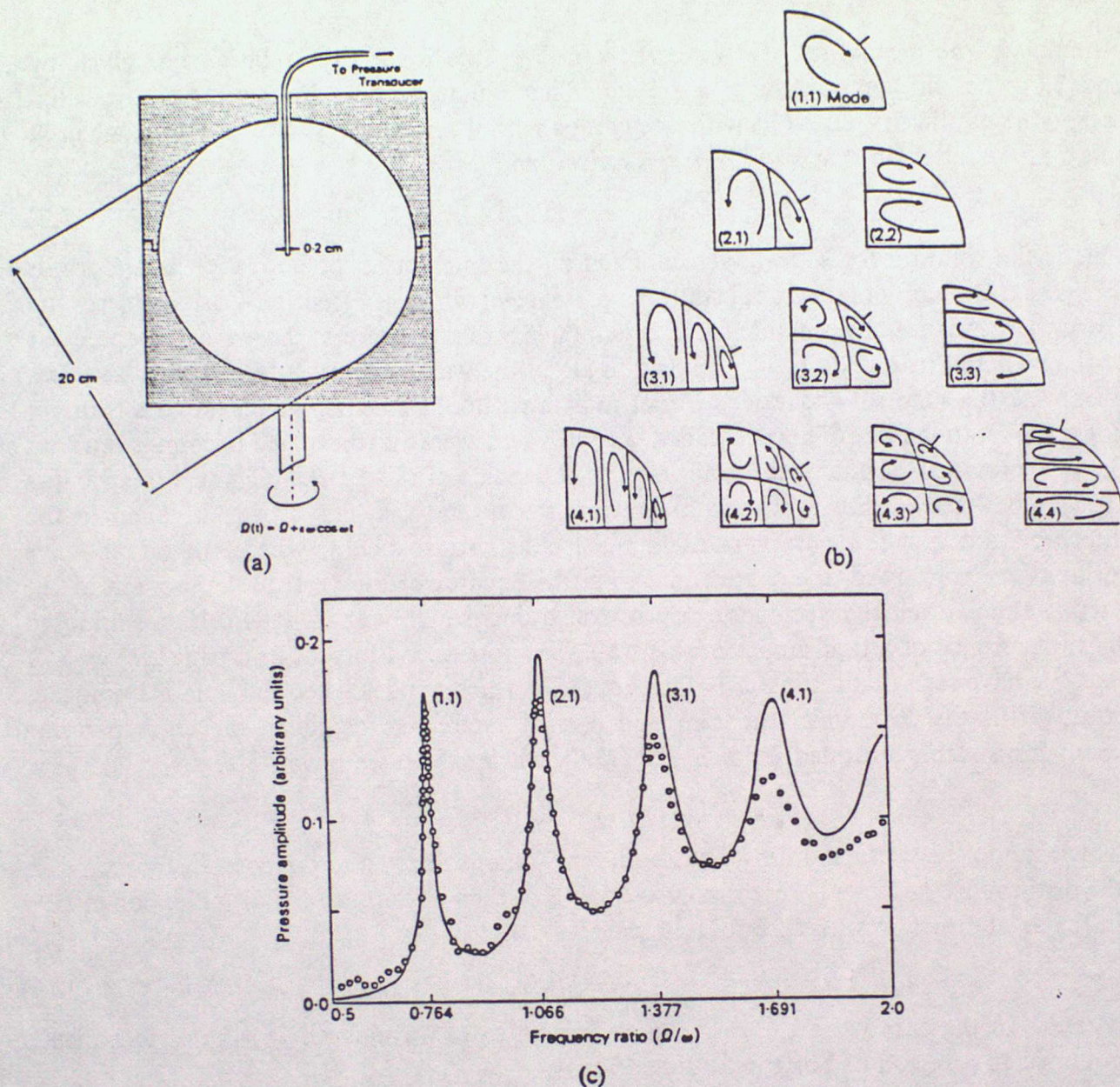


Figure 2. Axisymmetric inertial oscillations of a rotating liquid sphere (Aldridge and Toomre 1969): (a) Fluid container and pressure probe. The container (shaded), which was made of two perspex hemispheres fitted together at the equator, rotated about a vertical axis with angular speed  $\Omega + \epsilon\omega \cos \omega t$ . (b) Streamlines of meridional flow for some equatorially-symmetric modes of various values of  $(n, m)$  where  $n$  is the number of modes in a 'family' and  $m$  measures the ratio of transverse to axial scale. (c) Determinations of the amplitude of the pressure oscillation at the centre of the sphere for  $\epsilon = 8.0^\circ$  over a range of values of  $\Omega/\omega$ , showing four of the seven resonance peaks detected in the experiments. The full line is based on theory, which gives the appropriate  $(n, m)$  values for each resonance.

agree with theory to better than 1%. These experiments and Aldridge's further work (Aldridge 1972) on spherical shells have proved instructive to mathematicians concerned with ill-posed problems in the theory of differential equations. As Stewartson has emphasized, in the determination of eigen-frequencies from Eq. (3.5) it is necessary to solve a hyperbolic differential equation, which has real characteristics, under boundary-conditions of the Dirichlet-Neumann type, and the absence of a general theory of such equations provides little comfort for theoreticians concerned with wave motions in atmospheres, oceans, and the earth's liquid core, where the main geomagnetic field originates. (For references see Acheson and Hide 1973; Brown and Stewartson 1976; Hide and Stewartson 1972.)

Geophysical systems such as the atmosphere and oceans are subject to the combined constraints of rotation and stable density stratification. Elementary wave motions in such

systems are the inertial-gravity waves governed by the dispersion relationship given by Eq. (3.6) when all components of  $\kappa$  are real. That equation also admits certain physically-acceptable oscillatory solutions with one component of  $\kappa$  imaginary. For example, when  $\Omega$  and  $g$  are parallel (so that  $z = Z$ ),  $\kappa = (k, i\hat{l}, m)$  and  $\omega^2 = N^2 k^2 / (k^2 + m^2)$  we find

$$\hat{l} = \pm 2\Omega k / \omega = \pm 2\Omega (k^2 + m^2)^{\frac{1}{2}} / N. \quad (3.8)$$

This is the solution for edge-waves confined by the interaction of buoyancy and Coriolis forces to the vicinity of a vertical wall, the presence of which is essential. Coriolis forces are everywhere balanced by pressure forces and influence the structure of the wave perpendicular to the wall and its direction of propagation along the wall, without affecting the wave frequency or the shape of the trajectories of individual fluid elements, which move in straight lines parallel to the wall. These so-called 'Kelvin waves' were first discussed in connection with the interpretation of tidal records at ports on either side of the English Channel (see Krauss 1973). They are readily produced in the laboratory and they have been invoked in the interpretation of wind observations in the tropical stratosphere, where, so far as wave motions are concerned, the change in sign at the equator of the vertical component of the earth's angular velocity vector introduces constraints roughly analogous to those imposed by the presence of a rigid impermeable wall. (See note added in proof on page 28.)

We have seen that setting  $\omega = 0$  in Eq. (3.7), which applies when the fluid is homogeneous, yields the Proudman theorem and it is of interest to establish the corresponding result for a stably-stratified fluid. By Eq. (3.6), when  $\omega = 0$  we have

$$(2\Omega \cdot \kappa)^2 = -(N \times \kappa)^2 \quad (3.9)$$

which cannot be satisfied unless  $\kappa$  has both real and imaginary components. If, for example, the disturbance has a real horizontal wavelength  $\lambda_H$  then its amplitude falls off exponentially in the axial direction with an e-folding scale

$$\sim \Omega \lambda_H / \pi N, \quad (3.10)$$

whereas in the case when the disturbance has an axial wavelength  $\lambda_A$ , the disturbance is confined to a region of horizontal dimensions

$$\sim N \lambda_A / 4\Omega \pi, \quad (3.11)$$

the so-called 'Rossby radius of deformation', which gives the scale of some of the main energetic eddies in the atmosphere and oceans. By Eq. (3.9), when geostrophic balance obtains the axial and horizontal scales are roughly in the ratio  $2\Omega/N$  (Prandtl's 'ratio of scales', see Prandtl 1952, also Lineykin 1974), which goes to infinity when  $N \rightarrow 0$ , in accordance with Proudman's theorem.

#### 4. STEADY SOURCE-SINK FLOWS

(i) *Strictly two-dimensional systems.* The inertial oscillations considered in section 3 depend for their existence on the deflecting action of Coriolis forces on moving particles, so it is appropriate to inquire whether there could be circumstances in which rotation merely changes the pressure field, leaving unaffected the trajectories of individual fluid elements relative to the rotating frame. Mechanically-driven flows which, by virtue of the boundary conditions and the supposition that the fluid is homogeneous, are two-dimensional in planes perpendicular to the axis of rotation, have this property when, in addition, a certain quantity  $j$  is equal to zero. Here  $j$  is defined as the number of irreducible sets of closed curves that can be drawn in the region of  $(x, y)$  space of connectivity  $c$  occupied by the fluid across which the net flow of fluid does not vanish. In other words, Taylor's theorem (see section 2(iv), especially Eqs. (2.11) and (2.12)) holds when the flow is driven by relative

movement of two-dimensional boundaries and/or by sources and sinks of the 'dipole' type, but not when sources and sinks of the 'monopole' type are present.

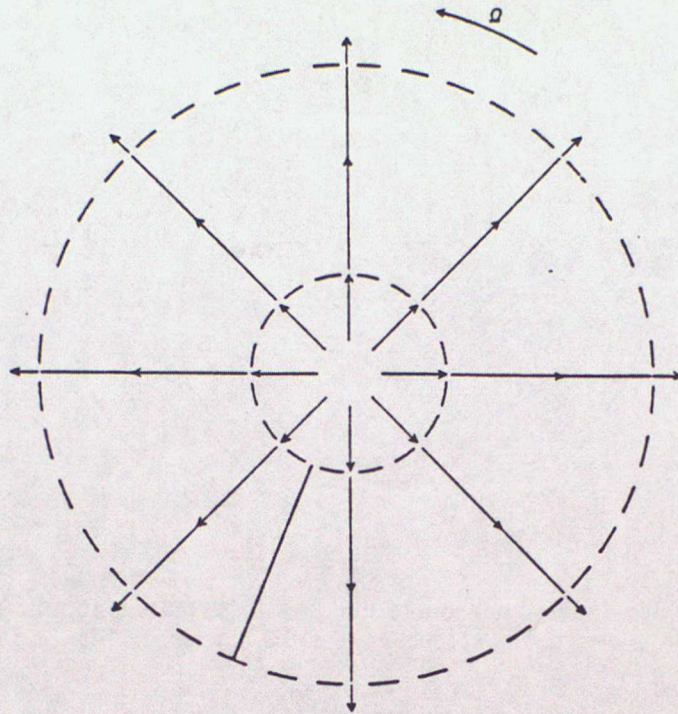


Figure 3. Streamlines of two-dimensional source-sink flow in a rotating annular system of inner radius  $a$  and outer radius  $b$  when, owing to the presence of a radial barrier (at  $\phi \doteq 250^\circ$ ),  $j = 0$ ,  $c = 1$  (see text).

Examples of source-sink systems of both  $j \neq 0$  and  $j = 0$  types are illustrated by Figs. 1, 2 and 3 of Hide (1968), in each of which fluid enters and leaves the system via permeable but rigid portions of the cylindrical side-walls at a total rate  $Q \text{ m}^3\text{s}^{-1}$ . Fig. 3 of the present paper illustrates a system of the  $j = 0$  type in the simplest case of all, where the source-sink distribution is independent of the azimuthal angle  $\phi$ . The velocity field is determined virtually everywhere by considerations of continuity (see Eq. (2.1)) when viscous effects are confined to thin boundary layers on the rigid impermeable radial barrier connecting the two cylindrical surfaces. Thus

$$\mathbf{u} = (u_r, u_\phi, u_z) = (q/2\pi r, 0, 0) \quad (4.1)$$

where  $r$  is the radial coordinate and  $q$  times the length of the system in the  $z$ -direction is equal to  $Q$ , and the corresponding azimuthal component of the pressure gradient is given by

$$r^{-1} \partial P / \partial \phi = r^{-1} (\Omega q / \pi) \quad (4.2)$$

(see Eq. (2.12)). The last equation shows immediately why the radial barrier is an essential feature of the system when  $\Omega \neq 0$ , for without the barrier, across which a pressure difference  $2\Omega \bar{\rho} q$  develops, it would be impossible to support the azimuthal pressure gradient.

When  $j \neq 0$  (as in the cases illustrated by Fig. 2 of Hide (1968)) rotation interacts with the basic source-sink flow to produce  $j$  gyres, a 'cyclonic' one around each distinct sink and an 'anticyclonic' one around each distinct source. The simplest case of all (see Fig. 4) corresponds to the system illustrated by Fig. 3 with the radial barrier removed, thus increasing the connectivity  $c$  from 1 to 2 and  $j$  (which in general satisfies  $j \leq c - 1$ ) from 0 to 1. With no radial barrier present there can be no azimuthal pressure gradient to prevent the sideways deflection of the flow by Coriolis forces. The resulting azimuthal motion can be calculated exactly; thus  $\mathbf{u} = (u_r, u_\phi, u_z)$  where  $u_r = q/2\pi r$ ,  $u_z = 0$  and

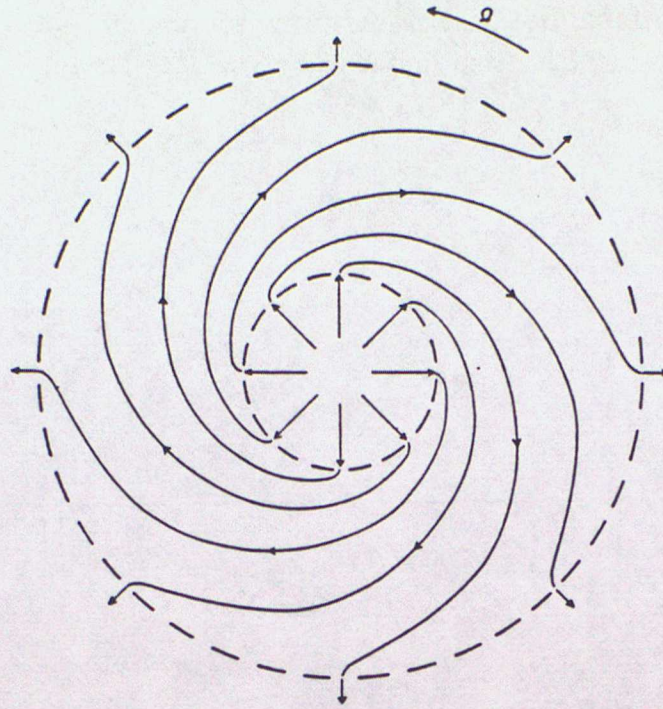


Figure 4. Streamlines of two-dimensional source-sink flow in a rotating annular system of inner radius  $a$  and outer radius  $b$  when, owing to the absence of a radial barrier (cf. Fig. 3),  $j = 1$ ,  $c = 2$  (see text).

$$u_{\phi} = \Omega \left\{ -r + \frac{1}{b^{S+2} - a^{S+2}} \left( \frac{b^2 a^2 (b^S - a^S)}{r} + (b^2 - a^2) r^{S+1} \right) \right\} \quad (4.3)$$

if  $a$  and  $b$  are the radii of the inner or outer cylindrical surfaces respectively and  $S \equiv q/2\nu$  ( $\nu$  being the coefficient of viscosity and  $q$  reckoned positive or negative according as the inner cylinder is the source or sink of fluid (cf. Eq. (4.1)). Fig. 5 illustrates the dependence of the radial profile of  $u_{\phi}$  on the Reynolds number  $|S|$ , for several values of  $S$  ranging from  $-\infty$  to  $\infty$ . When  $|S|$  is very small, viscosity ensures that the relative azimuthal motion  $u_{\phi}$  is very slow, but when  $|S| \gg 1$ , viscous effects are confined to a boundary layer on the sink of thickness

$$b/S \text{ or } a/|S| \text{ according as } q \gtrless 0. \quad (4.4)$$

The azimuthal flow elsewhere is such that individual fluid elements conserve their angular momentum, so that  $\zeta \equiv r^{-1} \partial(ru_{\phi})/\partial r$ , the axial and only non-zero component of relative vorticity  $\xi$ , is equal to  $-2\Omega$ ; this can be seen from the general expression

$$\xi = (0, 0, \zeta) = \left( 0, 0, 2\Omega \left\{ \left( 1 + \frac{1}{2}S \right) \left[ \frac{(b^2 - a^2)r^S}{b^{S+2} - a^{S+2}} \right] - 1 \right\} \right). \quad (4.5)$$

The corresponding absolute vorticity in the main body of the fluid is zero, implying – since the area integral of the absolute vorticity can be shown to equal  $2\pi(b^2 - a^2)\Omega$  for all  $S$  – that when  $|S| \gg 1$  the absolute vorticity is concentrated in the thin layer on the boundary where the fluid leaves the system. (This is a clear case of motions expelling absolute vorticity from the main body of the fluid and concentrating it at the rim, but by a process which can be fully specified, in contrast to some of the examples invoked during the controversy – still apparently unsettled (but see McEwan 1976) – started in the 1960s by certain speculations concerning the early stages in the development of hurricanes.)

(ii) *End-effects due to Ekman boundary layers.* Strictly two-dimensional flows are impossible to realize in practice, owing to the presence of end-walls in  $z = z_1$  and  $z = z_2$  (where  $z_2 > z_1$ ). The ‘end-effects’ produced by such walls range from minor local modifications when the basic two-dimensional flow has no relative vorticity and the end-walls are

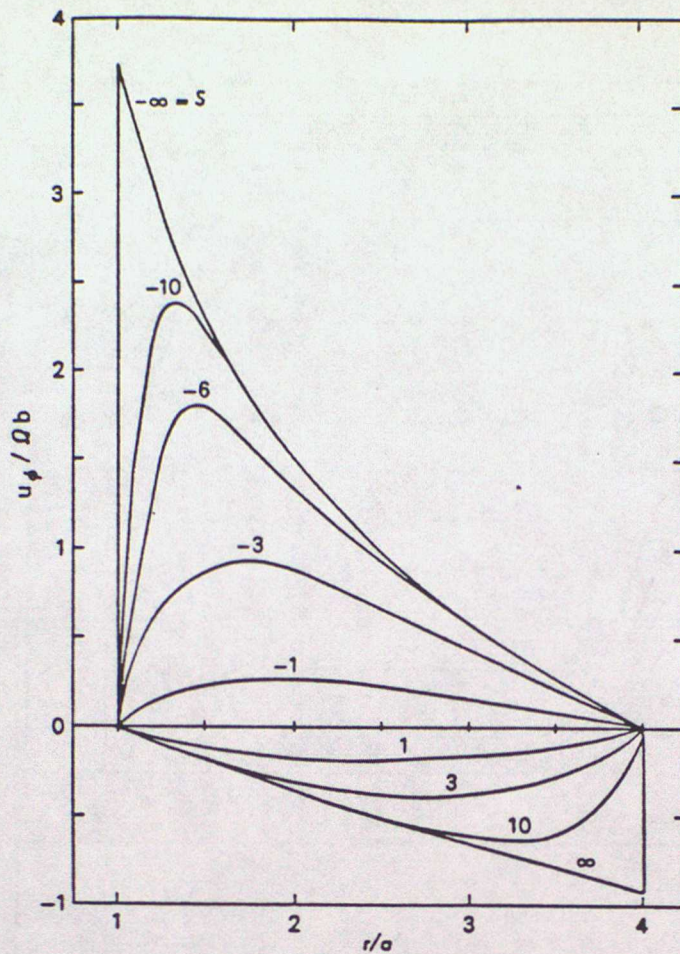


Figure 5. The variation of azimuthal velocity  $u_\phi$  with radius  $r$  for the system illustrated by Fig. 4 when  $b = 4a$ , calculated for several values of  $S \equiv q/2\pi v$ ,  $|S|$  being a Reynolds number based on the source strength. When  $|S| \gg 1$  individual fluid particles tend to conserve their angular momentum as they traverse the main body of the system, the corresponding relative vorticity  $\zeta$  being close to  $-2\Omega$ . A boundary layer of thickness  $b/S$  when  $S > 0$  (and  $a/|S|$  when  $S < 0$ ) and in which  $\zeta \sim |S|\Omega$  forms on the surface of the sink, but there is no corresponding boundary layer on the surface of the source.

everywhere perpendicular to  $\Omega$  (i.e. when  $\nabla_1 z_l(r, \phi) = \nabla_1 z_u(r, \phi) = 0$ ), to major changes in the flow pattern throughout the whole system when the basic two-dimensional flow possesses vorticity or the end walls are not everywhere perpendicular to  $\Omega$ .

Consider first the case when the end-walls are perpendicular to  $\Omega$ , so that  $\nabla_1 z_l = \nabla_1 z_u = 0$  and the separation distance

$$D \equiv z_u(r, \phi) - z_l(r, \phi) \quad (4.6)$$

is uniform (cf. Fig. 6). Supposing that the coefficient of kinematic viscosity  $\nu$ , though non-zero, is so small that the boundary layers that develop on each end-wall so as to satisfy the no-slip boundary condition there are small in thickness  $\delta$  (i.e.  $\delta \ll D$ ), we can readily show that

$$\delta = (\nu/\Omega)^{\frac{1}{2}}(1 + O(\varepsilon)) \quad (4.7)$$

where  $\varepsilon$  is the Rossby number (see Eq. (2.16)), implying that when the interior flow is quasi-geostrophic (i.e.  $\varepsilon \ll 1$  and  $E \ll 1$ , see Eq. (2.17)) the boundary-layer is highly ageostrophic with the 'Ekman' structure. The components  $(u_1, u_2)$  of  $\mathbf{u}$  parallel to the wall are given by

$$u_1 = \{U_1(1 - e^{-\sigma} \cos \sigma) \mp U_2 e^{-\sigma} \sin \sigma\}(1 + O(\varepsilon)) \quad (4.8)$$

and 
$$u_2 = \{U_2(1 - e^{-\sigma} \cos \sigma) \pm U_1 e^{-\sigma} \sin \sigma\}(1 + O(\varepsilon)) \quad (4.9)$$

where  $(U_1, U_2)$  are the corresponding quasi-geostrophic components at the edge of the

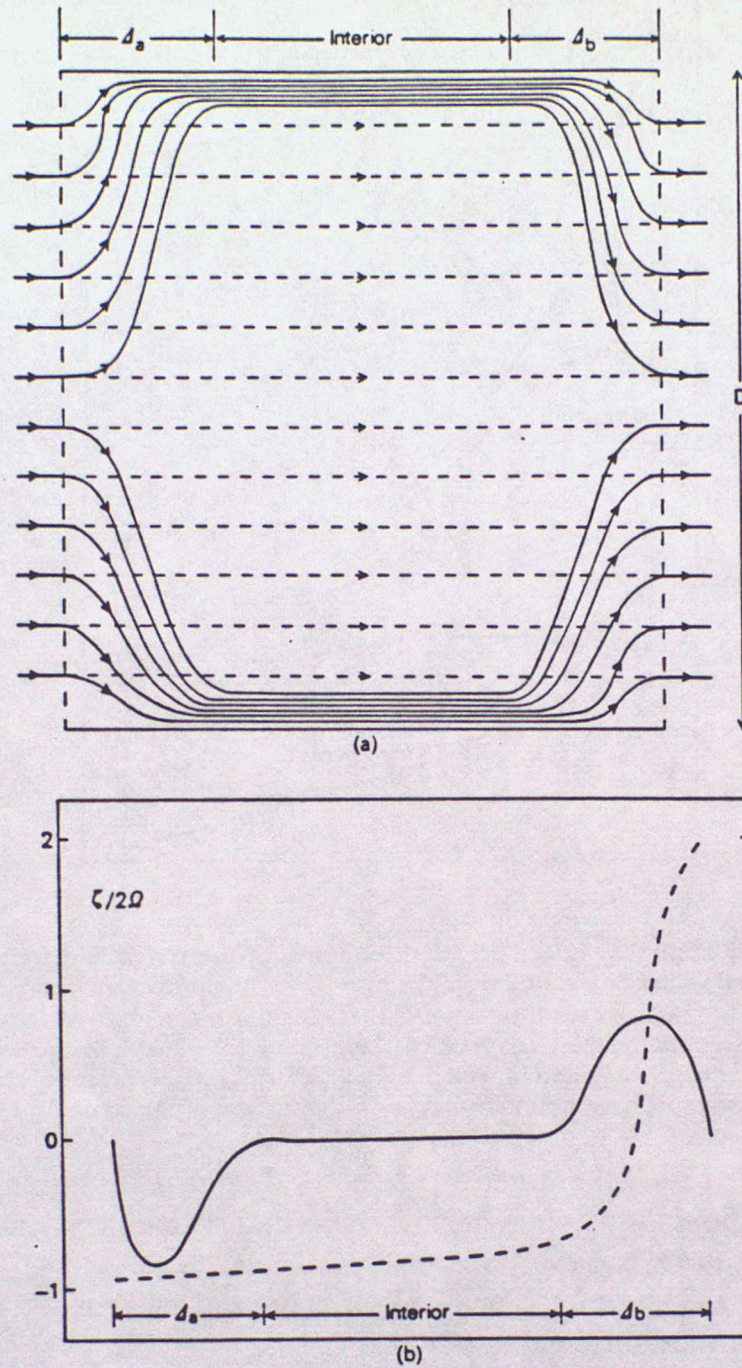


Figure 6. Illustrating the effect of end-walls separated by a uniform distance  $D$  on flows due to distribution of sources and sinks for which  $j \neq 0$  (see text), as exemplified by the simple case of an annular system (see Figs. 4 and 5) with  $j = 1$ . (a) shows the projection of streamlines on a meridian plane and (b) shows the corresponding radial variation of relative vorticity  $\zeta$  in regions remote from the Ekman boundary layers of thickness  $\delta = (\nu/\Omega)^{1/2}$  on the end-walls. The lightly-dashed line corresponds to the case when the end-walls are absent and the full line to the case when the end-walls are present. Suction due to the Ekman boundary layers reduces the radial motion  $u_r$  and the relative vorticity  $\zeta$  to zero in the main body of the fluid and gives rise to axial motion in boundary layers of thickness  $\Delta_a$  and  $\Delta_b$  on the side-walls.

boundary layer, where it meets the interior region,  $\sigma$  is a 'stretched' coordinate equal to  $x_3$ , the distance from the boundary, divided by  $\delta$ , and the upper (lower) sign is taken when  $\Omega$  is parallel (antiparallel) to the positive  $x_3$ -direction. There is a net cross-isobar flow in the boundary layer, and if the  $x_3$ -component of the vorticity in the interior region,  $\partial U_2/\partial x_1 - \partial U_1/\partial x_2$ , is non-zero, boundary layer 'suction' occurs, giving rise to a value of  $u_3$ , the component of  $\mathbf{u}$  normal to the boundary, which vanishes on the rigid boundary only and has the generally non-zero value

$$U_3 = \pm \frac{1}{2} \delta (\partial U_2 / \partial x_1 - \partial U_1 / \partial x_2) (1 + O(\epsilon)) \quad (4.10)$$

at the edge of the boundary layer (see e.g. Batchelor 1967; Greenspan 1968; Prandtl 1952).

Returning to the discussion of source-sink flows, we find that  $U_3$  vanishes in all cases of such systems having  $j = 0$  (as exemplified by Fig. 3), for in such cases the basic relative vorticity  $\partial U_2/\partial x_1 - \partial U_1/\partial x_2 = \pm\zeta = 0$  (where  $\zeta = r^{-1}\partial(ru_\phi)/\partial r - r^{-1}\partial u_r/\partial\phi$ ). The end-walls boundary layers are then passive in the sense that they merely reduce the relative flow from its non-zero value in the interior region to zero on the wall, where the no-slip boundary condition must be satisfied. This behaviour contrasts sharply with cases when  $j \neq 0$  (as exemplified by Fig. 4), where  $\zeta \neq 0$  and boundary layer suction completely changes the interior solution and gives rise to complicated three-dimensional boundary-layers on the side-walls (see Fig. 6).

The modified flow in the latter case consists of five regions (see Fig. 6): the inviscid region, in which the flow is quasi-geostrophic when  $\varepsilon \ll 1$  and  $E \ll 1$ , satisfying

$$\mathbf{u} = (u_r, u_\phi, u_z) = (0, Q\Omega^\pm/2\pi v^\pm r, 0)(1 + O(\varepsilon)) \quad (4.11)$$

(where  $\varepsilon = Q/2\pi v^\pm \Omega^\pm a^2 = Q/2\pi\delta\Omega a^2$  and  $E = \delta^2/D^2$ ), and four highly ageostrophic regions (see section 2(v)) comprising two Ekman layers of thickness  $\delta$  on the end-walls separated by the uniform distance  $D$  and boundary layers of thickness  $\Delta_a$  and  $\Delta_b$  on the side-walls in  $r = a$  and  $r = b$ , supposing that  $\Delta_a + \Delta_b \ll b - a$ . The transfer of fluid now takes place via these boundary layers, but it is theoretically significant that simple Ekman theory, without recourse to consideration of the complex structure of the side-wall boundary layers, can be used to determine  $\mathbf{u}$  in the inviscid interior with an error no more than  $O(\varepsilon)$ . Within that region all components of relative vorticity  $\xi$  now vanish (to  $O(\varepsilon)$ ) – in contrast to the case when the end-walls are absent, see Fig. 5 – since Proudman's theorem (see Eq. (2.19)) requires that geostrophic flow of a homogeneous fluid should satisfy  $\partial u/\partial z = 0$ , the first two components of which when combined with Eq. (4.10) give

$$\partial u_z/\partial z = -\delta\zeta/D \quad (4.12)$$

which is only compatible with the third component  $\partial u_z/\partial z = 0$  when  $\zeta = 0$ .

The mathematical analysis of the side-wall boundary layers is highly complex, even in the case when non-linear effects are negligible and the layers are consequently of the so-called 'Stewartson-type' with overall thickness  $(D\delta/2)^\pm$  (and therefore proportional to  $v^\pm$ ) and sub-structure on a scale  $D^\pm\delta^\pm$  (proportional to  $v^\pm$ ). Unfortunately, the error in the linear theory is  $\sim a\varepsilon/D^\pm\delta^\pm$  or  $b\varepsilon/D^\pm\delta^\pm$ , implying that non-linear effects must be taken into account in the treatment of the side-wall boundary layers even when linear (Ekman) theory suffices for the end-wall boundary layers. According to an approximate analysis (Hide 1968) of an axisymmetric system (see Fig. 6) and a supporting laboratory investigation, the thickness of the boundary layer on the source ( $\Delta_a$  when  $q > 0$ ) increases and that of the sink boundary layer ( $\Delta_b$  when  $q > 0$ ) decreases with increasing  $\varepsilon E^{-\pm}$  (and vice versa when  $q < 0$ ), but in such a way that the product  $\Delta_a\Delta_b$  remains  $\sim D\delta/2$  even when  $\varepsilon E^{-\pm}$  is quite large, with  $\Delta_b$  tending to the value  $2\pi v b D/Q$  (see Eq. (4.4) and Fig. 5) and  $\Delta_a$  to  $Q/4\pi v^\pm \Omega^\pm a$  when  $\varepsilon E^{-\pm} \gg 1$ . These results have been generally confirmed and extended by further work, including a combined numerical and laboratory investigation by Bennetts and Jackson (1974).

Because the flow is axisymmetric, it is a relatively straightforward matter to extend the foregoing analysis to cases when the end-walls are no longer perpendicular to  $\Omega$  provided that in shape they remain figures of revolution about the axis of symmetry, since differences from the case illustrated by Fig. 6 are then mainly only quantitative. Thus, when the bounding end-wall surfaces are concentric spheres of radii  $\hat{a}$  and  $\hat{b}$  ( $\hat{b} > \hat{a}$ ) (see Fig. 7) and relative flow is produced by a cylindrical source near one pole feeding a cylindrical sink near the other pole, the transfer of fluid, again, takes place via Ekman layers, which now have thickness

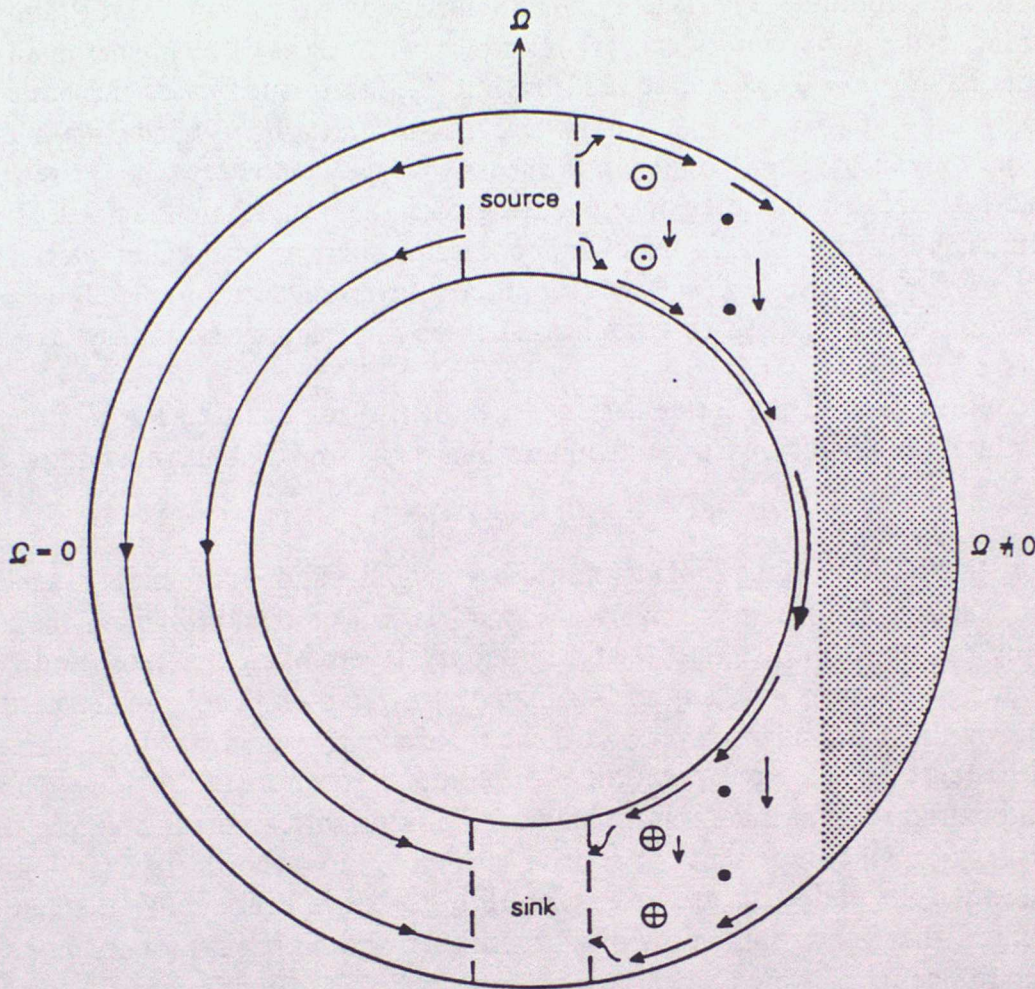


Figure 7. Axisymmetric source-sink flow in a spherical shell of fluid. The left side of the schematic diagram shows the streamlines for the case when the basic angular speed of rotation  $\Omega = 0$ . Fluid then moves directly from the source in the northern hemisphere to the sink in the southern hemisphere, with individual elements following trajectories for which  $r^2 + z^2 = \text{constant}$ . This flow pattern should be compared with that found in the rapidly-rotating case illustrated by arrows on the right side of the diagram. The transfer of fluid now takes place via Ekman boundary layers on the inner and outer spherical boundaries. Whilst the transfer via the boundary layer on the outer sphere decreases with decreasing latitude, that via the boundary layer on the inner sphere increases with decreasing latitude (see Eq. (4.13)) and continuity requires that there should be a compensating axial component to the flow in the interior region (see Eq. (4.14)). The azimuthal flow in the interior region is in geostrophic balance and vanishes, in accordance with Proudman's theorem (Eq. (2.19)) and the Ekman suction formula (Eq. (4.11)), in the stippled region where  $r$  exceeds the radius of the inner sphere.

$$\delta = v/(\Omega |\cos \psi|)^{\frac{1}{2}} \quad (4.13)$$

where  $\psi$  is the 'co-latitude', so that  $\delta$  increases with increasing distance from the poles. Owing to this  $\psi$ -dependence of  $\delta$ , at a given distance  $r$  from the axis the boundary layer on the outer sphere is thinner than the layer on the inner sphere and therefore transports less fluid towards the equator. In contrast to the cylindrical case illustrated by Fig. 4, continuity demands an axial flow  $u_z$  in the inviscid interior where  $u_z$  is independent of the axial coordinate (in keeping with the third component of Eq. (2.19)) and varies with  $r$  according to the expression

$$u_z(r) = \frac{Q}{4\pi b^2 a^2} \left\{ \frac{\hat{a}^2(1-r^2/\hat{a}^2)^{\frac{1}{2}}(1-r^2/b^2)^{-\frac{1}{2}} - b^2(1-r^2/b^2)^{\frac{1}{2}}(1-r^2/\hat{a}^2)^{-\frac{1}{2}}}{(1-r^2/\hat{a}^2)^{\frac{1}{2}} + (1-r^2/b^2)^{\frac{1}{2}}} \right\} \quad (4.14)$$

when  $r < \hat{a}$ , the azimuthal motion being related to  $u_z$  by the Ekman suction formula given by Eqs. (4.10) and (4.13). A striking feature of the flow is the absence in this geostrophic

limit of any motion in the fluid occupying the region between the imaginary cylindrical surface  $r = \hat{a}$  and the 'low-latitude' part of the outer bounding sphere which extends from  $r = \hat{a}$  to the 'equator' at  $r = \hat{b}$ . The geostrophic azimuthal flow in the region  $r \leq \hat{a}$  drops to zero at  $r = \hat{a}$  but its rate of change with respect to  $r$  does not, implying that a weak ageostrophic detached shear layer will be present near  $r = \hat{a}$ . This layer and the boundary layers on the cylindrical surfaces of the source and sink as well as the boundary layer at the equator of the inner sphere, where Ekman theory breaks down (as evinced by the behaviour of the r.h.s. of Eq. (4.13) when  $\psi = \pi/2$ ) are complex in structure and their theoretical investigation poses some very difficult mathematical problems. Again, however, the flow elsewhere can be determined by elementary theoretical considerations and unpublished experiments carried out in my laboratory demonstrate conclusively that this flow occurs in practice. (The study of source-sink flows is not, of course, directly relevant to dynamical meteorology, but it is nevertheless interesting to note that the tendency for the main constituent of the Martian atmosphere, carbon dioxide, to freeze out near the winter pole gives rise to a net poleward atmospheric flow and a concomitant increase in azimuthal wind speed; for references see e.g. Golitsyn 1973 or my Presidential Address for 1975 (Hide 1976).)

(iii) *Geostrophic contours and end-effects due to topography.* We now turn to the more complicated general case of non-axisymmetric system for which the axial distance  $D$  (see Eq. (4.6)) between the end-walls is non-uniform. We have seen in section 2 (see Eq. (2.23)) that in quasi-geostrophic flow of a homogeneous incompressible fluid, such as the interior flows in the cases discussed in (ii) above, changes in relative vorticity are brought about mainly by axial stretching, and indeed the axial vorticity in the side-wall boundary layers in the flow illustrated by Fig. 6 is strongly influenced by axial stretching due to Ekman boundary-layer suction at the end-walls. When, in addition to Ekman suction, end-wall topography contributes to axial stretching, by Eqs. (2.23), (2.19) and (4.12), the axial component of the quasi-geostrophic relative vorticity,  $\zeta$ , satisfies

$$\partial\zeta/\partial t + (\mathbf{u}_1 \cdot \nabla_1)\zeta \doteq 2\Omega[(\mathbf{u}_1 \cdot \nabla_1)D - \delta\zeta]/D \quad (4.15)$$

The relative importance of the topographic contribution to vorticity changes, as represented by the term  $2\Omega D^{-1}(\mathbf{u}_1 \cdot \nabla_1)D$  in Eq. (4.15), is measured by the ratio  $h/h_*$  where  $h$  is the amplitude of variations in  $D$  and

$$h_* \sim \varepsilon D + \delta. \quad (4.16)$$

Topographic end effects will not be important when  $h \ll h_*$ , but when  $h > h_*$  — and this is always the case for strictly geostrophic motion since  $h_*$  then vanishes — such effects are so strong that within the main body of the fluid the flow is steered (to  $O(\varepsilon)$ ) along geostrophic contours, defined as curves on which

$$D \equiv z_u - z_l = \text{constant}. \quad (4.17)$$

Another solution of the 'steering equation'

$$\mathbf{u}_1 \cdot \nabla_1 D = 0 \quad (4.18)$$

satisfied by  $\mathbf{u}_1$  is  $\mathbf{u}_1 = 0$ , and indeed there *are* circumstances in which the effect of topography is to produce stagnation, as in the case of the equatorial region of the spherical system discussed in (ii) above (see Fig. 7). Quasi-geostrophic motion is clearly impossible in regions where, owing to the geometry of the end-walls, continuous geostrophic contours cannot be found, and within such regions the flow, if it does not vanish, either oscillates rapidly or is characterized by strong transverse shear.

The effect of axisymmetric sloping end-walls on the source-sink flow illustrated by

Fig. 3 is particularly striking (see Fig. 8) — in contrast to the case illustrated by Fig. 4 and 6, for which the basic flow is parallel to the geostrophic contours and is therefore unaffected by

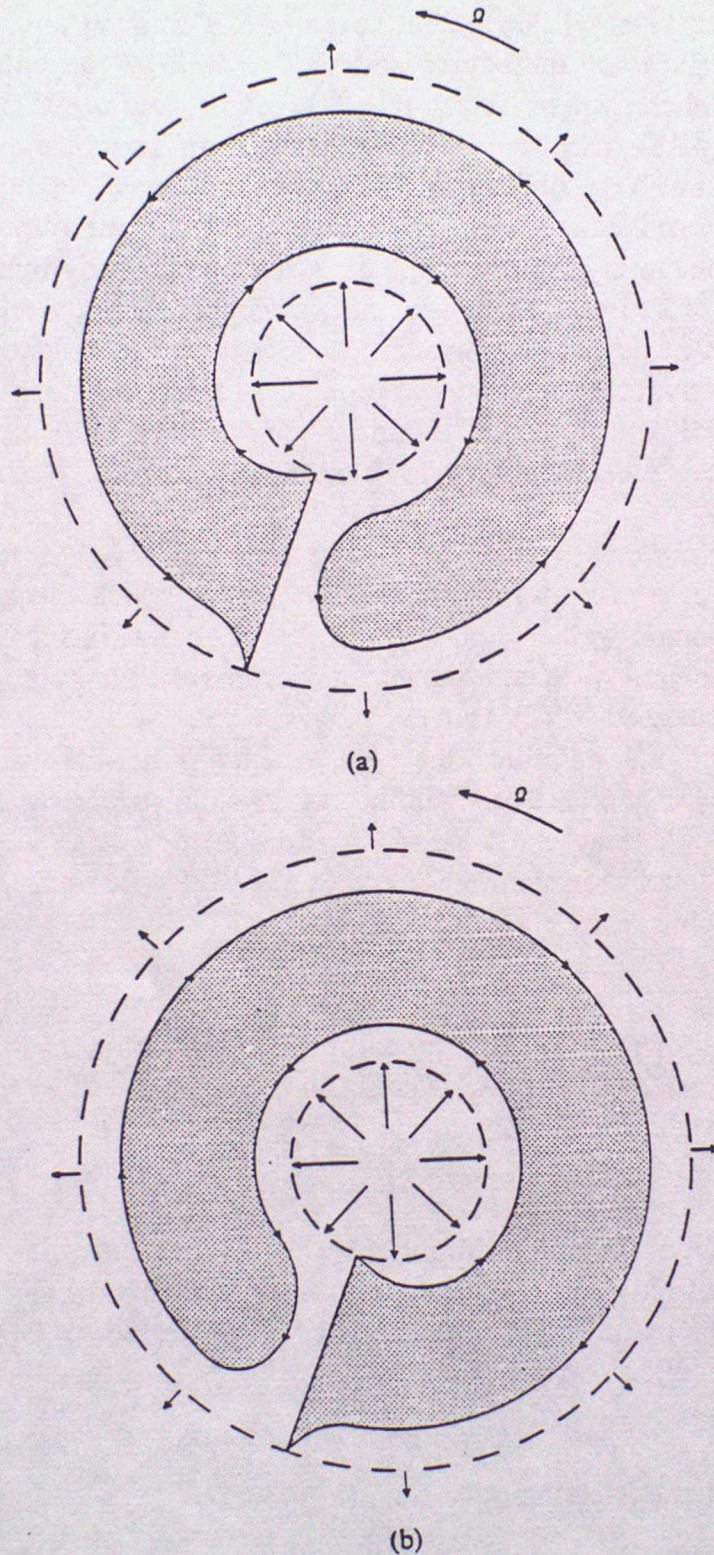


Figure 8. Schematic diagram illustrating the effect of axisymmetric sloping end-walls on flow due to a two-dimensional source-sink distribution in an annular system with a radial barrier. In the case when the distance  $D$  between the end-walls is uniform, streamlines are purely radial (see Fig. 3). Fig. 8(a) illustrates the case when  $dD/dr > 0$  (see text) and Fig. 8(b) the case when  $dD/dr < 0$ . In the main body of the fluid there can be no flow across 'geostrophic contours'  $r = \text{constant}$ , and owing to this major constraint on the flow, motion is largely confined to highly ageostrophic boundary layers on the cylindrical surfaces of the source and sink and on one side only of the radial barrier, where the transfer of fluid from the inner cylinder to the outer cylinder takes place via a 'western boundary current' when  $dD/dr > 0$  (see Fig. 8(a)) or an 'eastern boundary current' when  $dD/dr < 0$  (see Fig. 8(b)). The motion simply reverses direction, with no significant change in flow pattern, when the source and sink are interchanged, so that fluid enters the system via the outer cylinder instead of the inner cylinder and vice versa.

topographic stretching. Figure 8(a) illustrates the case when  $D$  increases with increasing distance from the axis (i.e.  $dD/dr > 0$ ) and  $D(b) - D(a) \gg h_*$  (see Eqs. (4.16) and (4.18)), and Fig. 8(b) the case when  $dD/dr < 0$  and  $D(a) - D(b) \gg h_*$ . In the main body of the fluid, there can be no flow across geostrophic contours, which are circles concentric with the axis of rotation, and, owing to this major constraint on the flow, motion is largely confined to highly ageostrophic boundary layers on the cylindrical surfaces on the source and sink and on one side or the other side of the radial barrier, where the transfer of fluid from the inner cylinder to the outer cylinder (when  $q > 0$ , the case illustrated) takes place in a 'western boundary current' when  $dD/dr > 0$  (see Fig. 8(a)) or an 'eastern boundary current' when  $dD/dr < 0$  (see Fig. 8(b)). The motion simply reverses direction, with no significant change in the general flow pattern, when  $q < 0$ , corresponding to the case when fluid enters the system via the outer cylinder rather than the inner cylinder. Within the 'western' or 'eastern' boundary current, the 'planetary vorticity' term  $2\Omega D^{-1}(\mathbf{u}_1 \cdot \nabla_1)D$  is balanced by the sum of the non-linear advective term  $(\mathbf{u}_1 \cdot \nabla_1)\zeta$  and the viscous term  $\nu \nabla_1^2 \zeta$  in the vorticity equation (see Eqs. (2.6), (2.11) and (4.15)).

It is possible to show that in its main dynamical effects the sloping end-walls with  $D$  increasing outwards is formally equivalent in the case of a homogeneous fluid to the latitudinal variation of the Coriolis parameter  $f$  (the vertical component of  $2\Omega$ , see Eq. (2.27)) when dealing with flow in a thin spherical shell (for references see Greenspan 1968). This is often called the 'beta-effect' in dynamical meteorology and oceanography, owing to the use of the so-called 'beta-plane' where local Cartesian coordinates are used (with the  $X$ -axis towards the east and the  $Y$ -axis towards the north) and  $f$  is taken as a linear function of  $Y$ :

$$f = f_0 + \beta Y \quad (4.19)$$

The best-known example of a western boundary current in nature is the Gulf Stream in the Atlantic Ocean (Stommel 1965), the earliest theoretical investigations of which were greatly aided by various laboratory studies of source-sink flows in systems akin to those illustrated by Figs. 8(a) and (b) (for review see Veronis 1973). Inserting a rigid full meridional barrier connecting the source to the sink in the spherical system illustrated by Fig. 7 gives rise to a cross-equatorial western boundary current reminiscent of the East-African low-level cross-equatorial jet-stream in the atmosphere and the Somali Current in the Indian Ocean.

(iv) *Other experiments with mechanically-driven flows.* Time and space do not permit the detailed treatment of further examples of experiments on basic processes in mechanically-driven systems, such as 'spin-up', which has received a great deal of attention (see Benton and Clark 1974; Buzyna and Veronis 1971; Greenspan 1968). Central to the understanding of these processes, as attested by the cases we have chosen to discuss in detail, is the Proudman theorem expressing, effectively, the tendency for slow disturbances to propagate preferentially in directions parallel to the rotation axis. The system illustrated by Fig. 6 is a convenient one for studying the disturbance produced by a localized bump on one of the end-walls or by a solid object placed in the interior region. The wake due to the presence of such an obstacle to the flow takes the form of a 'Taylor column' trailing at an angle  $\sim \varepsilon$  radians to the  $z$ -axis when  $\varepsilon \ll 1$  (see Hide *et al.* 1968). In the 'viscous' limit when  $\varepsilon \ll E^\pm$  ( $\ll 1$ ) the column is parallel to the  $z$ -axis, the flow within it is virtually stagnant, and the 'walls' of the column are highly ageostrophic detached shear layers of thickness  $\sim (D\delta)^\pm$  (see Greenspan 1968). Otherwise, i.e. when  $E^\pm \ll \varepsilon$  ( $\ll 1$ ) the Taylor column is of the so-called 'inertial type' and much more complicated in structure than in the viscous limit.

Recent studies of Taylor columns have included work on effects due to density stratification. On the experimental side, the combined effects of rotation and stratification are probably best studied by determining the flow produced by moving solid objects slowly through a fluid which otherwise rotates uniformly, as in Taylor's pioneering study of

homogeneous systems (see Taylor 1923, 1974). Various lines of theoretical and experimental evidence indicate that stratification restricts the penetration distance parallel to the rotation axis to a value given by Eq. (3.10) when the advective contribution to ageostrophic effects is more important than viscosity (for references see Mason 1976). The study of flow over and around topography in rotating non-homogeneous fluids is currently an active area of research in geophysical fluid dynamics and should in due course provide dynamical oceanographers and meteorologists with a better foundation for interpreting observations and with improved methods of representing effects due to topography in numerical models.

Experimental and theoretical investigations of channel flows have also featured in recent work. These studies, which include important generalizations of hydraulic theory to the case of rotating fluids, bear on certain problems in dynamical oceanography (see e.g. Stern 1975).

In our discussion thus far we have encountered several examples of highly ageostrophic shear layers on end-walls and side-walls and detached shear layers in the main body of the fluid. As a rule, instabilities develop on these shear layers when an appropriate Reynolds number based on the thickness of the layer exceeds a critical value  $\gtrsim 10$ , and experimental investigations have played a leading role in the study of these instabilities. Important work on Ekman layer instability has been carried out using systems essentially of the type illustrated by Fig. 6, and the stability of detached shear layers and of western boundary currents has been usefully investigated in systems driven by differential rotation between part or the whole of the upper end-wall and the other bounding surfaces (for references see Greenspan 1968).

##### 5. THERMALLY-DRIVEN FLOWS DUE TO AN IMPRESSED HORIZONTAL TEMPERATURE GRADIENT

Having considered a variety of mechanically-driven flows we conclude our discussion of experiments with rotating fluids with a brief account of systems driven by buoyancy forces due to impressed differential heating and cooling. For theoretical purposes it is often convenient to specify the impressed heating and cooling in terms of the hypothetical temperature field  $T_i(\mathbf{r}, t)$  corresponding to the actual temperature field that would obtain if the fluid in the system were replaced by a solid of the same thermal properties. Corresponding to  $T_i(\mathbf{r}, t)$  is a hypothetical density field specified by  $\theta_i(\mathbf{r}, t)$ , where  $\theta$  is related to  $T$  through the thermal coefficient of cubical expansion  $-d\theta/dT$ .

By Jeffreys' theorem (see Eq. (2.6)), hydrostatic equilibrium obtains in the special case when the horizontal gradient of  $\theta_i$  vanishes everywhere (and there is no mechanical forcing), but the equilibrium is unstable when the vertical gradient is anywhere top heavy (i.e.  $d\theta_i/dZ < 0$ ) and sufficiently large in magnitude to overcome dissipative effects due to viscosity, thermal conduction, etc. The investigation of the ensuing overturning motions, as exemplified by the well-known phenomenon of Bénard convection, has been the subject of a considerable amount of experimental and theoretical work (for references see Busse and Carrigan 1974; Chandrasekhar 1961; Gilman 1975; Spiegel 1972; Turner 1973), and this has included cases when general rotation is so rapid that Coriolis forces play a dominant role.

In the more general case when the impressed temperature gradient is not entirely vertical, fluid motions occur for all values of  $\partial\theta_i/\partial Z$  for (by Jeffreys' theorem)  $\mathbf{g} \times \nabla\theta_i \neq 0$  and hydrostatic equilibrium is consequently impossible. It is with such systems in cases when the ensuing motions are strongly influenced by Coriolis forces due to rapid rotation that this final section is largely concerned. These motions not only carry heat horizontally, thereby reducing the impressed horizontal temperature gradient, but they also carry heat

upwards, thereby *increasing* the upward component of the temperature gradient and the downward component of the density gradient.

Thermally-driven flows in rotating fluids subject to a horizontal temperature gradient have been studied extensively during the past twenty-five years (for references see Hide and Mason 1975). Many of the experimental findings are evidently quite general and therefore of wide theoretical interest, and on the meteorological side these findings were influential in the development of successful ideas concerning the large-scale motions in the atmosphere (see Lorenz 1967; Quinet 1974), at a time when such problems were well beyond the range of computers. Indeed, even modern computers are at a disadvantage in the investigation of the more complicated flow phenomena encountered — at first sight somewhat paradoxically — when the apparatus is rotated comparatively rapidly (see Eqs. (5.2) and (5.3) and Fig. 10).

The simplest system in which controlled and reproducible experiments have been carried out is the annular apparatus introduced by Hide in 1950 (see Fig. 9) for which, in the case when there are no internal heat sources ( $\bar{Q} = 0$  in the notation of Eq. (2.3)) but the bounding cylindrical side-walls in  $r = a$  and  $r = b$  are maintained at different temperatures  $T_a$  and  $T_b$ , respectively, the impressed temperature field satisfies

$$T_i = [T_b \ln(r/a) - T_a \ln(r/b)] / \ln(b/a). \quad (5.1)$$

Accurate determinations of the principal spatial and temporal characteristics of the fields of temperature and flow velocity over a wide range of precisely specified and carefully-controlled experimental conditions led to the discovery of several fundamentally different free types of flow (see Table 1), only one of which is symmetrical about the axis of rotation (see Fig. 10). The general character of the flow evidently depends largely on the values of certain external dimensionless parameters:

$$\Theta \equiv gd\Delta\rho/\bar{\rho}\Omega^2(b-a)^2 \quad (5.2)$$

and

$$\mathcal{F} \equiv 4\Omega^2 l_4/v^2, \quad (5.3)$$

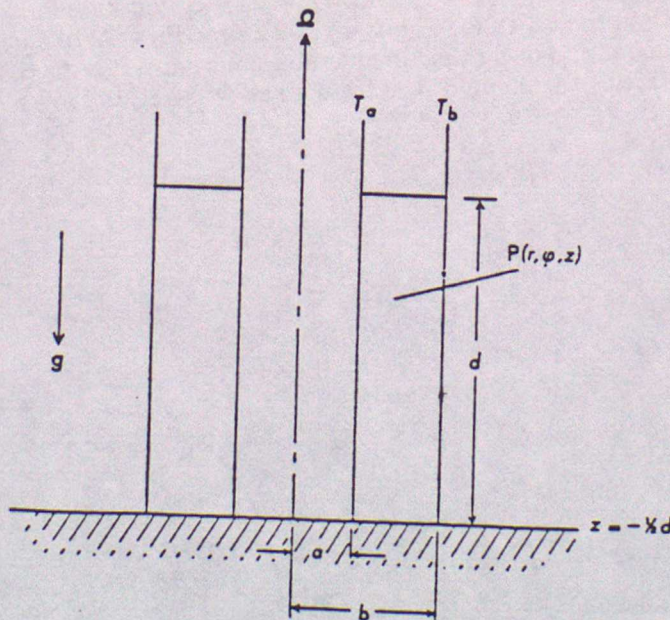


Figure 9. Schematic diagram of a rotating fluid annulus subject to a horizontal temperature gradient, drawn for the case when the upper and lower bounding surfaces are horizontal.  $P$  is a general point with polar coordinates  $(r, \phi, z)$  in a frame of reference rotating with the apparatus.  $\Omega = (0, 0, \Omega)$  is the angular velocity of basic rotation;  $g = (0, 0, -g)$  is the acceleration of gravity (which in magnitude is typically very much larger than  $\Omega^2 r$ ); the region occupied by the fluid is  $a < r < b$  and  $-1/2 d < z < 1/2 d$ ;  $T_a$  and  $T_b$  denote the respective temperatures at which the inner and outer cylindrical boundaries are held by means of temperature baths.

TABLE 1. BROAD CLASSIFICATION OF MODES OF FREE CONVECTION IN A ROTATING FLUID IN AN AXISYMMETRIC CONTAINER SUBJECT TO A HORIZONTAL TEMPERATURE GRADIENT

(1) AXISYMMETRIC
(2) NON-AXISYMMETRIC
(a) regular baroclinic waves
(i) steady waves
(ii) 'vacillation'
(wave shape, wave amplitude,
wave number, wave dispersion)
(b) irregular baroclinic waves
(geostrophic turbulence)

where  $g$  is the acceleration of gravity and typically  $\gg \Omega^2 b$ ,  $d$  the depth of the fluid,  $\Delta \rho$  the density contrast associated with the impressed density difference, i.e.  $\Delta \rho \equiv |\rho(T_a) - \rho(T_b)|$ ,  $\bar{\rho}$  is the mean density,  $\Omega$  the angular velocity of basic rotation and  $\nu$  the kinematic viscosity

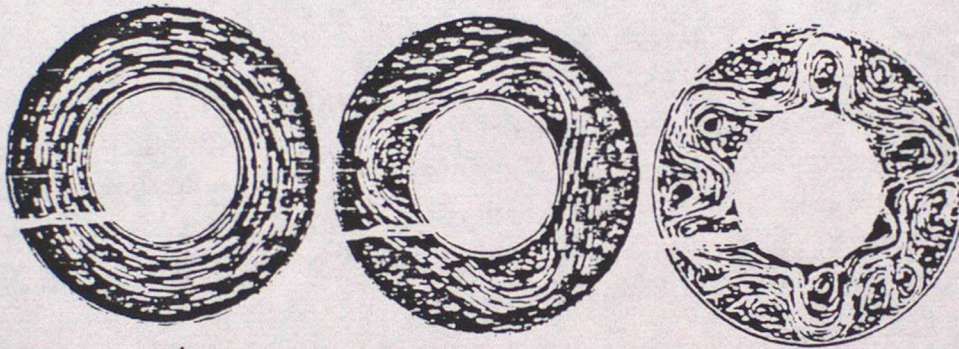


Figure 10. Streak photographs giving one example of each of the main modes of thermal convection in a rotating fluid annulus subject to a horizontal temperature gradient (see Figs. 9 and 11), namely (a) axisymmetric flow, (b) regular baroclinic waves and (c) irregular baroclinic waves, corresponding to different rates of (anticlockwise) basic rotation rate  $\Omega = 0.341, 1.19$  and  $5.02 \text{ rad s}^{-1}$  respectively. (Experimental details:  $a = 3.8 \text{ cm}$ ;  $b = 8.4 \text{ cm}$ ;  $d = 15.4 \text{ cm}$ ;  $T_a = 16.3^\circ\text{C}$ ;  $T_b = 25.8^\circ\text{C}$ ; working fluid - water; duration of time exposure for streak photographs was 1 s for Fig. 10(a) and 3 s for Figs. 10(b) and (c).) Note that the thick white streak in the lower left quadrant of each picture has no significance; it is the outline of a wire well above the surface of the fluid. (Taken from a review by Hide 1969.)

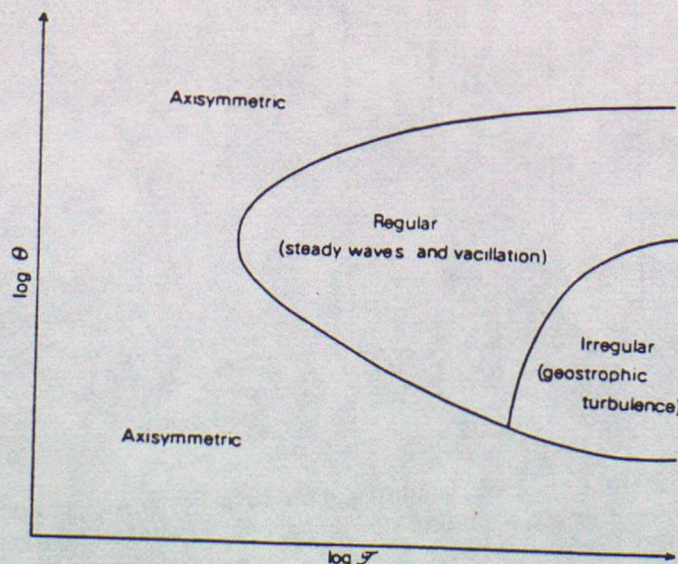


Figure 11. Schematic regime diagram illustrating the dependence of the mode of thermal convection in a rotating fluid annulus subject to a horizontal temperature gradient on the two principal dimensionless parameters required to specify the system, namely  $\Theta$  and  $\mathcal{F}$  (see Eqs. (5.2) and (5.3), Table 1 and Fig. 10).

of the fluid. The quantity  $l_4$  has the dimensions of length to the fourth power and over a fairly wide range of conditions is equal to  $(b-a)^5/d$ . When  $\mathcal{T}$  is less than a certain critical value of about  $2 \times 10^5$  (see Fig. 11), viscosity ensures that the motion is essentially symmetric about the axis of rotation for all values of  $\Theta$  (cf. Fig. 10(a)), but when  $\mathcal{T}$  exceeds this critical value there exists a certain range of  $\Theta$  within which the corresponding motions are highly non-axisymmetric and either regular (cf. Fig. 10(b)) or irregular (cf. Fig. 10(c)), depending on the values of  $\Theta$  and  $\mathcal{T}$ . The regular flows (as exemplified by Fig. 10(b)) usually exhibit periodic time variations which take the form of 'vacillations' (see Hide 1953, 1958) in wave-amplitude, wave-shape, or wavenumber, or of wave dispersion (see Table 1), but under certain conditions the amplitude of these periodic changes is so small that, apart from a steady drift of the wave pattern relative to the apparatus, the flow is virtually steady. In sharp contrast to this behaviour, the irregular flows, as exemplified by Fig. 10(c), exhibit complicated aperiodic fluctuations.

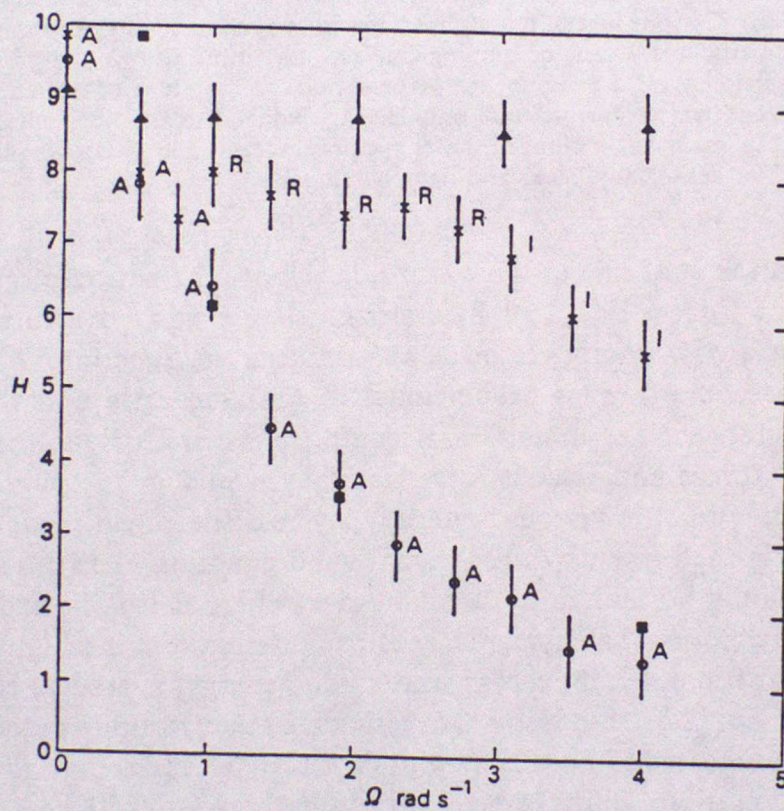


Figure 12. Illustrating the dependence of the heat transfer coefficient  $H$  (Nusselt number) on the basic rotation rate  $\Omega$  for thermal convection in a typical rotating fluid annulus subject to a horizontal temperature gradient (see Figs. 9, 10 and 11 and Table 1).  $H = 1$  corresponds to no convective heat transfer, just conduction (and radiation). The letter 'A' denotes axisymmetric flow, 'R' regular baroclinic waves and 'I' irregular baroclinic waves ('geostrophic turbulence'). Crosses on the error bars correspond to a system with plane horizontal end-walls, circles to sloping end-walls introduced so as to suppress non-axisymmetric flow (see Hide and Mason 1975) and triangles to a case when a rigid impermeable full radial barrier connecting the inner and outer cylinder was inserted so as to reduce the effect of rotation on advective heat transfer. The squares are values based on a simple theoretical model of heat transfer due to axisymmetric flow (Hide 1967) and are evidently in good agreement with the experimental measurements.

Here is not the place to present a detailed account of extensive experimental and theoretical work on various aspects of these flow phenomena (for reviews see e.g. Fultz *et al.* 1959; Hide 1969; Hide and Mason 1975), but it is of some interest to discuss certain findings that bear on the basic theoretical ideas presented in section 2. Of particular interest is the effect of rotation on heat transfer (see Fig. 12). In a system characterized by axial symmetry about the rotation axis, motions are confined to meridian planes when  $\Omega = 0$ , with lighter (warm) fluid rising and passing from the warm side to the cold side, and heavier (cool) fluid

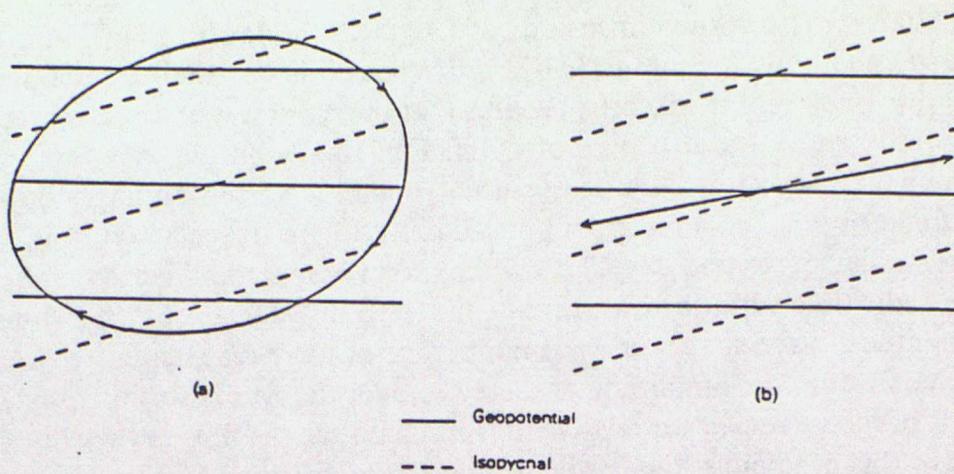


Figure 13. Illustrating 'sloping convection' (see text). In case (a),  $\Omega$  is zero or sufficiently small for direct axisymmetric meridional overturning to occur as a result of the impressed horizontal density gradient. At higher rates of rotation, case (b), Coriolis forces inhibit direct meridional overturning, and the motion now consists of non-axisymmetric baroclinic waves, or 'sloping convection', with motions and variations in the velocity, pressure and density field having  $\phi$  components, perpendicular to the plane of the diagram. Typical individual fluid elements move in trajectories that are only slightly inclined to the horizontal, at an angle which is essentially non-zero but less than the slope of the isopycnal surfaces, so as to ensure that on average denser fluid sinks and lighter fluid rises.

sinking and passing from the cool side to the warm side. Under the action of gravitational torques proportional to  $g \times \nabla\theta$  (see Eq. (2.6)), fluid elements undergo an overturning motion (see Fig. 13(a)), the associated vorticity vector being azimuthal in direction. When, on the other hand,  $\Omega \neq 0$ , gyroscopic torques proportional to  $(2\Omega \cdot \nabla)\mathbf{u}$  arise and these inhibit meridional overturning. Indeed, the inhibition is complete when Coriolis forces greatly exceed the other inertial forces and viscous forces, as they would in the main body of a rapidly rotating fluid (though not in viscous boundary layers or detached shear layers); the essential torque balance is then given by the thermal wind equation (2.18), from which it follows that  $\mathbf{u}$  is then mainly horizontal in direction everywhere if it is horizontal on the boundaries. Axisymmetric motions satisfying the geostrophic equations are highly inefficient not only at converting kinetic potential energy into kinetic energy, a process that requires overturning motions (see Eq. (2.5)), but also at advecting heat in directions perpendicular to  $\Omega$ , since  $u_r$  vanishes when  $\mathbf{u}$  satisfies Eq. (2.15) with  $\partial P/\partial\phi = 0$ . Horizontal advective heat transfer by axisymmetric motions will take place largely in the end-wall Ekman layers (see Eqs. (4.7)–(4.9)) and such transfer decreases rapidly with  $\Omega$ , roughly as  $\Omega^{-\frac{1}{2}}$  (Hide 1967). One therefore expects, and the experiments confirm, that if the flow were to remain axisymmetric as  $\Omega$  increases, the advective contribution  $H-1$  (when expressed in suitable dimensionless units) to the heat transfer should become vanishingly small (see Fig. 12). (Here  $H$  is the Nusselt number, defined as the total heat transfer divided by the heat transfer by conduction (and/or radiation) alone (see e.g. Hide 1958; Krieth 1968).)

In practice, however, the flow does not remain axisymmetric, unless very special steps are taken (see Fig. 12), and the dependence of  $H$  on  $\Omega$  is rather more complicated than a steady monotonic decrease. When, as a result of increasing  $\Omega$ ,  $H$  has dropped by no more than 20% or 30% (depending on the exact values of other parameters) below  $H(\Omega = 0)$ , regular non-axisymmetric wave-motions set in (see Fig. 10(b) and 11) and within the regular waves regime  $H$  remains fairly independent of  $\Omega$  (see Fig. 12). It is only when  $\Omega$  attains a sufficiently high value for irregular non-axisymmetric flow ('geostrophic turbulence') to occur (see Figs. 10(c) and 11) that  $H$  starts to drop again with increasing  $\Omega$ , behaviour which would appear somewhat paradoxical to engineers (see e.g. Krieth 1968) used to associating an *enhancement* of heat transfer with the onset of turbulent flow.

The mechanisms responsible for the transitions from axisymmetric to non-axisymmetric flow and from regular non-axisymmetric flow to irregular non-axisymmetric flow are of considerable theoretical interest. It has been demonstrated fairly conclusively that the non-axisymmetric flows, with their meandering jet streams, are fully-developed 'baroclinic waves' which owe their existence to an instability of the basic axisymmetric state. The available potential energy of that state is converted into kinetic energy of the waves by a process which has been termed 'sloping convection' (see Fig. 13(b)), in which typical individual fluid elements move in trajectories that are only slightly inclined to the horizontal, at an angle which is essentially non-zero but less than the slope of isopycnic surfaces. Baroclinic waves, with a horizontal scale given by Eq. (3.11), and associated frontal systems and jet streams are characteristic features of the earth's troposphere, where they play a key role in the planetary-scale transport of heat and momentum, and it can be expected on general theoretical grounds that baroclinic waves will occur not only at other levels in the atmosphere, but also in other natural systems, such as the terrestrial oceans and the fluid regions of rapidly-rotating planets and stars, including the sun.

So far as the transition from regular baroclinic waves to irregular flow ('geostrophic turbulence') is concerned, various lines of experimental evidence and theoretical reasoning (for references see Hide and Mason 1975) point to the conclusion that irregular flow arises when the baroclinic waves are 'barotropically unstable', with the kinetic energy of the main baroclinic mode passing, through non-linear interactions, to other scales of motion. The most striking evidence comes from determinations of  $m_{\max}$ , the number of waves around the annulus ( $m$ ) at the transition from regular to irregular waves. Reducing  $\Theta$  (see Eq. (5.2)) within the regular regime tends to increase  $m$  (equal to 3 in Fig. 10(b)) and the transition to irregular flow occurs when the azimuthal wavelength  $\pi(b+a)/m$ , has dropped to a value  $\pi(b+a)/m_{\max}$  close to 1.5 times the radial scale of the waves, according to the original annulus experiments, which covered a wide range of  $b/a$  and the other parameters (Hide 1953, 1958; see also Hide and Mason 1975). In such an anisotropic system where, owing to Coriolis forces, vertical motions are very much slower than horizontal motions and viscous effects are weak, one might expect the spirit of Fjørtoft's theorem to apply, even if not the letter (see section 2(iv) and Eq. (2.27)). By that theorem the main baroclinic wave cannot lose kinetic energy by non-linear interactions to smaller scales of motion without simultaneously losing energy to larger scales of motion, and when the azimuthal wavelength  $\pi(b+a)/m$  of the main baroclinic wave is comparable with the size of the apparatus, larger scales are not available and in consequence the wave is stable (see Fig. 10(b)). Only when  $\pi(b+a)/m$  is small enough,  $\approx 1.5$  times the radial scale according to the experiments, are the larger scales available; non-linear interactions then produce irregular flow by continually transferring kinetic energy from the main baroclinic wave to other scales of motion.

These results concerning the nature of the irregular regime of flow have important implications for dynamical meteorology and oceanography. They also enable us to understand the principal finding of the two or three isolated laboratory investigations of thermal convection in rotating fluids undertaken prior to 1950. More than a century ago Vettin made a qualitative study of the top-surface flow in a rotating tank of fluid with a lump of ice near the centre, and thereby noticed that the axisymmetric flow patterns found at low values of  $\Omega$  gave way to irregular non-axisymmetric patterns at higher values of  $\Omega$ . He also drew meteorological conclusions from his laboratory work (see Fultz *et al.* 1959), but these were unpalatable to his contemporaries, presumably because such an approach to meteorological problems came too soon, at a time when the atmosphere was very incompletely observed, theoretical meteorology was isolated from other branches of science, and the subject of fluid dynamics had not yet been transformed to its present healthy state from being an activity in which (to paraphrase some recent remarks by a leading expert) 'engineers

observed effects that could not be explained and mathematicians explained effects that could not be observed.\* Nowadays, fortunately, dynamical meteorologists and oceanographers make good use of basic fluid dynamics, including the full implications of the concept of geostrophy which, as we have found in our discussion of a range of experiments with rotating fluids, plays a central role in the interpretation of a wide variety of flow phenomena. Indeed, none would now dispute that the important problems in geophysical fluid dynamics can only be tackled seriously through a combination of observational, experimental and mathematical investigations, rendered crucial by keeping basic theoretical notions in mind.

## ACKNOWLEDGMENTS

In my work over the years on rotating fluids I have been greatly helped by many colleagues and students, and I am also indebted to several agencies and institutions for financial support and other resources.

## REFERENCES

- |  |      |  |
|--|------|--|
| Acheson, D. J. and Hide R.   | 1973 | Hydromagnetics of rotating fluids, <i>Reports on Progress in Physics</i> , 36, 159-221.  |
| Aldridge, K. D.  | 1972 | Axisymmetric inertial oscillations of a fluid in a rotating spherical shell, <i>Mathematika</i> , 19, 163-168.   |
| Aldridge, K. D. and Toomre, A.   | 1969 | Axisymmetric inertial oscillations of a fluid in a rotating spherical container, <i>J. Fluid Mech.</i> , 37, 307-323.  |
| Batchelor, G. K.   | 1967 | <i>An introduction to fluid mechanics</i> , Cambridge University Press.  |
| Bennetts, D. A. and Jackson, W. D. N.                                    | 1974 | Source-sink flows in a rotating annulus: a combined laboratory and numerical study, <i>J. Fluid Mech.</i> , 66, 689-705.                                       |
| Benton, E. R. and Clark, A.  | 1974 | Spin-up, <i>Annual Reviews of Fluid Mechanics</i> , 6, 257-280.  |
| Brown, S. N. and Stewartson, K.  | 1976 | Asymptotic methods in the theory of rotating fluids, <i>Proc. Symp. on Asymptotic Methods and Singular Perturbations</i> (New York, 1976).                     |
| Busse, F. H. and Carrigan, C. R.   | 1974 | Convection induced by centrifugal buoyancy, <i>J. Fluid Mech.</i> , 62, 579-595.   |
| Buzyna, G. and Veronis, G.   | 1971 | Spin-up of a stratified fluid: theory and experiment, <i>Ibid.</i> , 50, 579-608.  |
| Chandrasekhar, S.  | 1961 | <i>Hydrodynamic and hydromagnetic stability</i> , Oxford University Press.   |
| Charney, J. G.   | 1973 | Planetary fluid dynamics. In <i>Dynamical meteorology</i> (ed. P. Morel), D. Reidel Publishing Company, Dordrecht, Holland, 97-352.                            |
| Dutton, J. A. and Johnson, D. R.   | 1967 | The theory of available potential energy and a variational approach to atmospheric energetics, <i>Advances in Geophysics</i> , 12, 334-436.                    |
| Eckart, C.   | 1960 | <i>Hydrodynamics of atmospheres and oceans</i> , Pergamon Press, London.   |
| Eliassen, A. and Kleinschmidt, E.  | 1957 | Dynamical meteorology. In <i>Handbuch der Physik</i> , 48, 1-154, Berlin, Springer-Verlag.   |
| Fjørtoft, R.   | 1953 | On the changes in the spectral distribution of kinetic energy for two-dimensional, non-divergent flow, <i>Tellus</i> , 5, 225-230.                             |
| Fultz, D., Long, R. R., Owens, G. V., Bohan, W., Kaylor, R. and Weil, J. | 1959 | Studies of thermal convection in a rotating cylinder with some implications for large-scale atmospheric motions, <i>Met. Mon., Amer. Met. Soc.</i> , 4, 1-104. |
| Gilman, P. A.  | 1975 | Linear simulation of Boussinesq convection in a deep rotating spherical shell, <i>J. Atmos. Sci.</i> , 32, 1331-1352   |

\* The systematic study of rotating fluids might have commenced in the last century had mathematicians and physicists been prepared to investigate the theoretical implications of the discovery - from analyses of meteorological data - of geostrophic motion in the atmosphere. In the event, the discovery seems to have been played down if the following words (taken from a lecture delivered in 1869) of a former president of this Society can be taken as representative of the general attitude of contemporary scientists: 'A principle has been much before the public of late which was first urged by Professor Buys-Ballot of Utrecht. It may be stated as follows: Stand with your back to the wind and the barometer will be lower on your left than on your right (in the northern hemisphere). No matter how gently the wind blows, the law is found to be true. This fact, however, is of no use to us in enabling us to judge the coming weather.'

- Golitsyn, G. S. 1973 *An introduction to the dynamics of planetary atmospheres*, Hydrometeorology, Leningrad.
- Greenspan, H. P. 1968 *The theory of rotating fluids*, Cambridge University Press.
- Hide, R. 1953 Some experiments on thermal convection in a rotating liquid, *Quart. J. R. Met. Soc.*, 79, 161
- 1958 An experimental study of thermal convection in a rotating liquid, *Phil. Trans. R. Soc. Lond.*, A250, 442-478.
- 1967 Theory of axisymmetric thermal convection in a rotating fluid annulus, *Phys. Fluids*, 10, 56-68.
- 1968 On source-sink flows in a rotating fluid, *J. Fluid Mech.*, 32, 737-764.
- 1969 Some laboratory experiments on free thermal convection in a rotating fluid subject to a horizontal temperature gradient and their relation to the theory of the global atmospheric circulation, in *The global circulation of the atmosphere* (ed. G. A. Corby), London; Royal Meteorological Society.
- 1971 On geostrophic motion of a non-homogeneous fluid, *J. Fluid Mech.*, 49, 745-751.
- 1976 Motions in planetary atmospheres, *Quart. J. R. Met. Soc.*, 102, 1-23.
- 1968 On slow transverse flow past obstacles in a rapidly-rotating fluid, *J. Fluid Mech.*, 32, 251-272.
- Hide, R., Ibbetson, A. and Lighthill, M. J. 1975 Sloping convection in a rotating fluid, *Advances in Physics*, 24, 47-100.
- Hide, R. and Mason, P. J. 1972 Hydromagnetic oscillations of the Earth's core, *Rev. Geophys. and Space Phys.*, 10, 579-598.
- Hide, R., and Stewartson, K. 1973 *Methods and results of theoretical oceanography: 1, Dynamics of the homogeneous and quasi-homogeneous ocean*, Gebrüder Bornträger, Berlin, Stuttgart.
- Krauss, W. 1968 Convection heat transfer in rotating systems, *Advances in Heat Transfer*, 5, 129-251.
- Krieth, F. 1966 Dynamics of rotating fluids: A survey, *J. Fluid Mech.*, 26, 411-431.
- Lighthill, M. J. 1973 Lectures on sub-synoptic scales of motions and two-dimensional turbulence. In *Dynamical meteorology* (ed. P. Morel) D. Reidel Publishing Company, Dordrecht, Holland, 353-418.
- Lilly, D. K. 1974 Theory of the main thermocline (a review), *Akad. Nauk. Okeanograf. Kom., Okeanologiya*, 14, 965-981.
- Lineykin, P. S. 1967 *The nature and theory of the general circulation of the atmosphere*. World Meteorological Organization Publication No. 218.
- Lorenz, E. N. 1976 Forces on spheres moving horizontally in a rotating stratified fluid, *Geophys. Fluid Dyn.*, 7.
- Mason, P. J. 1976 Angular momentum diffusion and the initiation of cyclones, *Nature*, 260, 126-128.
- McEwan, A. D. 1972 *Weather forecasting as a problem in physics*, M.I.T. Press, Cambridge, Mass.
- Monin, A. S. 1974 Global invariants of atmospheric motions pp. 106-112 in *Physical and dynamical climatology*, World Meteorological Organization Monograph No. 347, Hydrometeorology, Leningrad.
- Obukhov, A. M. 1971 Geophysical fluid dynamics, *Lectures in Applied Mathematics*, 13, 1-60.
- Pedlosky, J. 1963 Geostrophic motion, *Rev. Geophys.*, 1, 123-173.
- Phillips, N. A. 1968 The Rossby wave, *Quart. J. R. Met. Soc.*, 94, 225-248.
- Platzman, G. W. 1952 *Essentials of fluid dynamics*, London; Blackie and Sons.
- Prandtl, L. 1916 On the motions of solids in a liquid possessing vorticity, *Proc. R. Soc. Lond.*, A92, 408-424.
- Proudman, J. 1974 A numerical study of vacillation, *Advances in Geophysics*, 17, 101-186.
- Quinet, A. 1976 The dynamics of unsteady currents, In *The sea*, Vol. VI, pp. 189-318. E. Goldberg, ed. John Wiley and Sons, New York.
- Rhines, P. B.

- |                 |      |   |
|-----------------|------|---|
| Spiegel, E. A.  | 1972 | Convection in stars. II. Special effects, <i>Ann. Rev. Astronomy Astrophys</i> , 10, 261-304.   |
| Stern, M. E.    | 1975 | <i>Ocean circulation physics</i> , Vol. 19. International Geophysics Series, Academic Press.  |
| Stommel, H.     | 1965 | <i>The Gulf Stream</i> , University of California Press.  |
| Taylor, G. I.   | 1917 | Motion of solids in fluids when the flow is not irrotational, <i>Proc. R. Soc.</i> , A93, 99-113.                                     |
|                 | 1923 | Experiments on the motion of solid bodies in rotating fluids, <i>Proc. R. Soc. Lond.</i> , A104, 213-218.                             |
|                 | 1974 | The interaction between experiment and theory in fluid mechanics, <i>Ann. Rev. Fluid Dyn.</i> , 6, 1-16.                              |
| Thompson, P. D. | 1961 | <i>Numerical weather analysis and prediction</i> , MacMillan Co., New York.   |
| Turner, J. S.   | 1973 | <i>Buoyancy effects in fluids</i> , Cambridge University Press.   |
| Van Mieghem, J. | 1973 | <i>Atmospheric energetics</i> , Clarendon Press, Oxford.  |
| Yeronis, G.     | 1973 | Large scale ocean circulation, <i>Advances in Applied Mechanics</i> , 13, 1-92. (ed. C. S. Yih, Academic Press, New York and London.) |

NOTE ADDED IN PROOF. According to Dr A. E. Gill (private communication), one example of Kelvin waves (see page 10 above) in the troposphere are the 'coastal laws' that propagate around the southern end of the African continent at all times of the year.

## LECTURE 9: SUPER-ROTATION &amp; ANGULAR MOMENTUM I. AN ANNULUS MODEL

1. Introduction

It has long been appreciated that the tendency for a fluid approximately to conserve axial angular momentum can place important constraints on the form and intensity of the flow in a rotating system. This is especially true of an axisymmetric system since the absolute angular momentum per unit mass,  $m$ , defined in cylindrical geometry by

$$m = r(\Omega r + v) \quad (1)$$

(where  $r$  is the cylindrical radius from the rotation axis,  $\Omega$  is rotation rate and  $v$  is azimuthal velocity) is governed (for an incompressible fluid) by

$$\partial m / \partial t + \mathbf{u} \cdot \nabla m = \mathfrak{S} / \rho \quad (2)$$

(where  $\mathfrak{S}$  is a source/sink term due to molecular viscosity and  $\mathbf{u}$  is the velocity in the meridional plane). Thus, in an inviscid fluid,  $m$  is precisely conserved following the motion in the meridional plane. Under these conditions, the flow is severely constrained by the distribution of  $m$  in the initial state - the total angular momentum must remain constant. If the flow is initially at rest in the rotating frame,  $m$  at subsequent times can never exceed  $\Omega r_{\max}^2$  (where  $r_{\max}$  is the maximum radial distance from the rotation axis) - prograde motion ( $v > 0$ ) at  $r = r_{\max}$  is excluded! Flows with a net local or global excess of angular momentum (said to be in super-rotation with respect to the inviscid state) must require viscous and/or non-axisymmetric effects to maintain that excess.

The above considerations are of interest in connection with the general circulation of atmospheres, since most atmospheres are observed to possess on average significant local and global excesses of angular momentum. To examine ways in which such an excess can be maintained in a perfectly axisymmetric flow, we consider in this lecture the super-rotation of viscous flows in a thermally-driven, rotating, cylindrical annulus (the ensuing discussion is largely summarised from papers by Read 1986a,b).

## 2. Effects of internal viscosity

Since an inviscid, axisymmetric system (initially at rest) cannot exhibit any super-rotation, it is natural to consider the effects of Newtonian (molecular) viscosity, while still preserving an axisymmetric flow. Viscosity removes the formal conservation of  $m$  but, for a steady flow, some useful constraints can still be derived (cf the discussion of Held & Hou 1980). With viscosity, Eq (2) can be written as

$$\partial m / \partial t + \nabla \cdot (\mathbf{u}m) = - \nabla \cdot \mathbf{F} \quad (3)$$

where  $\mathbf{F}$  is the diffusive flux of  $m$  due to viscosity which, for an isotropic fluid, is given by

$$\begin{aligned} \mathbf{F} &= - \nu r^2 \nabla \omega \\ &= - \nu r^2 \nabla (m/r^2) \end{aligned} \quad (4)$$

where  $\omega$  is the local relative angular velocity  $= v/r$ . If we consider any local maximum in  $m$  (necessarily, though not exclusively, associated with local super-rotation),  $m = m_0$  say, we may draw a closed  $m$  contour in the meridional plane at  $m = m_0 - \delta$  (where  $\delta$  may be arbitrarily small and positive, see Fig. 1). Integrating the steady form of (3) over the toroidal volume enclosed by the  $m_0 - \delta$  contour, we obtain

$$\begin{aligned} \iint \nabla \cdot (\mathbf{u}m) dV &= (m_0 - \delta) \int \mathbf{u} \cdot \mathbf{n} ds \\ &= 0 \text{ (by mass conservation)} \\ &= - \int \mathbf{F} \cdot \mathbf{n} ds \end{aligned} \quad (5)$$

Thus, either  $\mathbf{F} \cdot \mathbf{n} = 0$  everywhere, or else  $\mathbf{F}$  must possess both inward and outward components in different regions of the  $m$  contour (i.e.  $\mathbf{F}$  must act up-gradient w.r.t  $\nabla m$  somewhere in the flow). Since  $\mathbf{F}$  is anti-parallel to  $\nabla \omega$  (and not to  $\nabla m$  - see Eq (4)), a necessary condition for local super-rotation is that  $\nabla \omega \cdot \nabla m$  take either sign in the flow (NB it is not necessary to invoke 'negative viscosity' phenomena - fundamentally associated with non-axisymmetric effects).

### 3. An example in the cylindrical annulus

The above ideas can be illustrated in a numerical simulation of flows in a rotating fluid annulus, heated and cooled at the sidewall boundaries in the conventional way. The model is an axisymmetric version of that described in Lecture 7, except that all boundaries are stress-free (i.e.  $\nabla\omega \cdot \mathbf{n} = \mathbf{F} \cdot \mathbf{n} = 0$ , and the fluid cannot exchange  $m$  with the boundary via viscosity) apart from the lower surface, which is rigid and non-slip. The fluid was initialised as isothermal (at  $T = (T_a + T_b)/2$ ) and at rest in the rotating frame, then integrated in time until a steady state was reached.

A meridional overturning circulation is driven by the differential heating between the two sidewalls which is largely thermally-direct (see Fig. 2), although some smaller, indirect cells also occur owing to the effects of a diffusive instability (when the Prandtl number  $\gg 1$ ). During the spin-up of the flow,  $m$  is redistributed by the meridional circulation upwards and inwards towards the rotation axis, and accumulates near the top of the inner cylinder, generating a local maximum in  $\omega$ . Since  $\mathbf{F}$  is related to  $\nabla\omega$ , viscous diffusion transfers  $m$  radially outwards from the  $\omega$  maximum against its local gradient  $\nabla m$ . In the steady state, the outward diffusion of  $m$  exactly balances advection by the meridional circulation, and the distribution of  $\mathbf{F}$  and  $m$  is shown in Fig. 2(c). Note that fluid elements near  $r = b$  and  $z = d$  have acquired  $m > \Omega b^2$  in a wedge-shaped region of the flow. Since Eq (5) is satisfied not only for regions bounded by contours of  $m$  but also by impermeable boundaries, it also applies to the flow in Fig. 2, with  $\mathbf{F}$  up-gradient w.r.t  $\nabla m$  in some places and down-gradient in others. Adjacent to the lower non-slip boundary,  $\omega < 0$  along the outer part of the boundary and  $\omega > 0$  along the inner part, so that the net torque on the flow is zero (cf the distribution of mean zonal flow at the Earth's surface, with easterlies in the tropics and westerlies at higher latitudes).

If we define the quantitative super-rotation with respect to the angular momentum in an inviscid fluid at rest in the rotating frame, we obtain a measure of the global super-rotation

$$S = \iint v r^2 dr dz / \iint \Omega r^3 dr dz \quad (6)$$

which measures the total relative angular momentum against the absolute angular

momentum of the initial rest state ( $S > 0$  implies an excess of angular momentum over the rest state). A similar measure of local super-rotation can be defined as

$$s = m/\Omega b^2 - 1 \quad (7)$$

The example illustrated in Fig. 2 has  $S \approx s_{\max} \approx 0.35$ , so that the flow clearly exhibits both local and global super-rotation.

#### 4. Scale analysis of super-rotation

How do  $S$  and  $s$  depend upon the external parameters, and can any quantitative limits be placed on the maximum values of  $S$  and  $s$  attainable? These questions can be answered in part by a scale analysis of the governing equations, noting that  $S$  itself is a dimensionless parameter equivalent to a Rossby number based on the cylindrical radius

$$S \sim R_c = \bar{V}/\Omega \bar{r} \quad (8)$$

where  $\bar{r}$  and  $\bar{V}$  are typical radius and azimuthal velocity scales. The details of the analysis are too complicated to include here, but may be found in Read (1986a). We give a flavour of its methods and results below.

It is convenient to define a number of new dimensionless parameters in addition to  $S$  and Prandtl number  $P$  - including the Rayleigh number

$$A = g\alpha\Delta T L^3/\kappa\nu \quad (9)$$

where  $L \sim (b - a)$  and other parameters are conventional, the Ekman number

$$E = \nu/(2\Omega d^2) \quad (10)$$

conventional Rossby number

$$R_o = \bar{V}/(2\Omega L) \quad (11)$$

aspect ratios

$$\epsilon = d/L; \quad \eta = L/r \quad (12a,b)$$

and a further parameter

$$Q = A^{-1/2} E^{-1} \epsilon^{-3/2} \quad (13)$$

The latter is a measure of the (square of the) ratio of the thickness of the (non-rotating) thermal boundary layer at the sidewalls to that of the Ekman layer, and is a convenient dimensionless measure of the rotation rate with a useful physical interpretation (see Read 1986a). Anticipating the final result, we consider a range of intermediate rotation rates consistent with  $\epsilon^2/P^2 \ll Q < 1$ , for which it can be shown that  $\bar{\psi}/r \sim \kappa \epsilon^{3/4} A^{1/4}$ . Scaling the azimuthal component of the vorticity equation in the interior using

$$\Delta r = L \Delta r_*; \quad r = \bar{r} r_*; \quad z = d z_*; \quad \psi = \bar{\psi} \psi_*; \quad T - \bar{T} = \Delta T T_*; \quad (14)$$

(where starred items are dimensionless functions of order unity) we obtain

$$A^{-3/4} \eta^3 \epsilon^{3/4} [\nabla^2 \zeta_* - \zeta_*/r_*^2] = A^{-1/2} P^{-1} \epsilon^{1/2} [J(\psi_*, \zeta_*/r_*^2)] + \frac{\Delta T_h}{\Delta T} [\partial \bar{\psi} / \partial r_*] - R_o P \epsilon^{-2} Q^2 [\partial v / \partial z_*] - \frac{R_c R_o P \epsilon^{-2} Q^2}{c_o} [1/r_* \partial v^2 / \partial z_*] \quad (15)$$

where  $J(x,y)$  is the Jacobian representation of the non-linear terms, and  $\Delta T_h$  is the horizontal temperature difference in the interior ( $\sim \Delta T$  if the isotherm slope  $\geq 1$ ). For  $A$  and  $P \gg 1$ , and  $R_o$  and  $R_c > 1$ , the essential balance is between the buoyancy and centrifugal and Coriolis terms (gradient wind balance - if  $R_c \gg R_o$ , the centrifugal term dominates, resulting in a cyclostrophic balance), implying that if  $\Delta T_h \sim \Delta T$  (valid around  $Q = 1$ , see Read 1986a),  $\epsilon$  and  $\eta$  are large enough, and  $P$  is greater than the limit

$$P \gg (e^2/\eta)^{1/3} \quad (16)$$

(so that diffusion of heat in the interior is not significant), the upper limit on  $R_c$  is approximately

$$\max(R_c) < \epsilon(\eta/P)^{1/2} \quad (17)$$

The most rapidly super-rotating flows thus require large aspect ratios and cylindrical curvature, and moderate rotation rates and Prandtl number. The resulting flow is characterised by a gradient wind balance (with centrifugal terms dominating over Coriolis terms in extreme cases) in the interior vorticity equation. A further novel implication is that the Ekman layers are no longer linear in the azimuthal momentum equation, but are characterised by a balance between the viscous term and the non-linear inertial acceleration (rather than the Coriolis term). The results of this analysis have been verified using a numerical model which is described by Read (1986a), and some typical profiles of the magnitudes of the various terms in the main equations of motion for a simulation with  $\epsilon = 2$ , close to the maximum in  $R_c$ , are shown in Fig. 3.

#### REFERENCES

- Held, I. M. & Hou, A. Y., 1980. 'Nonlinear axially-symmetric circulation in a nearly inviscid atmosphere', J. Atmos. Sci., **37**, 515-533.
- Read, P. L., 1986a. 'Super-rotation and diffusion of axial angular momentum: I. "speed limits" for axisymmetric flow in a rotating cylindrical fluid annulus', Quart. J. R. Met. Soc., **112**, 231-251.
- Read, P. L., 1986b. 'Super-rotation and diffusion of axial angular momentum: II. a review of quasi-axisymmetric models of planetary atmospheres', Quart. J. R. Met. Soc., **112**, 253-272.

P. L. Read  
August 1986

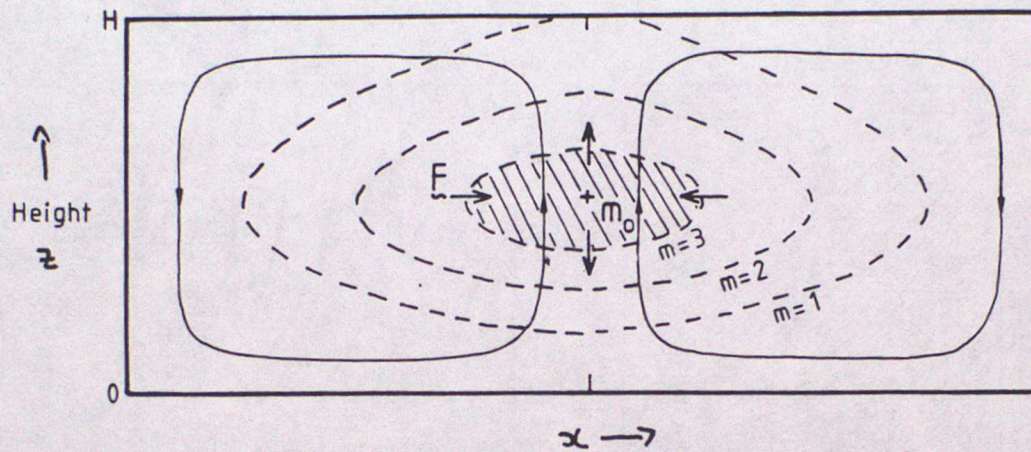


Figure 1: Schematic contour map in the meridional plane (e.g. radius-height plane in cylindrical geometry) of absolute angular momentum in a hypothetical axisymmetric flow. Constraints derived in the text for such a flow, associated with a balance between advection (in a meridional circulation - thin, continuous lines) and diffusion (fluxes illustrated by heavy arrows labelled  $F$ ), result in a need for  $F$  to act inwards in some places and outwards in others for a region enclosed by a closed  $m$  contour.

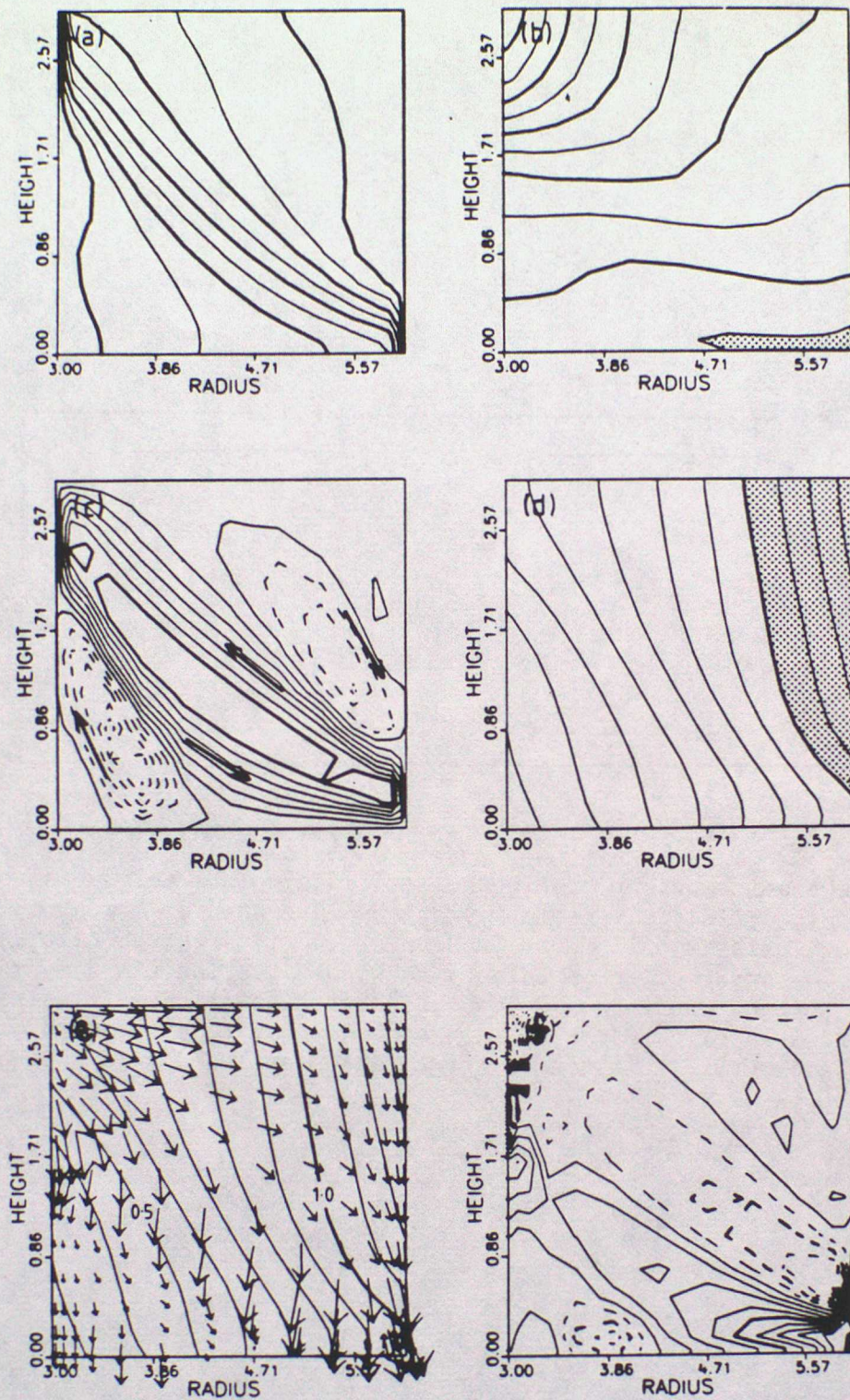


Figure 2. Contour maps of the steady-state fields for a numerical simulation of the thermally-driven axisymmetric circulation in a rotating fluid annulus with rigid, non-slip base, and stress-free side boundaries and top surface (case B, see text): (a) temperature (contour interval, 0.5 K); (b) angular velocity  $\gamma = v/r$  (see text, contour interval, 0.05 s<sup>-1</sup>; the region where  $\gamma < 0$  is shown shaded); (c)  $\chi$  (contour interval, 0.01 cm<sup>2</sup> s<sup>-1</sup>); (d)  $m/\Omega b^2$  (contour interval, 0.1; region where  $m > \Omega b^2$  is shown shaded). Negative contours are dashed. (e)  $m/\Omega b^2$  (contour interval, 0.1), with vectors of  $F$  superimposed; (f)  $-\nabla \cdot F$  (contour interval, 0.025 cm<sup>2</sup> s<sup>-2</sup>). Negative contours are dashed.

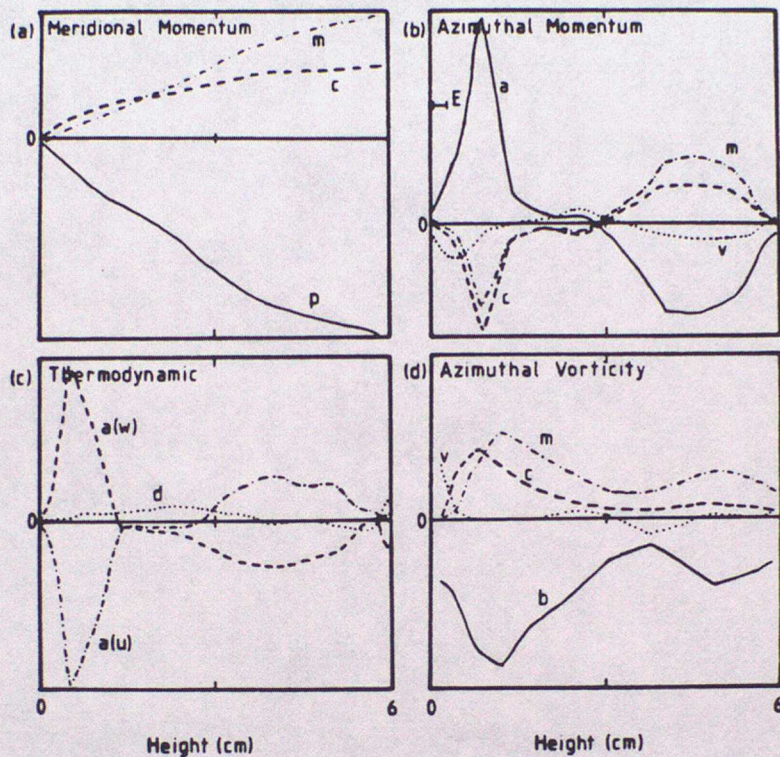


Figure 3: Profiles of the terms in a) the meridional momentum equation, b) the azimuthal momentum equation, c) the thermodynamic equation, and d) the azimuthal vorticity equation, calculated from a numerical simulation of strongly super-rotating flow in a differentially heated rotating annulus with stress-free base and sidewalls (see Read 1986a). Terms are plotted as a function of height at mid-radius, and correspond to a)  $c = 2\Omega v$ ,  $m = v^2/r$ ,  $p = (\partial p/\partial r)/\rho_0$ , b)  $a = \mathbf{u} \cdot \nabla v$ ,  $c = -2\Omega u$ ,  $m = -uv/r$ ,  $v = v(\nabla^2 v - v/r^2)$ ; c)  $a(w) = w\partial T/\partial z$ ,  $a(u) = u\partial T/\partial r$ ,  $d = \kappa\nabla^2 T$ ; d)  $m = 1/r \partial(v^2)/\partial z$ ,  $c = 2\Omega\partial v/\partial z$ ,  $b = g\alpha\partial T/\partial r$ ,  $v = v(\nabla^2 \zeta - \zeta/r^2)$ .

## LECTURE 10: SUPER-ROTATION AND ANGULAR MOMENTUM II. PLANETARY ATMOSPHERES

1. Introduction

The previous lecture considered the generation and maintenance of a super-rotating zonal flow in an axisymmetric, thermally-driven viscous fluid. In the present lecture, we draw on the insight provided by studies of such simple systems in the interpretation of the circulation of the atmospheres of the Earth and other planets of the Solar System. As remarked at the beginning of Lecture 9, most planets are observed to exhibit super-rotation in their atmospheres to a greater or lesser degree. To measure this super-rotation, we can define more general (zonal average) forms of  $S$  and  $s$ , by analogy with the parameters used in Lecture 9. Thus

$$S_o = \int_{-\pi/2}^{\pi/2} \int_0^{\infty} \int_a^{\infty} \rho u R^3 \cos^2 \phi \, dR \, d\lambda \, d\phi / M_o \quad (1)$$

where  $\lambda$  is longitude,  $\phi$  is latitude,  $a$  is the radius of the planetary surface,  $u$  is the zonal velocity component, and

$$M_o = \int_{-\pi/2}^{\pi/2} \int_a^{\infty} \rho \Omega R^4 \cos^3 \phi \, dR \, d\phi \quad (2)$$

$S_o$  is again a measure of the (mean) excess relative angular momentum of the fluid normalised by the absolute angular momentum of the atmosphere if it were stationary in the frame of the underlying rotating planet. For a thin, spherical atmosphere, it is often convenient to approximate  $M_o$  by

$$M_o = (8\pi/3) \rho_o \Omega a^4 H_s \quad (3)$$

where  $\rho_o$  is the density at the surface and  $H_s$  a mean density scale height. The local super-rotation is defined by

$$s = m/(\Omega a^2) - 1 \quad (4)$$

where the local angular momentum per unit mass is defined in spherical polar coordinates thus

$$m = R \cos\phi (\Omega R \cos\phi + u) \quad (5)$$

## 2. Super-rotation observed in planetary atmospheres

Axial angular momentum in the Earth's atmosphere is well known to be concentrated into the mid-latitude (sub-tropical) westerly jet streams. The global atmosphere thus super-rotates with typical values of  $S_0 = 1.5 \times 10^{-2}$  (e.g. see Hide et al. 1980), though with no local super-rotation (motion at the equator is generally easterly). If we interpret  $S_0$  as a global Rossby number by analogy with Lecture 9, the relatively low value for the Earth is simply an indication of the highly geostrophic nature of the bulk of the zonal motion in the atmosphere.

This is certainly not the case for the two planets Venus and Titan (the largest moon of Saturn), which rotate about their axes much more slowly than the Earth (sidereal periods of 243 days and 16 days respectively). Despite their very long planetary rotation periods, their atmospheres (at least around the tops of dense cloud layers) are observed to super-rotate comparatively very rapidly in the same sense as the rotation of the underlying planet. For Venus (for which a large amount of quantitative data are now available from US and Soviet spacecraft, e.g. see Schubert 1983), the atmospheric rotation period at the cloud tops is only  $\sim 4$  days (1/60 of the planetary period !!! - see Fig. 1) and the global super-rotation  $S_0$  is inferred to be  $\approx 10$ . With such a large value of  $S_0$ , the prevailing dynamical balance cannot be geostrophic, but is consistent with a cyclostrophic balance in the zonal vorticity equation between buoyancy torques and the centrifugal term - i.e. the 'thermal wind equation' becomes (in pressure coordinates)

$$\partial(u^2)/\partial(\ln p) = - R_g / \tan\phi \partial T / \partial\phi \quad (6)$$

where  $R_g$  is the gas constant (cf the case discussed in Lecture 9). The generation and maintenance of such a large super-rotation is still poorly understood in detail, and remains one of the outstanding problems in planetary

dynamical meteorology. For Titan, the available data are much more sparse, but the overall circulation appears to be very similar to that of Venus (see Flasar et al. 1981).

As discussed in Lecture 6, the major planets (Jupiter and Saturn) are very rapidly rotating, although the measurement of super-rotation is rendered difficult by the absence of an underlying planetary surface. For both planets it has become conventional to measure zonal motion with respect to a frame rotating with the planet's magnetic field ('System III') - believed to represent the rotation of the deep interior. In such a frame, the global super-rotation of each planet is extremely small (so far as it can be determined, since we can only measure it at the cloud tops). The local super-rotation near the equator, however, is significantly positive ( $\sim 10^{-2}$  for Jupiter - see Fig. 2 and Flasar 1986), associated with strong equatorial westerly jet streams. The generation and maintenance of such strongly super-rotating jets is again poorly understood.

The latest encounter by the Voyager 2 spacecraft with Uranus has revealed further intriguing problems concerning the super-rotation (or not!) of a planetary atmosphere. The rotation of Uranus has been a long-standing problem in astronomy a) because it is very hard to measure from the Earth (Uranus exhibits almost no visible features to observe its rotation); and b) by virtue of its extremely large obliquity with respect to its orbit (the rotation axis is oriented at  $98^{\circ}$  with respect to its orbital axis around the Sun) - which is not at all well understood. The Voyager images have enabled the atmospheric rotation to be measured at a few latitudes (about 8 in total! - see Smith et al. 1986), which suggest that the wind is westerly with respect to the magnetic field at nearly all latitudes, but with a (possibly easterly) minimum at the equator (i.e. little or no local or global super-rotation - see Fig. 3). It is of interest to note that, because of its large obliquity, Uranus' solar insolation (averaged over a Uranian year) is a maximum at its poles and a minimum at the equator. One might expect that this would result in a vertical transfer of  $m$  by a thermally-direct meridional circulation in the opposite sense (i.e. downwards) to that in an atmosphere with a heated equator and cooled poles, resulting in a net sub-rotation (i.e. a negative super-rotation) of the upper atmosphere (see Read 1986).

### 3. Angular momentum transfer in planetary atmospheres

In considering the transfer of angular momentum in an atmosphere, it is convenient to take as a starting point the properties of the axisymmetric (zonally-averaged) component of the circulation. As discussed above,  $S_0$  and  $s$  are frequently observed to exceed 1, suggesting a need to consider processes in addition to advection by the meridional and vertical motion fields, such as the viscous diffusion considered in Lecture 9. In a large-scale atmosphere, however, the effects of molecular diffusion are effectively negligible compared with other processes. It has long been accepted since the work e.g. of Jeffreys, Rossby and Starr (see Lorenz 1967) that the most important additional processes transferring angular momentum in a real atmosphere are the frictional interaction with the underlying surface, and the transfer of  $m$  by non-axisymmetric waves and eddies.

This might initially suggest that the discussion of axisymmetric viscous systems given above was not at all relevant to a planetary atmosphere. From a consideration of the zonal mean circulation, however, some useful similarities with the previous discussion becomes apparent, especially when taken in the context of wave-mean flow interaction theory (e.g. Andrews & McIntyre 1978; Edmon et al. 1980). For a non-axisymmetric flow, the zonally-averaged angular momentum equation becomes

$$\overline{\frac{\partial m}{\partial t}} + \overline{\mathbf{u}^* \cdot \nabla m} = -\nabla \cdot \mathbf{E} + \overline{\mathfrak{F}}/\rho \quad (7)$$

where  $\overline{\mathbf{u}^*}$  is the residual mean meridional velocity (which approximates to the Lagrangian mean circulation under certain conditions - see e.g. Edmon et al. 1980), defined in pressure coordinates by

$$\overline{\mathbf{u}^*} = \left[ \overline{v} - \frac{\partial \overline{\{(v'\theta')\}}}{\partial \theta} \frac{1}{dp} \right] / \partial p, \quad \overline{\omega} + \left[ \frac{\partial \overline{\{(v'\theta')\}}}{\partial \theta} \frac{1}{dp} \right] / (a \cos \phi) \quad (8)$$

where  $\overline{\omega} = Dp/Dt$ , and  $\mathbf{E}$  is a form of the so-called Eliassen-Palm (or EP) flux (actually  $-a \cos \phi$  x the usually quoted form of  $\mathbf{E}$ , so that a convergence of  $\mathbf{E}$  corresponds to an acceleration of the flow):

$$\mathbf{E} = a \cos\phi \left[ \overline{(u'v')} - \left\{ \frac{\partial u}{\partial p} (v'\theta') \right\} / \left( \frac{d\theta}{dp} \right) \right],$$

$$\overline{(\omega'u')} + \left\{ \frac{\partial(u \cos\phi)}{\partial\phi} / (a \cos\phi) - 2\Omega \sin\phi \right\} (v'\theta') / \left( \frac{d\theta}{dp} \right) \quad (9)$$

If  $\overline{\mathfrak{E}}/\rho$  is neglected, it is of interest to note that (7) has the same mathematical form as the axisymmetric angular momentum equation discussed in Lecture 9, so that  $\mathbf{E}$  is seen to be formally similar to the diffusive flux  $\mathbf{F}$  in viscous, axisymmetric models. Since  $\overline{\mathbf{u}}^*$  also satisfies a continuity equation similar to that of an axisymmetric  $\overline{\mathbf{u}}$ , the same arguments concerning the integral constraints on  $\mathbf{F}$  also apply to  $\mathbf{E}$  for toroidal volumes enclosed by  $m$  contours,  $\overline{\mathbf{u}}^*$  streamlines or impermeable boundaries (though note that  $\overline{\mathbf{u}}^*$  does not generally satisfy the same boundary conditions as  $\overline{\mathbf{u}}$ ). Thus, any local maximum in  $m$  must also be associated with EP fluxes which are up-gradient with respect to  $\nabla m$  in some places and down-gradient in others, unless other dissipative processes (such as viscosity, gravity wave-breaking etc.) contributing to  $\overline{\mathfrak{E}}/\rho$  are also significant.

An example for the Earth's atmosphere is shown in Fig. 4, in which the large-scale (quasi-geostrophic) EP fluxes are illustrated with respect to the distribution of  $m$ .  $\mathbf{E}$  in the tropics is largely horizontal and down-gradient, (with respect to  $\nabla m$ ), indicating a missing (up-gradient?) source of  $m$  in equatorial regions, probably due to the surface friction which is not accounted for in the EP flux as calculated. Note that there is no fundamental reason for  $\mathbf{E}$  to depend upon the mean zonal flow in the same way as  $\mathbf{F}$  (i.e. upon the angular velocity gradient), so that the discussion of viscous axisymmetric models can only provide qualitative information in a very general, non-specific way on how a super-rotating flow in a planetary atmosphere can be set up and maintained - essentially by a balance between advection in the meridional circulation and a diffusion-like transfer analogous to viscosity. It is of interest to remark, however, that a form of diffusion which tends to remove horizontal gradients of angular velocity (like molecular viscosity) has certain properties in common with eddy processes which tend to mix (absolute) vorticity - such as eddies arising from barotropic instability. Although such processes do not appear to be representative of eddies in the Earth's atmosphere (which is significantly baroclinic), there is some evidence for  $\overline{\nabla\omega \cdot \nabla m} > 0$  in atmospheres of Venus and Jupiter (in its equatorial jet) in a way intriguingly similar to the axisymmetric viscous flows discussed in Lecture 9 (see Figs 1 and

2, and Read 1986), with peaks in the mean angular velocity (indicated M) displaced from the equator itself.

#### 4. Angular momentum fluctuations and the length of the day

In addition to the effects of large-scale eddies in the atmosphere in transferring  $m$  between latitudes, the atmosphere can exchange  $m$  with the underlying planet via frictional interactions at the surface and pressure torques (which arise from east-west surface pressure differences across mountain ranges). In general, the distribution of mean zonal velocity across the Earth's surface is such that the total torque exerted by the atmosphere on the Earth (and vice versa) is close to zero - hence the loss of angular momentum due to drag on the mid-latitude westerlies is balanced by sources of  $m$  due to a similar drag on the surface easterlies in the tropics. This balance is never precise, however, because of general atmospheric variability, so that the atmosphere is continually exchanging  $m$  with the solid Earth. We have considered some general effects on the fluid atmosphere arising from this exchange, but it also has a measurable effect upon the total angular momentum (and hence on the instantaneous rotation rate) of the Earth itself. This can be detected through very careful measurements of the rotation of the Earth relative to background stars (astrometry - a branch of astronomy), though the magnitude of the effect on the rotation period or 'length of the day' is very small - if the entire atmosphere were brought to rest in the frame of the solid Earth, it would only alter the mean length of the day by a few milliseconds (ms)!

Fluctuations in the length of the day (l.o.d.) have been measured by astronomers for many years, and have indicated variability over a wide range of timescales (from days to decades). It was not until 1979, however, that meteorological data of sufficient quality became available (during FGGE) to measure accurately the total angular momentum of the atmosphere every day. A detailed comparison between this time series and that of the l.o.d. revealed a very good correlation over timescales of days to years (see Fig. 5, from Hide 1984). This correlation (and departures from it) have been found to be very useful and informative on a variety of problems in meteorology and geophysics, and the Office continues to maintain an archive of atmospheric angular momentum data (derived from ECMWF analyses) up to the present day.

The subject is currently a very active area of research in many centres throughout the world, and has lead, for example, to the 'rediscovery' of fluctuations in the global atmosphere with a period  $\sim 40$  days (cf Madden & Julian 1972). Variability on this timescale is readily apparent in the atmospheric angular momentum and l.o.d. time series, and is associated with fluctuations in both mid-latitudes and the tropics which are (at least partially) coherent. Recent theoretical interpretations have invoked a variety of different processes in the tropical atmosphere, including modified forms of equatorially-trapped Kelvin waves (Chang 1977), oscillations of the Hadley circulation associated with interactions between dynamics and moist convective heating (Goswami & Shukla 1984), and the propagation of barotropic Rossby waves between tropics and mid-latitudes (Simmons et al. 1983). None of these processes, however, has so far received widespread acceptance ....?

#### REFERENCES

- Andrews, D. G. & McIntyre, M., 1978. 'Generalized Eliassen-Palm and Charney-Drazin theorems for waves on axisymmetric mean flows in compressible atmospheres', J. Atmos. Sci., **35**, 175-185.
- Chang, C.-P., 1977. 'Viscous internal gravity wave and low frequency oscillations in the tropics', J. Atmos. Sci., **34**, 901-910.
- Edmon, H. J., Hoskins, B. J. & McIntyre, M., 1980. 'Eliassen-Palm cross-sections for the troposphere', J. Atmos. Sci., **37**, 2600-2616.
- Flasar, F. M., 1986. 'Global dynamics and thermal structure of Jupiter's atmosphere', Icarus, **65**, 280-303.
- Flasar, F. M., Samuelson, R. E. & Conrath, B. J., 1981. 'Titan's atmosphere: temperature and dynamics', Nature, **292**, 693-698.
- Goswami, B. N. & Shukla, J., 1984. 'Quasi-periodic oscillations in a symmetric general circulation model', J. Atmos. Sci., **41**, 20-37.

- Hide, R., 1984. 'Rotation of the atmospheres of the Earth and planets', Phil. Trans. R. Soc. Lond., **A313**, 107-121.
- Hide, R., Birch, N. T., Morrison, L. V., Shea, D. J. & White, A. A., 1980. 'Atmospheric angular momentum fluctuations and changes in the length of the day', Nature, **286**, 114-117.
- Lorenz, E., 1967. The Nature and Theory of the General Circulation of the Atmosphere, WMO No. 218, T.P. 115.
- Madden, R. A. & Julian, P. R., 1972. 'Description of global-scale circulation cells in the tropics with a 40-50 day period', J. Atmos. Sci., **29**, 1109-1123.
- Oort, A. H. & Peixoto, J. P., 1983. 'Global angular momentum and energy balance requirements from observations', Adv. in Geophys., **25**, 355-490.
- Read, P. L., 1986. 'Super-rotation and diffusion of angular momentum: II. a review of quasi-axisymmetric models of planetary atmospheres', Quart. J. R. Met. Soc., **112**, 253-272.
- Schubert, G., 1983. 'General circulation and dynamical state of the Venus atmosphere', in Venus (Hunten, D. M., Colin, L., Donohue, T. M. & Moroz, V. I., eds). University of Arizona Press, Tucson, pp681-765.
- Simmons, A. J., Wallace, J. M. & Branstator, G. W., 1983. 'Barotropic wave propagation and instability, and atmospheric teleconnection patterns', J. Atmos. Sci., **40**, 1363-1392.
- Smith, B. A. (and 39 authors!), 1986. 'Voyager 2 in the Uranian system: imaging science results', Science, **233**, 43-64.

P. L. Read  
August 1986

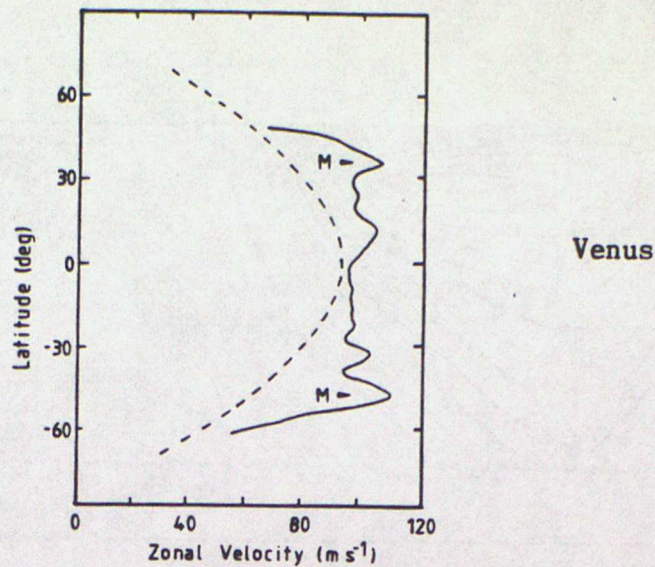


Figure 1. Latitudinal profile of mean zonal velocity at the tops of the clouds on Venus, adapted from the Mariner 10 data of Limaye and Suomi (1981). Also shown (dashed) is the velocity profile corresponding to a uniform angular velocity with latitude, equivalent to a rotation period of 4.8 days. The latitudes of maximum observed angular velocity are indicated by M.

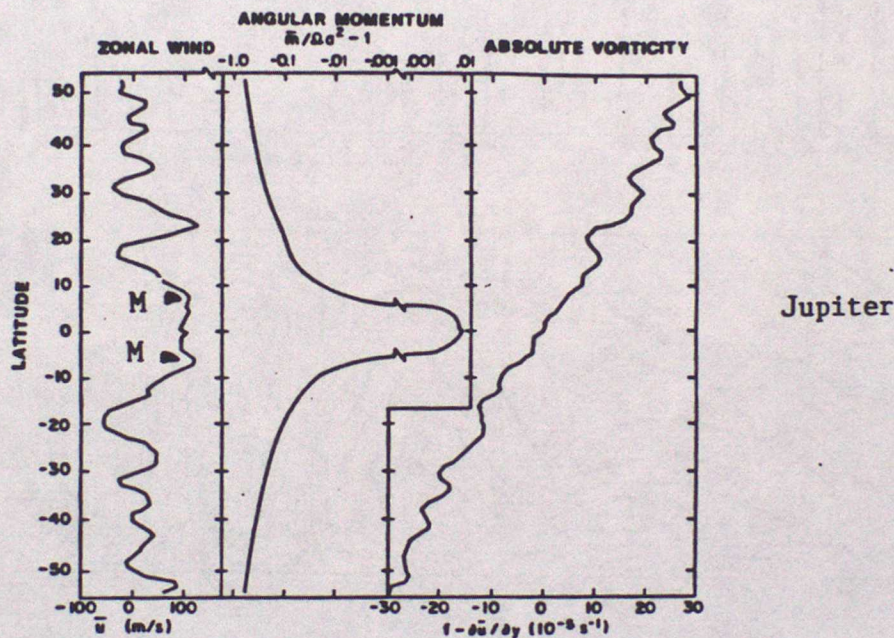


FIG. 2. Left panel: Mean zonal winds as a function of latitude, derived from the tracking of clouds in Voyager 2 images by Limaye *et al.* (1982). Central panel: Excess of angular momentum per unit mass over that corotating at the equator a distance 71,500 km from the center of Jupiter. Right panel: The component of the absolute vorticity for the zonally averaged winds which is normal to the oblate geopotential surface of Jupiter. To a good approximation this is given by  $f - \partial\bar{u}/\partial y$ , if the Coriolis frequency,  $f$ , and meridional coordinate,  $y$ , are defined in terms of planetographic latitude (see Appendix).

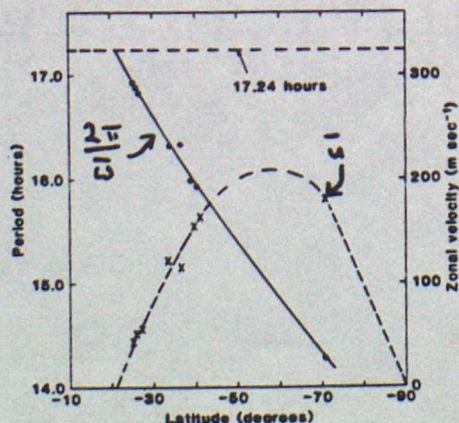


Fig. 3. Measured zonal velocities for the southern hemisphere as a function of planetocentric latitude. The points connected by the solid curve are rotation periods determined from individual spot motions. The error is less than 0.1 hour in all cases. The points connected by the dashed curve are the corresponding zonal velocities relative to the 17.24-hour period of the magnetic field (12). The point at  $-70^\circ$  was obtained from violet images and may therefore refer to a higher altitude than the other points, which were obtained from orange images.

Uranus

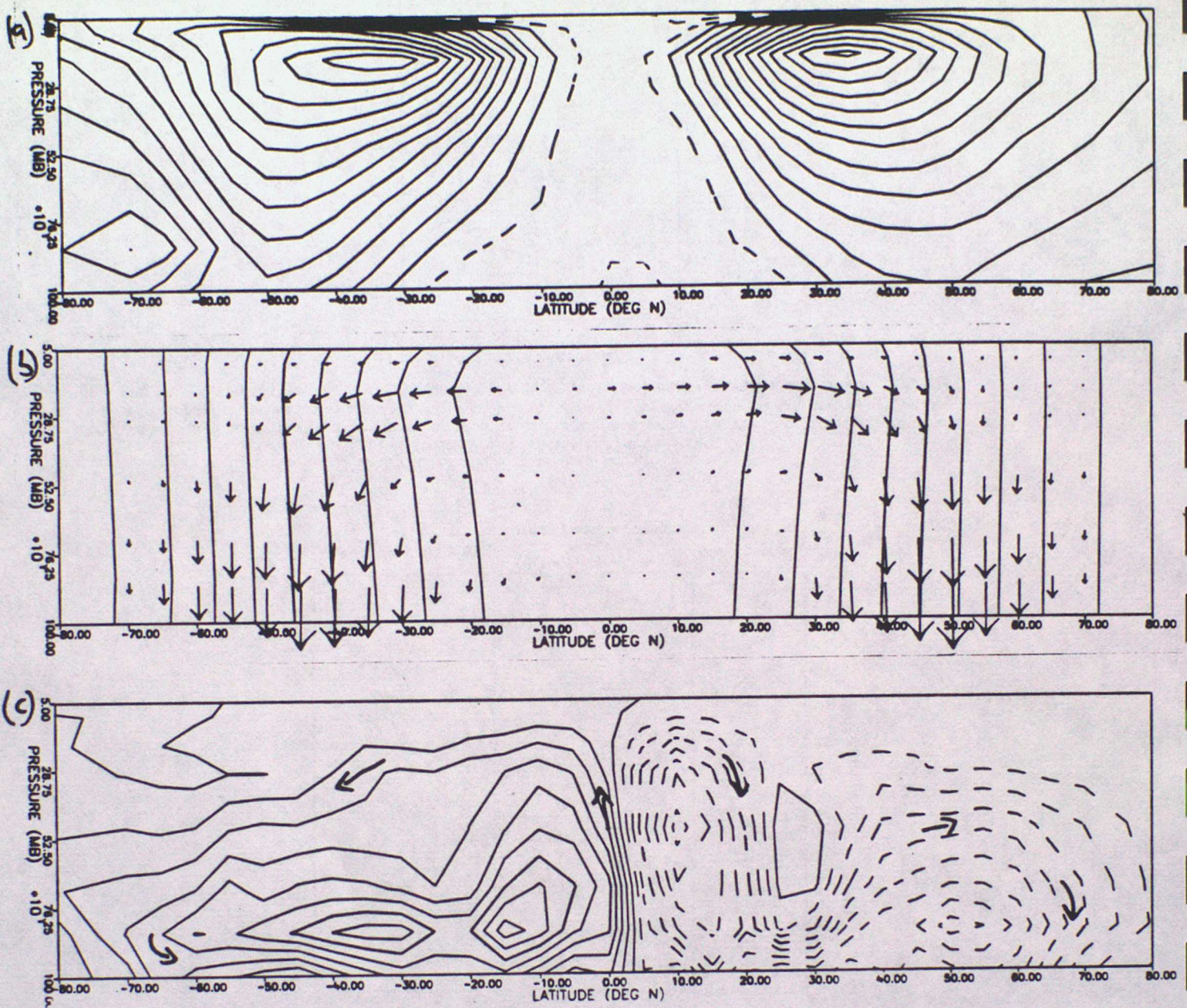


Figure 4: Sections a) of mean zonal flow, b) absolute axial angular momentum  $\bar{m}$  and EP flux vectors (quasi-geostrophic form - e.g. see Edmon et al. 1980) and c) streamfunction for the residual mean meridional circulation  $\bar{u}^*$  (see text) for the Earth's atmosphere. Data are for the annual mean from Oort & Peixoto (1983), using the same methods as those of Edmon et al. (1980), but plotted according to the convention used in the text (i.e. with  $\bar{E}$  representing the flux of angular momentum and  $-\nabla \cdot \bar{E}$  corresponding to an acceleration of the mean zonal flow). Contour intervals are a)  $2.25 \text{ m s}^{-1}$ , b)  $3 \times 10^8 \text{ m}^2 \text{ s}^{-1}$ , c)  $6 \times 10^{16} \text{ m}^2 \text{ s Pa}$  and vectors are normalised to a maximum length of  $3.3 \times 10^{17} \text{ m}^3 \text{ s}^{-2}$ . Negative contours are dashed, and the largest (most equatorward) contour in b) is at  $2.7 \times 10^9 \text{ m}^2 \text{ s}^{-1}$ .

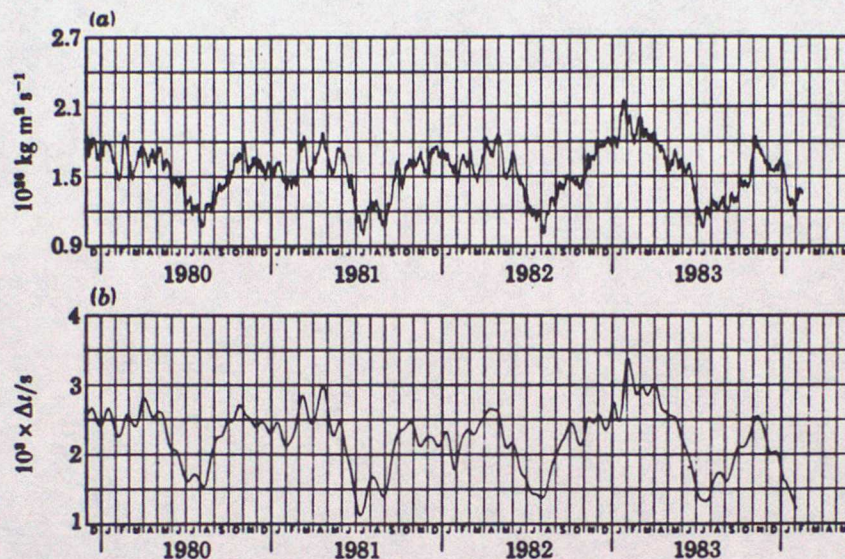


FIGURE 8. Angular momentum fluctuations of the atmosphere (a) and changes in the length of the day (b) from 1 December 1979 to 15 February 1984. There is good agreement between time-variations of the corresponding axial atmospheric effective angular momentum and  $\Delta t$ , implying that short-term changes in the length of the day can be accounted for virtually entirely in terms of axial angular momentum exchange between the atmosphere and solid Earth, without having to invoke significant non-meteorological excitation on these short timescales. These results effectively confirm and extend the work of Hide *et al.* (1980) (see also BHWW), which was based on the most comprehensive meteorological data sets ever obtained, albeit for the limited duration of the two Special Observing Periods (4 January–5 March and 1 May–30 June) in 1979 of the FGGE. By continuing these calculations on a routine basis with the best meteorological and length-of-day data available it will be possible to investigate in detail the non-meteorological processes that influence the rate of rotation of the solid Earth on longer timescales. (The length of the day is  $86400 + \Delta t$  s.)